Hydrophobic polyelectrolytes: An examination of their cooperative partitioning in a 2-phase oil/water system and lipid membrane interactions

Lennart van den Hoven

A master's thesis for the Nanomaterials Science Master Program

Supervisors:

Prof. Dr. Willem K. Kegel

MSc. James L. Martin Robinson

Dr. Alex van Silfhout

Van 't Hoff Laboratory for Physical and Colloid Chemistry

Debye Institute for Nanomaterials Science

Utrecht University

31-05-2023

Utrecht University

Abstract

Hydrophobic polyelectrolytes (HPEs) are polymers that contain hydrophobic and chargeable groups. The chargeable groups can be weak acidic- or basic groups making the HPEs pH responsive. Due to the amphipathic nature of the HPEs, they can strongly interact with lipid bilayer membranes. Depending on the chain architecture and the type of membrane, it is possible for HPEs to solubilize membranes by forming nanodiscs, an ability which can be used to extract membrane proteins together with their native lipid environment.

The pH dependent transitioning between a hydrophobic- and hydrophilic state can be quite sharp. The sharpness of the transition seems to be of a cooperative nature. The pH dependent cooperative partitioning is observed in various transitions such as coil to globule, micellization and nanodisc formation.

In this research the cooperative transition of poly (6-amino hexanoic acid) in at 2-phase oil and water system is examined. The results are compared to model developed by *J. L. Martin Robinson, W. K. Kegel, Cooperative transitions involving hydrophobic polyelectrolytes, PNAS,* ***120****, (2023)* [1] which is used to predict how the sharpness of the transition and transition pH depend on the polymer length. The results show that the sharpness of the transition increases with increasing polymer length and showed a linear relationship between polymer lengths and the value of M. The transition pH stays relatively equal for all three different polymer lengths. Both these observations are correctly predicted by the model. Experiments to test the influence of ionic strength of the sharpness of the transition show that at low ionic strength the transition becomes broader and shifts to higher pH values. This is attributed to less charge screening at low ionic strength, resulting in a pKa split for the acid groups and increase in hydrophobic energy penalty on an individual polymer.

Membrane interaction experiments are preformed using DMPC lipid membrane vesicles and an Eosin Y labelled polymer. The brightfield- and fluorescent microscopy images show that the polymer interacts with the membranes in a 3-11 pH range. At first it seems that at pH 3 the polymer accumulates more in and around the membranes resulting in a higher contrast between membranes and background. But due to some problems with the fluorescent intensity of the dye, the only conclusion from this experiment is that the polymer does not dissolve the membranes but does interact with them at pH 3-11, which is expected at low pH but not so much at high pH. This is attributed to the large carbon sidechain making it possible for the polymer to move into the membranes, even at high pH, while keeping its charges far enough away from each other.

Contents

1 Introduction

Hydrophobic polyelectrolytes (HPEs) are polymers with chargeable groups attached to a hydrophobic backbone. These chargeable groups can often be acidic- or basic groups and this can make the HPE pH-responsive upon changing the pH when dissolved in an aqueous solution. A change in pH can induce a conformational change of the HPE and this is called a coil to globule transition (figure 1). When the pH is below the pKa of an acidic HPE, the HPE will want to minimize the hydrophobic surface in contact with the aqueous solvent and form a globule. The opposite is true for when the pH is above the pKa of the HPE and now the deprotonation of the acid groups creates charges which cause the HPE to extend into a coil [2]. The pH induced conformational transition can occur over a very narrow pH-range and is not only restricted to a coil to globule transition. The sharpness of the transition cannot be explained by the conventional Langmuir adsorption isotherm but is more adequately described by a modification of the Monod, Wyman and Changeux -model (MWC). This model was first developed when examining oxygen binding to hemoglobin because the experimental values for oxygen binding did not match the theory of Langmuir adsorption [3]. In the MWC-model, the sharpness of the transition occurs due to a competition between two states where one has more affinity for the ligands then the other, but does come with an additional conformational energy penalty [4]. *Martin Robinson et al.* showed that the cooperative nature of the pH induced conformational transitions of HPEs can be described by a statistical mechanical model. This model gives insights into the behaviour of different HPEs with respect to the sharpness of the transition and the transition pH [1]. The model can be used to describe various different cooperative transitions as is depicted in figure 1.

Another interesting property of HPEs, is that depending on their architecture, they can strongly interact with lipid membranes. Due to their amphipathic nature, HPEs have the ability to solubilize lipid membranes and form nanodiscs [5] (figure 1). First the HPE binds to the surface of the membrane due to hydrophobic- and electrostatic interactions. The HPE can then insert its hydrophobic groups into the acyl chains of the core of the lipid membrane bilayer. The hydrophilic charged groups of the HPE will stick out of the membrane and the HPE will wrap around the lipids to form a nanodisc and solubilize the membrane [6]. The formation of nanodiscs can be used to extract membrane proteins together with their native lipid environment. Membrane proteins play a crucial role in a lot of cellular processes but extracting them from a lipid membrane can be quite difficult. Detergents can be used to break up the membrane and free the membrane proteins, but this can lead to a loss of native lipid interactions with the membrane proteins, sometimes resulting in inactivation or aggregation of the membrane protein. This can be circumvented by using HPEs to form nanodiscs around the membrane protein freeing the membrane protein in its native lipid environment. The membrane protein nanodiscs can be extracted by using affinity purification [7].

Scheidelaar et al. showed that the pH at which membrane solubilization occurs can be varied depending on the hydrophobicity of the HPE. Styrene maleic acid copolymers (SMA) were used to solubilize phospholipid vesicles. By varying the ratio of styrene and maleic acid in the copolymers, it was possible to control the hydrophobicity of the SMA polymers. They showed that the pH at which solubilization occurs increased when the hydrophobicity of the polymers increased [8]. The transitions between different hydrophobic and hydrophilic states for the SMA in their research, showed a sharp transition which hinted to cooperative behaviour.

A possible application for HPEs is that they have the potential to be used in selectively targeting tumour cells. The pH of extracellular tissue around tumour cells is 0.3 to 0.7 pH-unit lower then healthy tissue. This is called the Warburg effect and it occurs because tumour cells produces most of their energy through anaerobic glycolysis. This type of glucose metabolism is less efficient then aerobic glycolysis and produces lactate, which lowers the pH around the tumour cells [9]. HPEs with a sharp pH-transition could have the potential to be used to directly solubilize tumour cells without damaging healthy tissue. They might also be used to encapsulate drug molecules and selectively release their therapeutic cargo near the tumour cells.

The goal of this research is to examine the pH induced cooperative conformational changes displayed by HPEs while transitioning between a hydrophobic- and a hydrophilic state via a statistical mechanical

model developed by *Martin Robinson et al.* [1]. This will be done by synthesizing and quantitively characterizing different HPEs made from poly 6-aminohexanoc acid acrylate (PAHA). First the cooperative transition of the HPEs while partitioning in an oil and water system will be examined. Parameters which will be varied are ionic strength and polymer chain length. The results will be used to test the accuracy of the statistical mechanical model. The statistical mechanical model will then be used to explain and predict the cooperative behaviour of the HPEs. It is expected that the sharpness of the transition will be dependent on the amount of ionizable groups on the HPE and that the transition point will depend on the hydrophobicity of the individual monomer units of the HPE. Secondly, the interaction of the HPEs at different pH with respect to lipid bilayer membranes will be examined. This will be done by fluorescently labelling the HPEs and imaging this with fluorescent microscopy. Due to the fact that the hydrophobic- and hydrophilic groups are on the same monomer unit for 6-aminohexanoic acid acrylate, it is expected that the HPEs will not be able to solubilize membranes. This is because the rotational freedom between hydrophobic- and hydrophilic groups is important for membrane solubilization. This is the case for HPEs that consist of repeating hydrophobic- and hydrophilic units like SMA. The rotational freedom of the backbone makes it easier for the polymer to stabilize on the hydrophobic/hydrophilic interface, making it more surface active and better at solubilizing membranes. PAHA has both hydrophobic and hydrophilic groups on the same monomer unit so it cannot rotate them independently from each other and it is expected that this renders them unable to solubilize membranes. It is also hypothesized that concentration of polymer in solution at low pH will decrease because the ionized groups will be protonated resulting in the migration of the polymer in and around the lipid membrane bilayer.

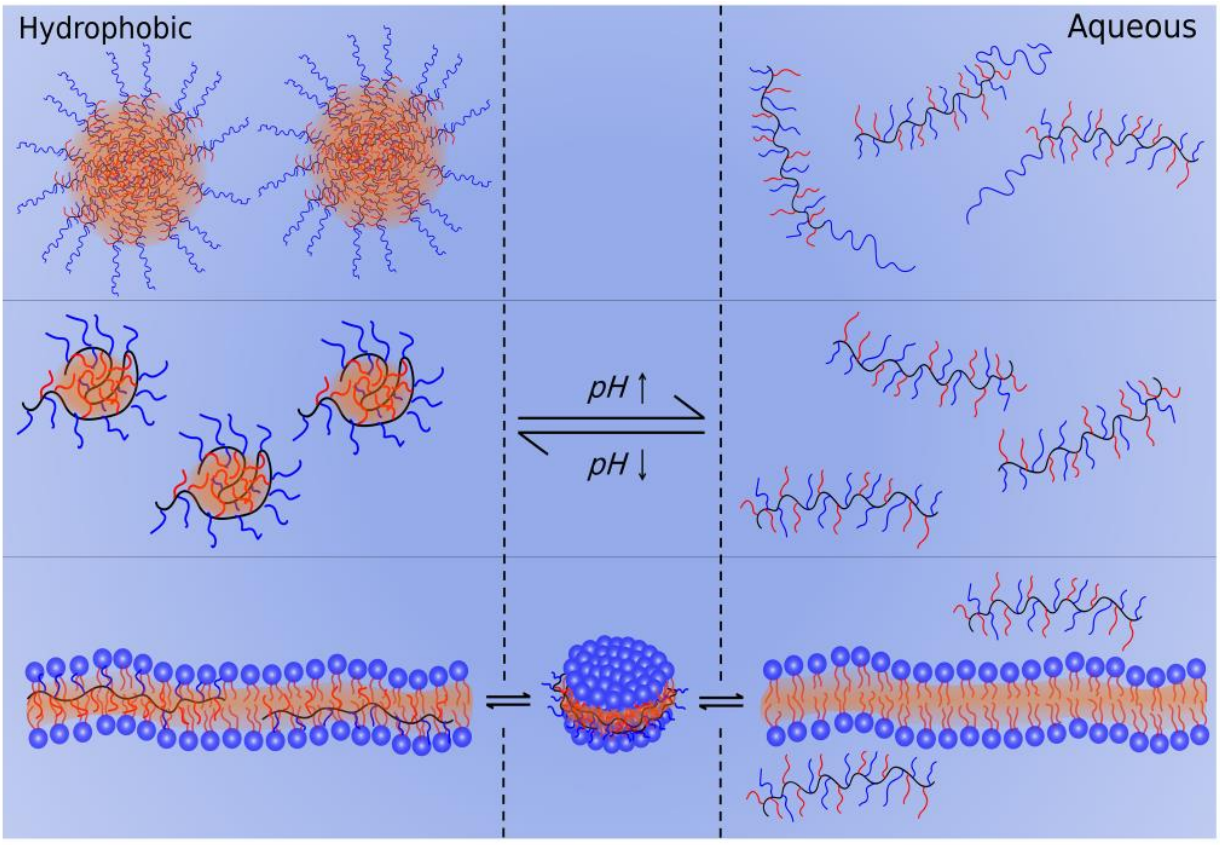

Figure 1: Three different pH responsive cooperative transitions for HPEs. Top) Micellization. Middle) Coil to globule transition. Bottom) Nanodisc formation, note that the transitions are between an hydrophobic and hydrophilic state. For nanodisc formation there are three states since the polymer can be in the membrane bilayer, free in solution or form an intermediate nanodisc state. Figure taken from [1].

2 Theory

In this chapter the theoretical foundations on which this research is built upon are further explained in detail. Certain (sub)chapters are primarily based on chapters for books or dictates and will be noted at the start of the chapter.

2.1 Cooperative transitions

Proteins play a vital role in cellular processes and can often be switchable. This means that they appear to be able to turn on or off depending on the binding of different types of ligand molecules. The active site of the protein can be altered upon ligand binding, which can increase or decrease the activity of the protein. This type of communication between binding sites of the protein is called allostery. When the binding of a ligand onto a substrate increases the affinity for other ligands to bind to the same substrate is called cooperativity [10]. The cooperative binding can be much sharper then the Langmuir adsorption theory for ideal binding onto a substrate [11]. The big difference between allostery and cooperativity is that for cooperativity there is not necessarily a conformational change induced upon ligand binding, but the ligand binding itself increases the binding affinity of the ligands onto the substrate. There is no interaction between groups on the substrate and the ligands appear to cooperate with each other to increase the extend of binding more sharply [10]. Because of this it is more appropriate to call the HPE transitions cooperative, since ligand binding does not necessarily induce a conformational change of the active sites (polymer itself can change conformation) but rather increases the affinity of other ionizable groups to be (de)protonated.

Allosteric transitions can be very sensitive and they were first quantitatively described by Jacques Monod, Jeffries Wyman and Jean-Pierre Changeux. The MWC-model was first developed when examining the allosteric behaviour displayed when oxygen binds to hemoglobin. The MWC-model describes two conformational states in which the hemoglobin can be in: the tense state (T) which has a low affinity for the ligands and the relaxed state (R) which has a high affinity for the ligands but comes with an additional conformational energy penalty. This means that when the ligand concentration is high enough it can overcome energy barrier associated with a conformational change to the R-state and this will lead to a sudden rapid uptake of ligand molecules. It is also important to note that the MWC-model states that the allosteric proteins are polymers (or oligomers) with repeating identical units [4]. This statement leaves open the possibility that not necessarily only proteins can display cooperative behaviour but also more simple molecules like HPEs, which is the focus of this research. Another way of looking cooperative systems is by the ensemble model for cooperativity. This model states that the cooperative behaviour of macromolecular systems arises form properties of the free-energy landscape of the system. Disruptions of the free-energy landscape can be ligand binding but also (de)protonation or interactions with other proteins which can lead to cooperative behaviour [12]. To induce a cooperative response a perturbation in the energy landscape can be created by binding ligands to help overcome the energy barrier needed to change conformation. By writing the probability to find a particular state of the substrate as the statistical weight divided by the partition function, the ensemble model enables an alternative explanation for cooperative behaviour that is purely based on thermodynamics and enables an approach in which only the energies of different states needs to be known or predicted [13].

An example of cooperative behaviour of HPEs is depicted in figure 2. In the research of *Ma et al.* polymers were made consisting of different ratios of 2-(dipropylamino) ethyl methacrylate (DPA-MA) and 2-(dibutylamino)ethyl methacrylate (DBA-MA). The DBA-MA monomer is more hydrophobic than the DPA-MA monomer so by varying the monomer ratio it is possible to control the hydrophobicity of the polymers. To the polymers either a fluorophore or a fluorescent quencher were added. Depending on the pH of the solution the HPE molecules can either be in free solution (because the amine is protonated) or can form a micelle to minimize the hydrophobic surface of the polymers that are in contact with the solution (Figure 2a). When a micelle is formed, the fluorophore and the fluorescence quencher are close to each other so there will be less fluorescent signal detected. The transition between a coil and a micelle is very sharp and it is shown that this is of a cooperative nature (Figure 2b). Figure 2b also shows that the

transition pH shifts to lower values when the hydrophobicity of the polymer increases. This can be explained by the fact that there are two energies which will affect the behaviour of the polymer. There is a favourable binding energy of binding a proton on the amine group and there is an unfavourable hydrophobic energy penalty for leaving hydrophobic groups in solution. A more hydrophobic polymer will therefore pay a higher energy penalty for staying free in solution so it will need a lower pH of the surrounding solution (higher H^+ -concentration) to compensate for this energy penalty and this explains why the transition pH gets lower with increasing polymer hydrophobicity [14].

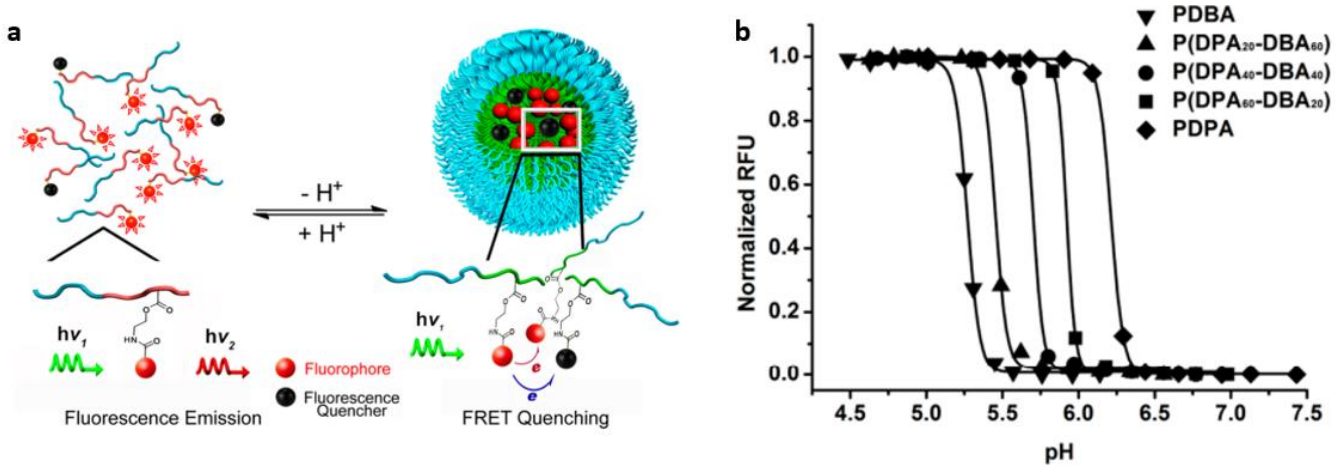

Figure 2: a) Schematic representation of the conformational change from an extended coil to a micelle when increasing the pH. Note that when the micelle is formed the fluorophore and the fluorescence quencher are close to each other so less fluorescent signal will be emitted. b) Cooperative transitions of basic HPEs (amines) with different hydrophobicity which shows a good degree of control over the transition pH. Figure taken form [14] and adapted.

2.2 The Canonical Ensemble

This subchapter is to give a detailed explanation of the Canonical Ensemble theory and is primarily based on chapter 5 from *Physical Chemistry 2: Classical Thermodynamics and introduction to Statistical Thermodynamics*, by W. K. Kegel [15]. Which relies on *Statistical Thermodynamics* by E. Schrödinger [16] and *An introduction to Statistical Thermodynamics* by T. L. Hill [17]. Additional sources will also be used and will be cited.

Statistical thermodynamics can be used to describe certain physical properties of a macroscopic system by looking at a very large collection of these systems and viewing them as one large super system. These properties can be deducted via a statistical approach and the reason for doing this is because it is otherwise almost impossible to describe the properties of a single macroscopic system due to the large number of variables present in the supersystem (each particle has 3 coordinates and there are often a huge number of particles present in the supersystem). By using statistical thermodynamics these variables can be reduced to only three because a thermodynamic state of a system only needs 3 variables to describe its state (V, T, N, or S, V, N, etc.). A way to statistically describe a system is by using the Canonical Ensemble theory.

The canonical ensemble describes a large supersystem which is isolated from the environment and of which the total energy is constant. This supersystem is divided into N smaller systems which are all identical copies of the system that is studied. These systems all have fixed values for N, V and T but they are able to exchange energy/heat between them. The canonical ensemble is dictated by two main rules which are called the postulates. The first postulate states that the time average of the system of interest is the same as the ensemble average in the limit of $N \rightarrow \infty$. This means that the average energy of a single system over time is the same as the ensemble average, which is the sum of all individual energies of the single systems multiplied by 1/N (total amount of systems) in the limit $N \rightarrow \infty$. This is an important postulate because it enables a relation between the average energy of a single system compared to the

average energy of the entire system (which explicitly consists of a collection of the single systems). The second postulate states that all microstates of the single systems, that are consistent with a specified thermodynamic state in the supersystem, have an equal probability to occur. This means that there is no preference for the single system between microstates that correspond to the same thermodynamic state [18].

Let's assume for simplicity that we have a supersystem which is divided in single systems which can all have energies ranging from E_1 all the way to E_j. The amount of systems that have energy E_1 is called the occupation number n_1 so these numbers can also range from n_1 to n_j. It is now possible to write an equation for the number of ways the energy states of the single systems can be distributed over the supersystem as:

$$W(n_1, \dots \dots n_j) = \frac{N!}{\prod_j n_j!} \quad (1)$$

Note that n_j is the occupation number of single systems in state j in the supersystem, so W is the total amount of ways it is possible to distribute a single system over the supersystem. W is often also called the weight of the configuration [19]. The occupation numbers must obey the following two conditions:

$$N = \sum_j n_j \quad (2)$$

$$E_t = \sum_j n_j E_j \quad (3)$$

So, Eq. 2 shows that the total amount of systems in the supersystem is equal to the sum of all occupation numbers and Eq. 3 shows that the total energy of the isolated supersystem is equal to the sum of the occupation numbers multiplied by the energy of the state which they occupy. The total amount of states of the supersystem can be written as:

$$\Omega = \sum''_{n_j \dots n_j} W(n_1, \dots \dots n_j) \quad (4)$$

This can be done because the sum of each possible distribution of the single systems (W) in the supersystem will simply be the total amount of states the supersystem can have due to the second postulate. Note that $\sum''_{n_j \dots n_j}$ implies that only sets are summed which obey the boundary conditions in Eq. 2 and 3. Also due to the second postulate, the average occupation number is given by:

$$< n_j > = \frac{\sum''_{n_j \dots n_j} n_j W(n_1, \dots \dots n_j)}{\Omega} \quad (5)$$

The second postulate says that each microstate of an energy state, in which a single system can be, has and equal probability to occur. This means that by multiplying the occupation number by the amount of possible ways to distribute the single systems (W) it will give you all the possible states for the supersystem to be in. If this is then divided by the total amount of states of the supersystem this will result in the average occupation number. The probability to find a system in state j is then:

$$P_j = \frac{<n_j>}{N} \quad (6)$$

An important assumption is made that because the super system consists of a very large amount of single systems (lim $N \rightarrow \infty$) the average distribution can also be written as the most probable distribution. This is because the value of N is so large, that the most probable distribution and distributions which vary slightly from the most probable distribution will dominate the value for the average occupation number (figure 3). This results in:

$$P_j = \frac{n_j^*}{N} \quad (7)$$

Where n_j^* is the most probable distribution of the set of occupation numbers. Because we say that the most probable distribution for W will dominate the value of Ω we can write:

$$\ln \Omega = \ln W_{max} \tag{8}$$

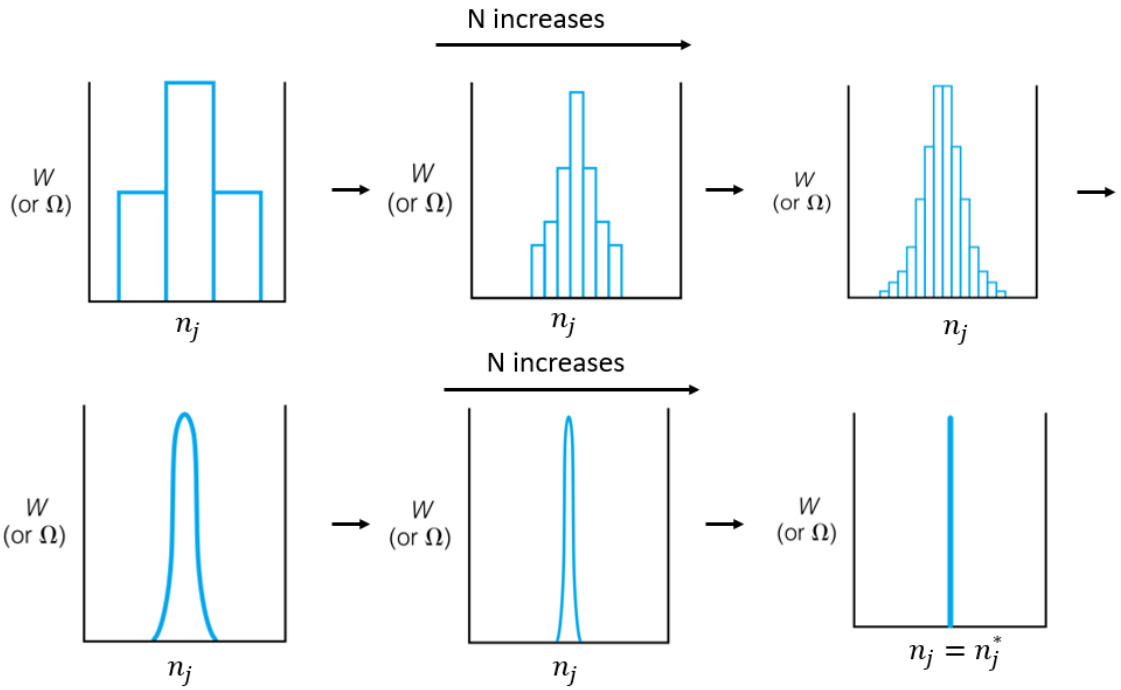

Figure 3: Illustration of how the number of ways to distribute the particles over the supersystem (W) changes with increasing number of particles (N). Note that the distribution gets more narrow with increasing number of particles and that when N → ∞, the distribution becomes so narrow that it becomes clear that one distribution dominates the number for W and this is called the most probable distribution (n_j^*). Figure taken from [40] and adapted.

Note that Eq. 8 only holds for the lim N → ∞, because then the asymptotic functions approach 1. Figure 3 shows that when N is very large the most probable distribution dominates the value of W or Ω. Now a new way of writing Eq. 8 has to be found because it will allow for a way of expressing the probability as a function of the energies. This can be done as follows:

$$\ln W = \ln \frac{N!}{\prod_j n_j!} = \ln N! - \ln \prod_j n_j! = \ln N! - \sum_j \ln(n_j!) \tag{10}$$

We can now use the Stirling approximation ($\ln n! = n \ln n - n$) to write [19]:

$$\ln W = N \ln N - N - (\sum_j (n_j \ln n_j - n_j)$$

$$= N \ln N - N - (\sum_j n_j \ln n_j - \sum_j n_j) \tag{11}$$

The important step here is to separate out the second summation into two different sums. Eq. 2 states that $N = \sum_j n_j$, so substituting this into Eq. 11 results in:

$$\ln W = \sum_j n_j \ln \sum_j n_j - \sum_j n_j \ln n_j \tag{12}$$

The only thing that is left to do now is to find the maximum of ln W by making use of the two constraints written in Eq. 2 and 3. For this it is possible to use Lagrange's method for undetermined multipliers. This results in the following equation:

$$\ln W - \alpha \sum_j n_j - \beta \sum_j n_j E_j \tag{13}$$

To find the maximum of Eq. 11 the derivative needs to be taken with respect to n_j and set to zero. After some basic algebra the solution to this is given in [15], [17] and [19] and looks like:

$$\ln(\sum_j n_j) - \ln n_j^* - \alpha - \beta E_j = 0 \tag{14}$$

Which can be written as:

$$n_j^* = Ne^{-\alpha-\beta E_j} \tag{15}$$

For Eq. 2, one can sum the most probable distribution of the occupation number which will also result in the total amount of states in the super system. So, by making use of $N = \sum_j n_j^*$, and substituting Eq. 15 in this, the result is:

$$N = \sum_j n_j^* = \sum_j Ne^{-\alpha-\beta E_j}$$

$$N = Ne^{-\alpha} \sum_j e^{-\beta E_j}$$

$$e^{\alpha} = \sum_j e^{-\beta E_j} \tag{16}$$

By substituting Eq. 16 into Eq. 15 and making use of Eq. 7 the probability to find a single state j can be written as:

$$P_j = \frac{e^{-\beta E_j}}{\sum_j e^{-\beta E_j}} \tag{17}$$

This is a very important finding because it is now possible to write the probability to find a single state j simply as a Boltzmann distribution divided by the sum of the distributions of all other energy states. The partition function (PF) can be written as:

$$Z(T,V,N) = \sum_j e^{-\beta E_j} \tag{18}$$

The PF is a very important finding because it enables a new way of expressing thermodynamic quantities by using a statistical approach. This means that it now possible to calculate macroscopic properties of the system from the behaviour of the microscopic particles. The only thing left to do now is to find out what the value for the Lagrange multiplier β is. This is done very well in *Physical Chemistry* from Julio de Paula and Peter Atkins [19]. It relies on a new way of writing the PF for an ideal one atomic gas:

$$Z(T,V,N) = \frac{V}{\Lambda^3}, \qquad \text{with } \Lambda = h\left(\frac{\beta}{2\pi m}\right)^{\frac{1}{2}} \tag{19}$$

Eq. 3 and 18 can now be combined to:

$$E = -\frac{N}{Z}\sum_j E_j\, e^{-\beta E_j} \tag{20}$$

It's possible to rewrite this expression by using: $E_j\, e^{-\beta E_j} = -\frac{d}{d\beta} e^{-\beta E_j}$, which will result in:

$$E = -\frac{N}{Z}\sum_j \frac{d}{d\beta} e^{-\beta E_j} = -\frac{N}{Z}\frac{d}{d\beta}\sum_j e^{-\beta E_j} = -\frac{N}{Z}\frac{dZ}{d\beta} \tag{21}$$

Taking the derivative of Z with respect to β results in:

$$\frac{dZ}{d\beta} = \frac{d}{d\beta}\frac{V}{\Lambda^3} = V\frac{d}{d\beta}\frac{1}{\Lambda^3} = -3\frac{V}{\Lambda^4}\frac{d\Lambda}{d\beta}, \quad \text{with} \quad \frac{d\Lambda}{d\beta} = \frac{1}{2\beta^{\frac{1}{2}}}\frac{h}{(2\pi m)^{\frac{1}{2}}} = \frac{\Lambda}{2\beta} \tag{22}$$

The energy of the monoatomic gas can be expressed as:

$$E = -\frac{N}{Z}\frac{dZ}{d\beta} = -\frac{N}{Z}\cdot -3\frac{V}{\Lambda^4}\cdot\frac{\Lambda}{2\beta} = \frac{3N}{2\beta Z}\cdot\frac{V}{\Lambda^3} = \frac{3N}{2\beta Z}\cdot Z = \frac{3N}{2\beta} \tag{23}$$

A known expression for the energy of a monoatomic gas is given by $E = \frac{3}{2}NkT$ which follows from calculating the internal energy (U) by using the PF in Eq. 19 and $U = kT^2\left(\frac{\partial lnQ}{\partial T}\right)$. The expression for E can be combined with Eq. 23 to give an expression for β:

$$\frac{3N}{2\beta} = \frac{3}{2}NkT, \quad \text{so } \beta = \frac{1}{kT} \tag{24}$$

Substituting Eq. 24 into Eq. 18 gives the final expression for the partition function:

$$Z(T,V,N) = \sum_j e^{-\frac{E_j}{kT}} \tag{25}$$

This shows that the PF is essentially a summation over all possible Boltzmann distributions of all different energy states. This is one of the most important and fundamental findings of statistical thermodynamics and it can be shown that the PF is related to all thermodynamic quantities, which makes the PF a bridge between statistics and thermodynamics.

2.3 The Grand Canonical Ensemble

The PF that is described in chapter 2.2 can now be extended to the Grand Partition Function (GPF). The GPF can be found when examining the Grand Canonical Ensemble. The Grand Canonical Ensemble describes a large supersystem which has constant chemical potential (μ), volume (V) and temperature (T) but the supersystem is open so particles can move freely in and out of the system. The GPF can be found similarly to chapter 2.2 and is done in chapter 2 of *Toy models in physical and molecular biology* by W. K. Kegel [3]. The big difference between the PF and the GPF is that and extra term needs to be found when performing the Lagrange method because now an extra boundary condition is used to represent the total amount of particles present in the ensemble.

$$\sum_{J,N} N \cdot n_{J,N} = N_t \tag{26}$$

Here $n_{J,N}$ represents the occupation number of a system J in the supersystem and N is the number of particles that are present in that system resulting in the total amount of particle's (N_t). Using the Lagrange method and making use of the Stirling approximation the result for the probability to find a system in state J is as follows [17]:

$$P_{J,N} = \frac{n^*_{J,N}}{N} = \frac{e^{-\beta E_{J,N}}\ e^{-\gamma N}}{\sum_{J,N} e^{-\beta E_{J,N}}\ e^{-\gamma N}} = \frac{e^{-\beta E_{J,N}}\ e^{-\gamma N}}{\Xi} \tag{27}$$

The value of γ is determined in [17] to be -μ/kT. Where μ is the chemical potential that describes how much energy is released when extracting particles from a particular phase. The GPF (Ξ) can be written in terms of the PF (Eq. 25) by separating the two summations over N and J, which leads to:

$$\Xi = \sum_N \left[e^{\frac{\mu N}{kT}} \sum_J e^{-\frac{E_{J,N}}{kT}} \right] = \sum_N e^{\frac{\mu N}{kT}}\, Z(T,V,N) = \sum_N \lambda^N\, Z(T,V,N) \tag{28}$$

In Eq. 28, λ is called the fugacity and is a value for how easily a particle can move between the systems in the supersystem. The GPF can be used to develop a statistical mechanical model for the partitioning of the polymers in a 2-phase oil/water system.

2.4 The Grand Canonical Ensemble for a 2-state system

This subchapter is based on chapter 2 of *Toy models in physical and molecular biology* by W. K. Kegel [3] and *Cooperative transitions involving hydrophobic polyelectrolytes* by J. L. Martin Robinson and W. K. Kegel [1].

The main goal of this research is to investigate the cooperative nature of transitions of HPEs and to find a way to predict their behaviour. A statistical mechanical model was developed in order to give insights into the cooperative nature of the transition, which is done by examining the pH mediated transition of HPEs in an oil/water system. 1D Adsorption of either H^+ or OH^- onto the polymer chain (depending on basic- or acidic groups) is assumed (Figure 4).

Where M is the total amount of ionizable groups on the substrate and N is the amount of ligand molecules that are bound to the substrate. By assuming that the adsorption is uncorrelated the GPF for a single conformation state of the polymer (Eq. 28) changes to:

$$\Xi_s = \sum_N^M \binom{M}{N} \lambda^N\, Z(T,V,N) \tag{29}$$

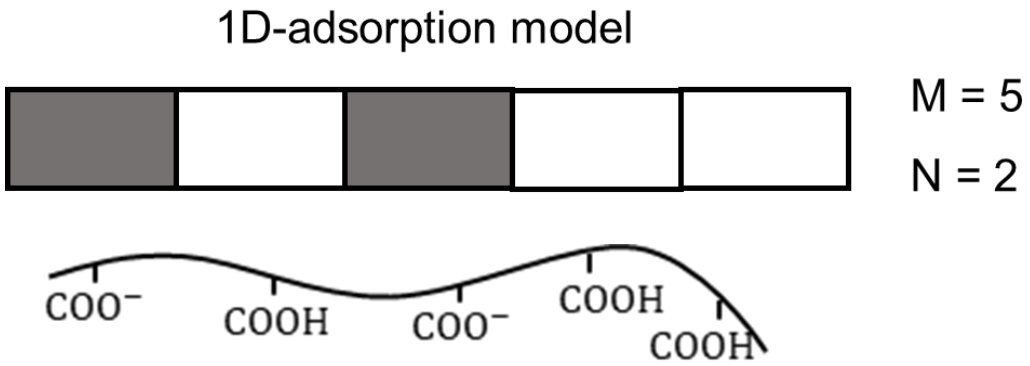

Figure 4: Schematic representation of the 1D- adsorption model. The biding ligands in this case are hydroxide ions which deprotonate the acid groups. For the model all binding sites are considered to be identical and binding of one ligand does not influence the binding of other ligands onto the template.

Due to uncorrelated adsorption there are a number of different ways for the ligands to bind to the adsorption sites hence the term $\binom{M}{N}$. This is because binding is a combination in which the order of binding does not matter for the final state of the polymer. It worth noting that the adsorption is probably not entirely uncorrelated since deprotonating one acid group will influence the pKa of the acid group next to it but this is ignored for now.

Two assumptions are made in order to adjust the GPF to the experimental system. A HPE in this case has acidic groups, so OH^- adsorbs onto the substrate. Because the 1D adsorption models assumes a single molecule system, the only particles that move are the OH-ions (HPE moves to other phases but in adsorption process only OH-ions move). Hence, we assume that the chemical potential of the solution is given by $\mu = kT\ln[OH^-]$. The other assumption is that the energy of the states in the system is given by $E_j = -NkT\ln K$, which comes form the expression for the Gibbs free energy in equilibrium. This changes Eq. 29 to:

$$\Xi_s = \sum_N^M \binom{M}{N} e^{\frac{NkTln[OH]}{kT}} \cdot e^{\frac{NkT\,lnK}{kT}} = \sum_N^M \binom{M}{N} [OH]^N K^N \tag{30}$$

The GPF can now be rewritten making use of the Binominal Theorem [20] as:

$$\Xi_s = (1 + [OH^-]K)^M \tag{31}$$

The K, in this case, is the reaction constant for deprotonating an acid group by binding a OH-ion to it. One can show that $K = \frac{[A^-]}{[HA][OH^-]}$ and can be rewritten in the following way:

$$K_w = [OH^-][H^+]$$

$$K_a = \frac{[A^-][H^+]}{[HA]}, \text{ so}$$

$$K = \frac{K_a}{K_w} \tag{32}$$

When combining Eq. 31 and 32 this results in:

$$\Xi_s = \left(1 + [OH^-]\frac{K_a}{K_w}\right)^M = \left(1 + \frac{1}{[H^+]}K_a\right)^M = (1 + 10^{pH} \cdot 10^{-pK_a})^M = (1 + 10^{pH-pK_a})^M \tag{33}$$

An energy term needs to be added to the GPF for a single conformational state to include the conformational energy penalty associated with the molecule being in this conformational state. This penalty will be higher for the aqueous state since the substrate has more affinity for the ligands, which comes with an energy penalty. The aqueous state in this case is comparable to the relaxed state of hemoglobin in the MWC model where the affinity for the ligands is also high. The GPF is now expressed as:

$$\Xi_s = \exp(-\frac{G_s}{kT})(1 + 10^{pH-pK_a})^M \tag{34}$$

Where G_s is the conformational energy penalty of the substrate in state *s* since changing conformation comes with an energy cost.

In the experimental system there are two phases in which the polymer only has a high affinity for the ligands in the aqueous phase. To specify the GPF to the experimental system one can say that the GPF can be written as a sum of the statistical weights of all possible conformational states. Here is assumed that there are only two possible conformational states: a hydrophobic state in the oil phase with low affinity for the ligands and a hydrophilic state in the water phase with high affinity for the ligands. In practice often more intermediate conformational states will be likely present within the system but these are ignored for now. The GPF for the 2-phase experimental system can be written as:

$$\Xi = \sum_s^S \Xi_s = \Xi_H + \Xi_{aq} \tag{35}$$

As mentioned before, by using UV-VIS spectroscopy it is possible to measure the fraction of polymer that has moved from the hydrophobic oil reservoir to the hydrophilic aqueous reservoir. The GPF in Eq.35 can be used to write an equation for the fraction of polymer in the hydrophobic conformational state. This can be done by dividing the statistical weight of the conformational state (Ξ_s) by the total GPF as written in Eq. 35 to give the fraction of polymer in this state. We say that the statistical weight of the reference state (hydrophobic state) equals 1 ($\Xi_H = 1$). This can be rationalized by the assumption that the pKa in Eq. 34 in the oil phase is very large since it is very unfavourable to deprotonate an acid group in the oil phase and create a charge. This results in $(1 + 10^{pH-pK_a})^M \approx 1$, because 10^{pH-pK_a} goes to zero. We then assume that the conformational energy penalty in the hydrophobic state is 0 since this is the ground state of the system and the polymer has no conformational energy penalty there. In essence this is saying that the hydrophobic state is the reference state to which the aqueous state is referenced. Taking a value of 1 for the hydrophobic state also makes the expressions more straightforward. The fraction of polymer in the hydrophobic state is given by:

$$f_H = \frac{\Xi_H}{\Xi} = \frac{\Xi_H}{\Xi_H + \Xi_{aq}} = \frac{1}{1+\exp\left(-\frac{g_H M_H}{kT}\right)\left(1+10^{pH-pK_a}\right)^M} \tag{36}$$

The fraction of polymer in the aqueous state is the left-over fraction ($f_{aq} = 1 - f_H$). The conformational energy penalty ($g_H M_H$) is the unfavourable energy penalty term for the hydrophobic free energy that the polymer must pay when it moves form the hydrophobic phase into the water phase. Note that a more general way of writing the hydrophobic conformational energy penalty is applied in the form of $G_s = g_H M_H$. In the experimental system, the conformational penalty in the aqueous phase is almost entirely dictated by the hydrophobic energy penalty that each a single hydrophobic monomer unit in the chain (g_H) must pay in order to move into the water. The hydrophobic energy penalty for a single monomer unit (g_H) is positive, since it is unfavourable to put a hydrophobic polymer into a hydrophilic solvent like water. Multiplying this by the total amount of hydrophobic monomers (M_H) in the chain will result in the total conformational energy penalty (G_s).

A big advantage of using this model to describe the cooperative behaviour of HPEs, is that it is not limited to the type of experimental system that is used. The requirements are that there are well defined states which can stabilize in different hydrophobic or hydrophilic reservoirs in the system and that the conformational change between the states is driven by changes in the pH. The model can be used for various different systems such as micellization, membrane solubilization and coil to globule transitions and this makes it widely applicable.

If the model is to be applied to lipid membrane solubilization experiments an extra conformational state will be present. The HPEs can be fully inside the lipid membrane (hydrophobic state), they can be free in the aqueous solution (aqueous state) and they can be partly in the lipid membrane and partly in the aqueous solution when forming a nanodisc (disc state). This will result in an extra GPF for the disc state given by:

$$\Xi_D = \exp(-\frac{G_{HD}}{kT})(1 + 10^{pH-pK_a})^{M_D} \tag{37}$$

Here the conformational energy penalty for disc formation (G_{HD}) is smaller than hydrophobic conformational energy penalty in the aqueous phase (G_H). This is because when forming a nanodisc, some

hydrophobic parts of the HPE can insert itself into the hydrophobic reservoir in the lipid bilayer. This makes the hydrophobic surface of the HPE that is in contact with the solution smaller then when its fully in the aqueous phase hence this makes the energy penalty for disc formation lower than the hydrophobic energy penalty in the aqueous state. When the number of chargeable groups in the disc state (M_D) is equal to the number of chargeable groups in the aqueous state (M), disk formation is always stable with respect to the aqueous state. This is because $G_{HD}<G_H$, so the statistical weight (GFP of single state) of the disc state (Ξ_D) is larger than the statistical weight of the aqueous state (Ξ_{aq}). This results in M_D being smaller then M ($M_D<M$) and this is likely due to some charged groups being inserted into the disc. This again highlights the applicability of the model because it can be used for multiple different type of experimental systems.

The transition point:

An important parameter which can be explained by the model is the transition point. The transition point occurs when the fraction of polymer is equal in the water- and oil phase so $\Xi_{aq} = \Xi_H = 1$. With this condition an equation can be written for the transition pH [21]:

$\Xi_{aq} = \exp\left(-\frac{g_H M_H}{kT}\right)(1 + 10^{pH_{trans}-pK_a})^M = 1$, which can be rewritten to

$$pH_{trans} = pK_a + 0.4343\,\frac{g_H}{kT}\,\frac{M_H}{M} \qquad (38)$$

It is important to note that the assumption is made that $(1 + 10^x) \approx 10^x$, which only holds if x>>1 (x in this case is pH_{trans} – pKa) so this means that Eq. 38 is only valid for cases in which the pH is higher than the pKa of the ionizable group. Eq. 38 is an important finding because it shows that the transition pH dictated by the monomer ratio between the hydrophobic monomers and monomers with ionizable groups $\left(\frac{M_H}{M}\right)$. By varying this ratio, it is possible to change the transition pH and at let it occur at higher or lower values. HPEs with a large $\frac{M_H}{M}$ – ratio will transition at higher pH values since more hydroxide ions will be needed in order for the polymer to move into the water phase and overcome the hydrophobic energy penalty.

The sharpness of transition:

The model in Eq. 36 predicts that the value of M is a measure for the cooperativity of the polymer (figure 5). In this case, a large value will mean a large cooperativity, which will result in a sharp transition that happens in a very narrow pH range. Figure 5 depicts this, where M=1 shows no cooperativity and increases to ultra-sensitive cooperativity for M=20.

The sharpness of the transition is also influenced by the amount of intermediate states of the HPE. More intermediate states will lead to transition broadening because intermediate states will differ in energy penalty from the original hydrophobic state. The intermediate states will now lead to conformational change at different pH values then the original hydrophobic states and this will lead to transition broadening. Low ionic strength can lead to transition broadening and the hypothesis is that at low ionic strength, the pKa of individual acid groups on the HPE can differ. The pKa split occurs because at low ionic strength the Debye length is large, so individual acid groups will experience each other's charge more strongly. The model predicts that a pKa split leads to more intermediate states because it leads to extra terms in the GPF. Another way transition broadening can occur is due to chemical dispersity between different HPEs in the sample. As discussed before, the transition point is dictated by the hydrophobic- to hydrophilic monomer ratio of the polymer ($\frac{M_H}{M}$ – ratio). Chemical dispersity leads to polymers which have different $\frac{M_H}{M}$ – ratios and will thus transition at slightly different pH. This results in transition broadening

because the polymers will change conformation at slightly different pH values and thus making the transition less sharp.

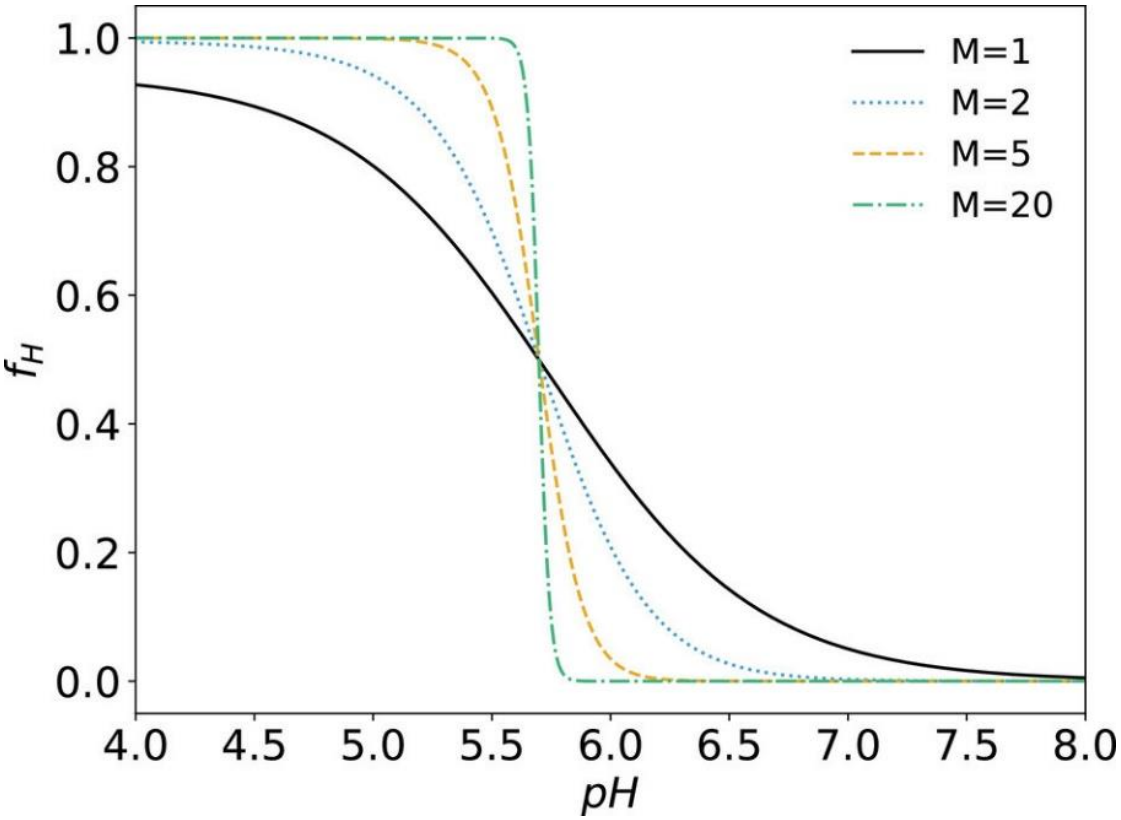

Figure 5: Schematic illustration of how the sharpness of the transition is influenced by the amount of ionizable groups present on the HPE. Note that for a value of M=1 the polymer displays no cooperativity whereas for M=20 there is ultrasensitive cooperativity. The figure also predicts that cooperative behaviour can be observed for shorter polymers with M-values larger than 5. Figure taken form [1].

2.5 The experimental system

One of the main goals of this research is to investigate if the conformational transition of HPEs is of a cooperative nature and if this can be quantified into a statistical mechanical model. In order to do this a simple but effective experimental system had to be developed (figure 6). The experimental system consists of two connected phases: the aqueous phase and the oil phase, which in this case is 1-pentanol. The HPE can move freely between phases and the concentration of polymer in the oil phase can be measured using UV-VIS spectroscopy. Upon increasing the pH, the polymer will move from the oil phase into the aqueous phase because it can deprotonate its acidic groups which is energetically favourable. The same can be said for the reverse transition since decreasing the pH will protonate the acidic groups on the HPE, increasing the hydrophobicity and resulting in the migration of the polymer from the aqueous phase to the oil phase. The system is designed in this way because it essentially forces the polymer to partition into either one of the two phases. The driving force for the partitioning into the aqueous phase is dependent on the change in pH and this parameter can be easily varied in this experimental system. Another big advantage of using this system is that is widely applicable to a wide range of HPEs. Partitioning experiments involving micelles or membrane solubilization have limitations with respect to the type of HPE that can be used since not all HPEs can solubilize membranes or form micelles. The only

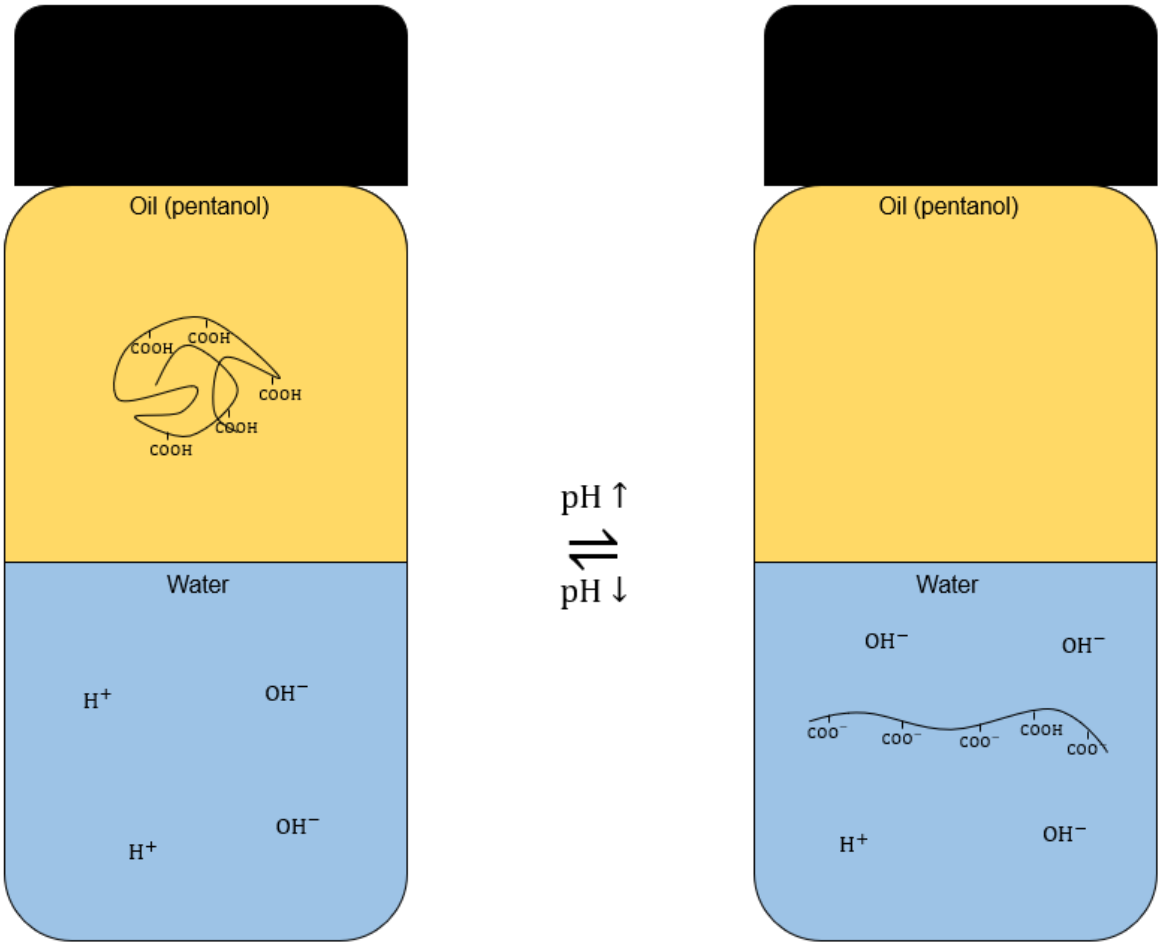

Figure 6: Schematic illustration of the experimental system. The experimental system consists of two phases between which the polymer can move freely. It is not clear what conformation the polymer has in each phase and it is expected that depending on the pH certain acid-groups will not be deprotonated in the aqueous phase. This is because the deprotonation of one group will probably influence the pKa of the group next to it.

restriction for this experimental system is that the HPEs need to contain ionizable groups which can be (de)pronated depending on pH and hydrophobic groups. This is in essence the definition of a pH sensitive HPE, so the system can be applied to almost all of them. The wide applicability of the system makes it easier to compare cooperative transitions for different types of HPEs and this can help in a better understanding of how the chemical structure of the HPE influences the transition.

Note that in figure 6, the HPE is drawn as a globule in the oil phase and as an extended coil in the aqueous phase but it is still not exactly clear what the exact conformation is of the polymer in the two different phases. For the model however, conformational state of the polymer is solely dependent on where in the system the polymer is present. This leads to two different conformational states: a hydrophobic state (in the oil phase) and an aqueous state (in the water phase). It is very likely that there are a lot more intermediate conformational states possible for the polymer and as mentioned before this can lead to transition broadening.

The volume of the phases, with respect to each other, should be kept as constant as possible. This is because the GPF for the HPEs describes the conformation of the individual molecules. The GPF can be used to determine the fraction of polymer in each state but the GPF in essence, describes the conformation of each single individual HPE chain. The molecular partition function can be written as [15]:

$$q = q_t q_{int}, \text{ with}$$

$$q_t = \left(\frac{2\pi mkT}{h^2}\right)^{3/2} V \qquad \text{and} \qquad q_{int} \approx q_R q_v q_{el} \tag{39}$$

Where q_t is the translational PF and q_{int} is the internal PF. The internal PF is not dependent on the volume in which the particle is present but translation is. For this experimental system the polymer particles can translate through the system so the translational PF has to be considered.

The partitioning of a substance between two phases can be described by the partitioning coefficient (K_p). In a 2-phase oil and water system it is given by:

$$K_p = \frac{c_H}{c_{aq}} = \prod_j \left(\frac{q_j}{V_j}\right)^{\nu_j} = \frac{q_H}{V_H}\left(\frac{q_{aq}}{V_{aq}}\right)^{-1} = q_{int,H}\, q_{int,aq}^{-1} = \frac{\Xi_H}{\Xi_{aq}} \quad (40)$$

Where c_H is the concentration of polymer in the hydrophobic phase and c_{aq} is the concentration of polymer in the hydrophilic state. The partitioning coefficient can be related to the statistical weights of the phases by looking at the partition coefficient in chemical equilibrium [15]. By dividing the total partition function by the volume of the phase, only the internal PF is left. In the experimental system, the internal PF is described by the GPF described in chapter 2.4. The number fraction of polymer in the hydrophobic state can be described by:

$$f_H = \frac{c_H V_H}{c_H V_H + c_{aq} V_{aq}} \quad (41)$$

By dividing the numerator and the denominator by $c_H V_H$, it is possible to rewrite Eq. 41 resulting in:

$$f_H = \frac{1}{1 + K_p^{-1}\frac{V_{aq}}{V_H}} \quad (42)$$

By keeping the volumes equal, Eq. 42 becomes equal to Eq. 36 because $K_p^{-1} = \frac{\Xi_{aq}}{\Xi_H} = \Xi_{aq}$. This highlights the importance of keeping the volumes of the 2 phases with respect to each other as constant as possible because this volume ratio can influence the measured hydrophobic fraction. In the experiments this is done by saturating the buffers with pentanol and the pentanol with water. By doing this volume changes are minimized to avoid changes in the f_H caused by volume effects after mixing of the phases.

2.6 RAFT polymerization

In order to accurately investigate the effect of the chain length of the HPEs on the sharpness of the transition it is very important to synthesize HPEs of different lengths that do not have a very high polydispersity per batch. A very good polymerization method for this is reversible addition fragmentation chain transfer polymerization (RAFT). RAFT polymerization was first discovered in 1998 when *Chiefari et al.* reported a new polymerization technique that used a chain transfer agent (CTA), which has a thiocarbonylthio-group that helps transfer radicals between chains [22]. RAFT polymerization has since then gained a lot more popularity due to the fact that it is easy to perform, is applicable to a wide range of monomers and leads to polymers with a low polydispersity index (PDI). The PDI describes the weight distribution of the individual polymers in the sample and is given by:

$$PDI = \frac{\overline{M_w}}{\overline{M_n}},\ with \quad \overline{M_n} = \frac{\sum N_i M_i}{\sum N_i} \quad and \quad \overline{M_w} = \frac{\sum N_i M_i^2}{\sum N_i M_i} = \sum w_i M_i \quad (43)$$

The number average molar mass ($\overline{M_n}$) gives a value for the average molar mass present in the sample by multiplying the molar mass by the mole fraction of all different polymers. The weight average molar mass ($\overline{M_w}$) is given by the sum of the molar mass multiplied by their weight fraction. The PDI describes how narrow the distribution is for the different polymer sizes in the sample. A monodisperse polymer will have a PDI of 1 so the PDI can never be lower than 1 [23]. Typical PDI values for the RAFT polymerization which was followed in this research are 1.03-1.17 and this indicates a low polydispersity in the samples [24].

The key component of the RAFT mechanism is the use of the CTA (figure 7a). The RAFT polymerization starts with an initiation reaction that generates a radical which can react with the monomer (step 1 and 2). The activated monomer can now react with the CTA which creates an equilibrium between active and dormant chains (step 3 and 5). The rate of addition and fragmentation is higher than that of propagation so less than one monomer is added each cycle. The end of each chain is protected by the CTA leading to

less termination events. The result of this is that all chains grow at a similar rate and this gives rise to a very low PDI (figure 7b). The fact that less termination events occur makes post modification of the polymers easier since the polymer chains have a more similar structure. The chain architecture of each chain however, can slightly differ due to the fact that either an initiator molecule can start the reaction or the R-group of the CTA and the effects of this on the experimental system will be further explained in chapter 3.5 [25].

Another controlled polymerization technique is atom transfer radical polymerization (ATRP). ATRP uses a metal-ligand complex which are often copper salts but can also be other transition metals such as Ru, Fe, Mo or Os. The metal ligand complex can react with alkyl halides to form an active species. This active chain can now begin to grow by reacting with monomers and start propagating but when it encounters another metal complex it can react and form a dormant chain again. The equilibrium between propagating chains and dormant chains is what controls the polymerization in the ATRP process. A big advantage of ATRP is that it is very widely applicable to a large variety of monomers [26]. A disadvantage however, is that it is often quite hard to polymerize monomers which have acid groups on them using ATRP. The COO^- groups can bind to the electro positive metal complex or they can protonate the ligands on the metal complex and this can decrease the catalytic activity [27]. For this reason, RAFT polymerization was chosen as the method of choice, because it can also be applied to polymerize monomers with acid groups. This is due to the fact that RAFT uses a CTA to transfer the radicals during polymerization and the CTA is an organic molecule which catalytic activity is not influenced by the acid groups on the monomer.

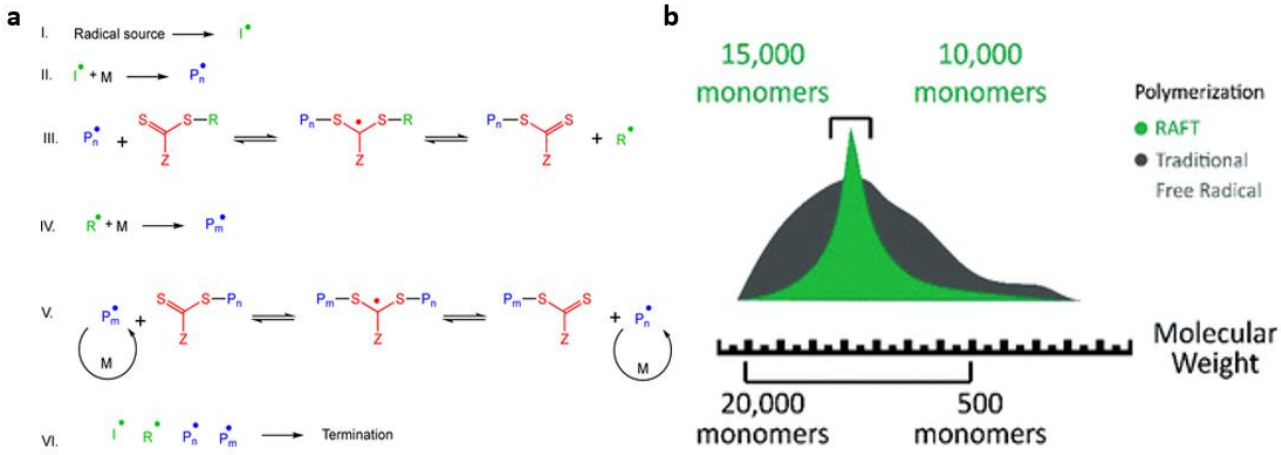

Figure 7: a) Mechanism for RAFT polymerization. b) Difference in polydispersity between RAFT polymerization and traditional free radical polymerization. Note that the distribution for RAFT is significantly smaller then free radical polymerization. Figures taken form [25] and [41].

2.7 Analytical techniques

The purpose of this subchapter is solely to give a brief indication which analytical techniques will be used in this research. The purpose is not to give the reader a detailed description on how the analytical techniques work but rather on how they are applied in this research.

[1]HNMR spectroscopy:

Nuclear magnetic resonance spectroscopy is one of the most used spectroscopic methods to identify the molecular structure of unknown samples. Depending on the atomic- and mass number, the nuclei of atoms can have a magnetic moment due to their spin. By applying a magnetic field, certain atoms will have magnetic moments which align with the direction of the magnetic field and this results in a split between two different energies and these can be detected. After applying a radiofrequency pulse, the magnetic moment of neighbouring nucleus can influence the resonance frequency of the probed nucleus which results in a split in the detected signal. This is called spin-spin coupling and it enables a qualitative way to analyse the chemical bonding between the atoms in the molecule [28]. In this research [1]HNMR spectroscopy

is used to determine the structure of the acrylate monomers and to see if the RAFT polymerization of these monomers was successful. Appendix A2 shows the ^{1}HNMR spectrum of a 6-amino hexanoic acid acrylate monomer. ^{1}HNMR spectroscopy can be used to label the peaks and identify individual groups on the molecule. The peaks that are most interesting are the ones near 6 ppm. These are from the H-atoms on the acrylate group. During a successful polymerization, these groups react to form the polymer backbone. By comparing the 6-amino hexanoic acid acrylate spectrum with the polymer spectrum it is possible to deduct if the polymerization is successful when the peaks near 6 ppm have disappeared. The integral values below the peaks represent the number of H-atoms creating the signal and they are relative to a reference peak. The peak at 12 ppm is distinctive for the H-atom on the acid group so an integral value of 0.25 corresponds to 1 H-atom. This correlates nicely with the labelled peaks which is also a good indication that 6-aminohexanoic acid acrylate was formed. The unlabelled peak at 3.2 ppm is probably residual H_2O not removed during the polymer workup.

UV-VIS spectroscopy:

UV-VIS spectroscopy uses the property that molecules can adsorb or emit light of various wavelengths. The light used in UV-VIS spectroscopy is in the range of 200-700 nm. Molecules adsorb and emit light with wavelengths which are characteristic for each molecule. The amount of light adsorbed by the molecule correlates linearly with the concentration of the molecule by the Beer-Lambert law (A=e l c). The Beer-Lambert law is a measure for the amount of light that can pass through a sample has a linear relation with respect to the concentration. A limitation of the BL-law is that the turbidity of the medium can be an issue. Only light that passes through the sample is measured but this does not take into account the light that is scattered by the medium. A cloudy emulsion can therefore not be accurately measured because the transmittance of the light through the medium is simply too low. Another limitation is that it works best for very dilute solutions. At high concentration the solute particles can start to interact with the solvent molecules and this can influence the molar extinction coefficient. At very high concentration the solute, in essence, becomes the solvent. The concentration of the solute also influence the refractive index of the medium. This can lead to changes in the path that the light takes through the sample and this can also influence the amount of light that is detected [29]. In this research UV-VIS spectroscopy is used to determine the concentration of polymer in the oil phase after the two-phase partitioning experiment. The polymer concentration is the used to calculate the fraction of polymer in the oil phase at different pH.

Dynamic light scattering (DLS):

Colloidal particles can scatter light in various directions and the intensity of the scattered light can vary depending on the size of the particles. Interference of the scattered light beams can occur due the fact that individual particles can move independently from each other. The particles will now scatter light beams at slightly different moments in time which causes interference that can either be constructive or destructive. The intensity of the light can be used to calculate the correlation function for the colloidal particles. The correlation function can be used to determine the size of the colloidal particles because smaller particles will have a correlation function which decreases faster than larger particles since smaller particles move faster and show less correlation in space and time [30]. DLS is used in this research to determine the size of the lipid membranes.

SEC-HPLC:

Size exclusion chromatography (SEC) is an analytical technique that can be used to separate molecules depending on their size. A mobile phase liquid phase is lead through a tube which is filled with porous material and called the stationary phase. The material from which the stationary phase is made can vary depending on the type of sample that has to be analysed. The sample is dissolved in the mobile phase and pumped through the stationary phase. Small molecules will be able to diffuse into the smallest pores of the stationary phase while this tends to happen less for large molecules. Because of this, large molecules will move through the stationary phase faster than small molecules and this leads to separation. Note that SEC solely separates molecules depending on their size and not on their molecular weight since the diffusion is only limited by the size of the molecule [29]. In this research HPLC was used to determine the size and polydispersity of the different polymers (Appendix B). The measurement failed, probably because the concertation of the polymers was to low and the refractive index change of the polymers in DMF was too

low to be properly detected. The poly(ethylene glycol) standards did end up being detected which supports the claim that the polymer concentration was too low.

Microscopy:

Microscopy was used to image the membrane interaction experiments. Bright field images were taken to examine the size and shape of the lipid membranes. Photons (light) can be used to excite a molecule from the ground state to the excited state. The excited state often has vibrational energy levels close to energy level of the excited state, to which the adsorbed photon can lose some of its energy. The result of this is that when the photon is emitted from the molecule it will have a lower energy then it had when it adsorbed [28]. This is called a red shift or Stokes shift and is quite common in fluorescently active molecules. The Stokes shift can be used in florescence microscopy by filtering out certain wavelengths of light to create an image that only highlights the parts of the sample that emit fluorescent light. The ray diagram shows a schematic representation of the how a fluorescent microscope works (figure 8). The light from the light source first passes through an excitation filter through which only a very narrow range of wavelength can pass. The selected light then reflects on a dichroic mirror, through an objective that focusses the light beam, onto the sample. The transmittance of a dichroic mirror depends on the wavelength of the light [31]. In this case shorter wavelengths get reflected while longer wavelengths can pass through the mirror. The light from the sample passes through the dichroic mirror and past an emission filter. The emitted light will have a larger wavelength than the absorbed light so it is possible to separate this out from the other light by using the emission filter. An ocular or detector can be used to image the emitted light form the sample. A fluorescently labelled polymer was used to investigate the interaction of the polymers with the membranes. The fluorescent dye molecule was Eosin Y and this molecule was chosen because it shows little change in fluorescence intensity over a wide pH range of 4 to 14 [32]. The brightfield images show where the membranes are in solution and the fluorescent images show where the polymer is with respect to the membranes.

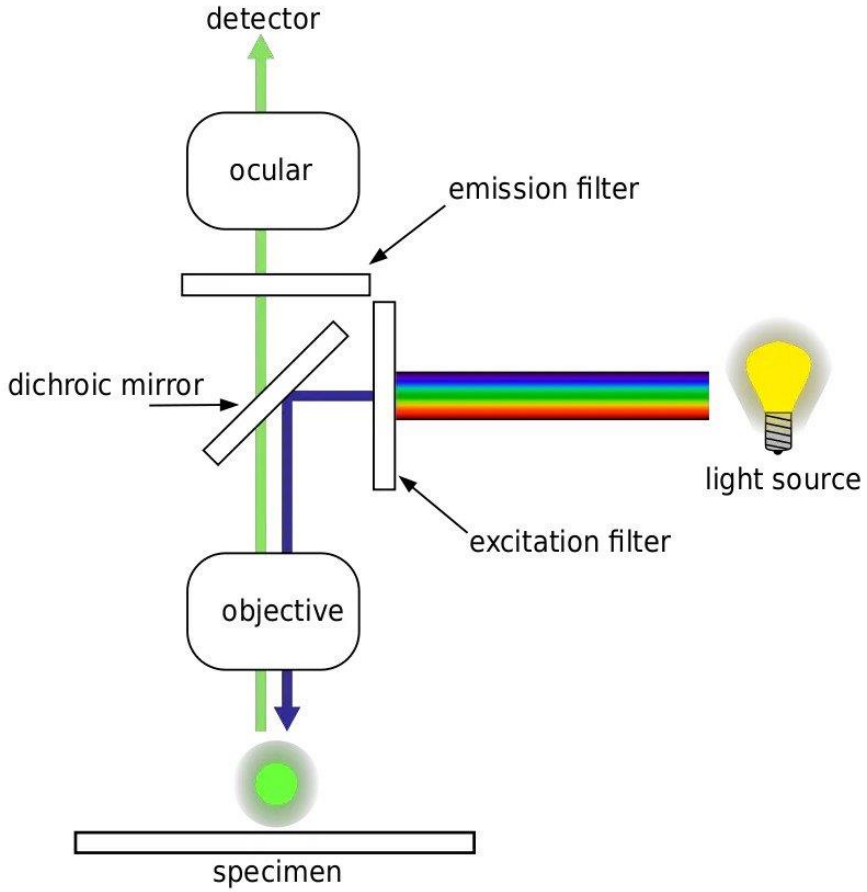

Figure 8: Ray diagram of a fluorescent microscope. Figure taken form www.microbeonline.com. https://microbeonline.com/fluorescence-microscope-principle-types-applications/

3 Experimental method

In this chapter several experimental methods and experiments will be described. The goal is to educate the reader in the different processes and procedures that had to be followed in this research.

3.1 Materials

The materials used in this research can be found in table 1.

Name	Abbreviation	Lot number	Supplier
Magnesium sulfate, anhydrous, 99.5% min	$MgSO_4$	M22H020	ThermoScientific
Acryloyl chloride, ≥97%, contains ~400 ppm phenothiazine as stabilizer	X	STBF0002V	Aldrich Chemistry
Chloroform (stab. /Amylene) HPLC	X	10042411	Biosolve
Diethylether (stab./BHT) AR	X	0010002475	Biosolve
6-AminoHexanoic acid, 99%	X	10230859	ThermoScientific
E-Capralactone, 99%	X	10237308	ThermoFisher
Triethylamine, high purity grade	Et_3N	22A0456103	VWR life science
Hydrochloric acid, pure, fuming, 37% solution in water	HCl	A0408705	Acros Organics
Sodium hydroxide, EMSURE®, ISO, pellets for analysis	NaOH	B0999498 407	Merck
Ethyl acetate	X	0020000239	Biosolve
Ethanol, EMSURE®, ACS, ISO, Reag. Ph Eur, absolute for analysis	EtOH	I1150283 124	Merck
Pentanol, puriss. P.a., ACS reagent, ≥99.0% (GC)	PeOH	BCBW1679	Sigma Aldrich
2,2'-Azobis(2-methylpropionitrile), 98%	AIBN	STBJ8049	
4-CYANO-4-[(ETHYLSULFANYLTHIOCARBONYL)SULFANYL]PENTANOIC ACID	CTA-1	X	Polymer source, inc
N,N-Dimethylformamide, ASC reagent, ≥99.8%	DMF	SZBF1680V	Sigma Aldrich
1,2-dimyristoyl-sn-glycero-3-phosphocholine	DMPC	850345P-1G-D-279	Avanti
Citric acid	X	BCBF5362V	Sigma Life Science
Tri-sodium citrate dihydrate, EMSURE®, ACS, ISO, Reag. Ph Eur, for analysis	X	AM1413148 014	Merck
Fluorescein O-methacrylate, 97%	X	MKBS9672V	Sigma Aldrich
Eosin Y	X	J2822	ChemCruz
Dichloromethane, anhydrous, 99.7%, packaged under argon in resealable ChemSeal bottles, stab. with amylene	DCM	Y16D823	Alfa Aesar
Silica gel, high purity grade (Davisil Grade 633), pore size 60 Å, 200-425 mesh particle size	X	MKBT7657V	Sigma-Aldrich
Tetrahydrofuran, 99.9%, extra pure, anhydrous, stabilized with BHT	THF	A0445811	Thermo scientific
Emsure® ACS, ISO, Reag. Ph Eur, Sodium chloride for analysis	NaCl	K53695504150	Sigma Aldrich
Emsure® Potassium chloride for analysis	KCl	K52100136028	Sigma Aldrich
Emsure® Potassium hydroxide for analysis	KOH	B1020333413	Merck
Dimethylsulfoxid d6 99,8 Atom%D	DMSO	1011302	Roth
Sodium azide reagentPlus®, ≥99.5%	NaN_3	STBJ5435	Sigma Aldrich

3.2 Monomer synthesis

Two types of monomers were synthesized in this research. The monomers could vary in size and hydrophobicity but they had some similarities. All monomers had an acrylate on one side and an acid group on the other side of the monomer. This subchapter describes the different synthesis steps for both monomers.

3.2.1 6-hydroxyhexanoic acid monomer

At the start of the research the goal was set to synthesize a monomer form 6-hydroxyhexanoic acid acrylate which is depicted below. For the synthesis, a paper from *Brodszkij et al.* was used and sometimes slightly adjusted [24]. First 0.1 moles (4 g) of NaOH was dissolved in 15 mL of milliQ water. Then 0.09 moles (9.7 mL) of ε-caprolactone was slowly dripped in over 30 minutes using a (World Precision Instruments, AL-1000) syringe pump (diameter 19.05 mm, flowrate 0.32 mL/min). After all ε-caprolactone was added, the solution was left stirring for 1 hour. The solution was then washed three times with 30 mL of diethyl ether. The organic phase was collected and evaporated under reduced pressure using the rotavap. A white precipitate was formed. 1 M HCl solution was added to the white precipitate until pH 3 was reached (pH checked with Merck, supelco, MQuant®, pH-indicatior strips). The acidic solution was washed twice with 50 mL of chloroform and twice with 50 mL of ethyl acetate. The organic phases were combined and dried using $MgSO_4$. The organic phase was evaporated under reduced pressure using the rotavap and a colourless liquid was formed. The product was dissolved in 175 mL of diethyl ether and 0.04 moles (5.2 mL) of triethyl amine was added. Then 0.05 moles (3.6 mL) of acryloyl chloride was dripped in over 30 minutes using the syringe pump (diameter 11.99, flowrate 0.12 mL/min). The solution was then washed three times with 120 mL of milliQ. The organic phase was collected and dried with $MgSO_4$. The organic solvent was evaporated using the rotavap and a clear, viscous liquid was formed. The ^{1}HNMR- spectrum is depicted in appendix A1 and it shows some inconsistencies. The spectrum shows the 6-hydroxyhexaonic acid acrylate for which it looks like that the integral values match the structure of the molecule. The peak split at the peak at 2.2 and 4.0 ppm however indicates that the molecule could have reacted with itself to from a dimer. This probably happened during the acidification step because the acid catalysed esterification can occur. Several different procedures were tried where for example the acidification time was varied or a lower temperature rotavap evaporation was used but it was deemed too difficult to synthesize a clean 6-hydroxyhexanoic acid monomer. Because of this an alternative synthesis was performed using 6-amiohexanoic acid as a starting material.

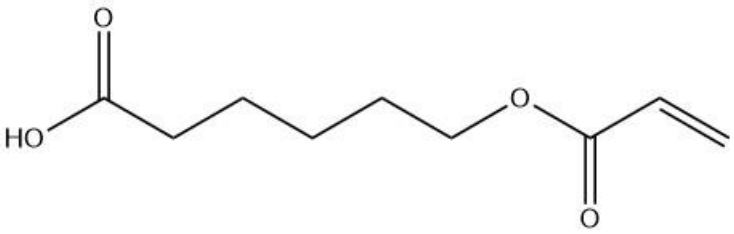

Monomer 1

3.2.2 6-aminohexanoic acid monomer

After several failed attempts at synthesizing monomer 1 an alternative synthesis needed to be found. It was decided to use 6-aminohexanoic acid as a precursor molecule for the synthesizing monomer 2 which is depicted below. The main advantages were that 6-aminohexanoic acid was cheap and that it could be bought in its pure form. This meant the ring opening and acidification step were not necessary anymore and this saved time and made the chemical process a lot more sustainable. The synthesis was based on a paper form *Hetzer et al.* were several different monomers were synthesized [33]. First 0.1 moles (4.5 g) of NaOH and 0.04 moles (5 g) of 6-aminohexanoic acid were dissolved in 30 mL of milliQ water. The mixture was cooled in an ice bath. Then 0.05 moles (3.8 mL) of acryloyl chloride was added dropwise over 30 minutes using a syringe pump (diameter 11.99 mm, flowrate 0.12 mL/min). After adding the acryloyl chloride, the solution was stirred for 2 more hours. A 1:1 mixture of 37% HCl and milliQ water was added

until pH 1 was reached. The white precipitate that formed was dissolved in 40 mL of ethyl acetate. The water phase was washed three times with 30 mL of ethyl acetate. The organic phases were combined and washed with 100 mL of HCl solution with pH 1. The organic phase was dried using $MgSO_4$ and the ethyl acetate was evaporated using the rotavap. A white precipitate formed. This precipitate was then dissolved in 2 mL of absolute ethanol and pipetted into 40 mL cold diethyl ether where a suspension formed. The solution was centrifuged using a Beckman Coulter, Allergra X-12R centrifuge at 2616 g for 10 minutes. The supernatant was discarded and the residue was dried by gently blowing N_2 gas on it. The white powder was analysed and the ^{1}HNMR- spectrum (appendix A2) showed that indeed 6-aminohexanoic acrylate was formed.

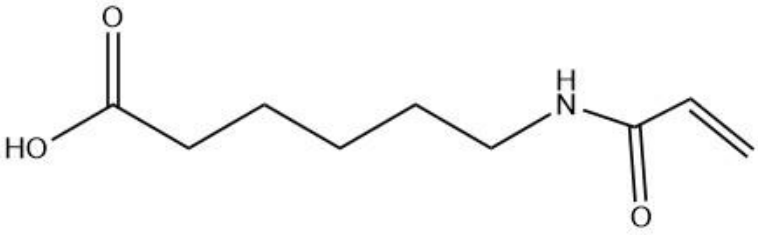

Monomer 2

3.3 Eosin Y- acrylate synthesis

First 0.001 moles (0.64 g) of Eosin Y was weighed and dissolved in 100 mL dry THF. Then 0.0011 moles (0.153 mL) of triethyl amine was added to the mixture. 0.0011 moles (0.089 mL) of acryloyl chloride was dissolved in 4 mL of dry THF and slowly dripped into the solution using the syringe pump. The solution was kept in an ice bath and under stirring for 1 hour. The solution was taken out of the ice bath and then left stirring for another 24 hours. The THF was evaporated using the rotavap. Column chromatography was performed using a silica gel column. The eluent used was a 97:3 mixture of chloroform and acetone. Three fractions were captured of which the first contained the Eosin Y-acrylate which was obtained after evaporating the eluent by gently blowing N_2 gas on it. The product was dissolved in eluent and filtered to avoid any leftover silica gel in the sample. The eluent was then again evaporated by gently blowing N_2 gas on it [34]. The ^{1}HNMR spectrum (appendix A3) shows that there is no peak at 9.8 ppm. This peak comes from the alcohol group present on Eosin Y. During the reaction the alcohol group reacts with the acryloyl chloride to form the Eosin Y- acrylate. The fact that this peak is not present in the spectrum is a good indication that the reaction was successful. Later experiments also showed that it was possible to randomly polymerize the Eosin Y- acrylate with monomer type 2 so this was also a good indication that the reaction was successful.

3.4 Polymer synthesis

The polymer synthesis was based on a paper from *Brodszkij et al.* and was repeated for several different types of polymers [24]. First monomer, AIBN and CTA were be dissolved in DMF in a small vile. Table 2 shows the amount of reactants used in the polymerization reactions. The chain length was dictated by the molar ratios of the reactants that were added. The components added to make the polymer were monomer, AIBN and CTA in molar ratios of X : 0.2 : 1 (with X being the targeted chain length). A fluorescent dye would sometimes also be randomly copolymerized into the polymer. This was done by dissolving 1 molar equivalent of the dye together with the three other reaction components. The solution was then degassed for 1 hour by bubbling N_2 gas through it. The solution was then placed in a preheated oil bath at 75 °C and left overnight under constant stirring. The solution is reprecipitated by pipetting it in cold diethyl ether. A suspension formed which was centrifuged at 2616 g for 10 minutes. The supernatant was discarded and the residue was dried by blowing N_2 gas on it. The residue was dissolved in ±3 mL of absolute ethanol and reprecipitated into cold ethyl acetate. The formed suspension was again centrifuged and the supernatant was discarded. The sample was dried by an N_2 stream and the sample was further dried under vacuum for 1 day. The ^{1}HNMR spectra of the polymers is shown in appendix A4-A9. The polymer spectra differs from the monomer spectra because the 3 peaks near 6 ppm are not present in the polymer spectra. These peaks are from the acrylate group that is present in monomer but this group

reacts during the polymerization. The fact that these peaks were not present in the polymer spectra was a good indication that the polymer synthesis was successful.

Name of polymer	Type of monomer	Amount of monomer (mg)	AIBN (mg)	CTA-1 (mg)	Dye (mg) (molar ratio of dye to monomer is 1:20)	DMF (mL)	Targeted chain length
PAHA-20	Monomer 2	249.66	2.3	19.14	X	1.8	20
PAHA-20-1	Monomer 2	250.30	2.3	18.71	X	1.8	20
PAHA-20-F	Monomer 2	259.39	2.3	18.54	Fluorecein-O-Methacrylate (29.08)	1.8	20
PAHA-40	Monomer 2	243.57	1.118	8.80	X	1.8	40
PAHA-80	Monomer 2	251.06	0.059	5.36	X	1.8	80
PAHA-20-E	Monomer 2	248.82	2.3	18.74	Eosin Y – acrylate (50.08)	1.8	20
PAHA-20-2	Monomer 2	255.29	2.3	19.72	X	1.8	20

3.5 Oil/water interface partitioning experiment

The oil/water interface partitioning experiments were performed in 4 mL glass viles and the two phases were water and 1-pentanol. 1-Pentanol is slightly soluble in water so to avoid volume changes water saturated pentanol and pentanol saturated buffer solutions were uses. The buffer stock solution was made by dissolving 0.13 moles (26.87 g) of citric acid, 0.5 moles (36.55 g) of KCl, 0.001 moles (62.84 mg) of sodium azide and 0.2 moles (17.03 g) of 1-pentanol in 750 mL of milliQ water. The sodium azide was added to avoid bacterial growth that could contaminate the buffers. 10 viles were filled with 25 mL of buffer solution and titrated up to the desired pH with 0.7 M KOH. The polymers were dissolved in water saturated pentanol and the concentrations are listed in table 3.

Type of polymer	mg of polymer	mL of 1-pentanol	Concentration in mg/ml	Type of experiment
PAHA-20-1	6.3	10	0.63	Low ionic strength
PAHA-20-1	9.14	15	0.61	Low ionic strength
PAHA-20-1	9.7	15	0.65	High ionic strength
PAHA-20-1	9.3	15	0.62	High ionic strength
PAHA-20-2	17.44	30	0.58	Effect of polymer length
PAHA-40	27.67	25	1.11	Effect of polymer length
PAHA-80	39.81	23	1.73	Effect of polymer length
PAHA-20-2	18.19	25	0.73	Effect of polymer length (repeats)
PAHA-40	29.21	25	1.17	Effect of polymer length (repeats)

PAHA-80	38.50	25	1.54	Effect of polymer length (repeats)

The 2-phase systems were made by adding 2 mL of buffer and 2 mL of polymer solution to a 4 mL vile. The vile was sealed, shaken and put on the roller bank for ±3 days. After this the pentanol phases was separated and analysed using a BMG labtech Clario Star plus microplate reader UV-VIS machine. An important property of the polymers was that they adsorbed light in the 200-700 nm range. This was possible because during the RAFT polymerization all living chains will end up with the Z-group of the CTA (figure 9) [25]. The Z-group, which was a thiocarbonylthio-group, showed a distinctive broad absorption peak at 308 nm. Because of this it was possible to measure the difference in concentration of the stock solution against the samples taken from the 2-phase experiments and this could be used to calculate the hydrophobic fraction of polymer [35].

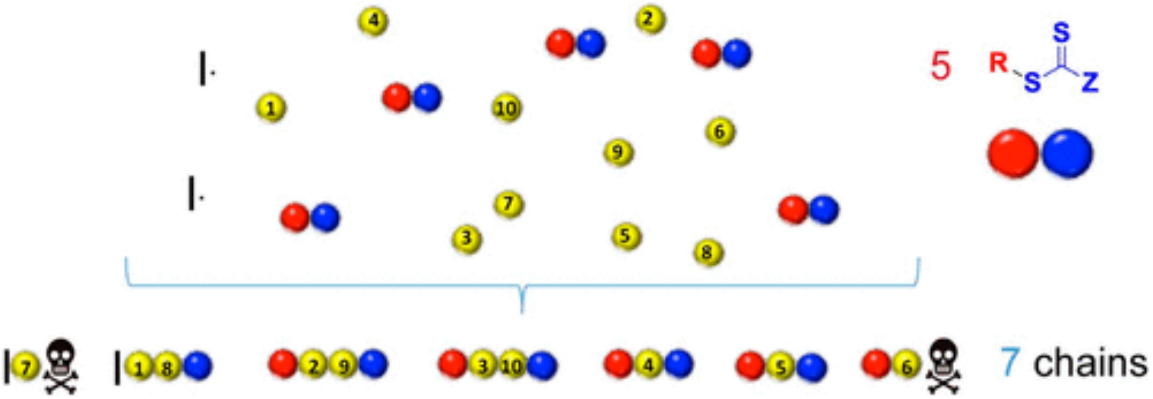

Figure 9: Schematic representation of radical transfer during RAFT polymerization. Note that all living chains will end up with the Z-group of the CTA. Figure taken form [25].

3.6 Lipid membrane synthesis

The lipid membrane synthesis was based on a thesis written by A. Kopf [36] and was sometimes slightly adjusted. First 0.02 millimoles (12.5 mg) of DMPC was dissolved in 2.5 mL of chloroform in a 100 mL flask. This flask was placed in a water bath at 45 °C. N_2 gas was gently blown on the solution and the flask was gently swirled to create a thin lipid film. The lipid film was further dried under vacuum for 1 hour. A citrate buffer was then made by dissolving 0.003 moles (0.59 g) citric acid and 0.0025 moles (0.66 g) tri-sodium citrate dihydrate in 50 mL milliQ water and titrating it with 1 M NaOH until the desired pH was reached. The lipid film was then placed in a water bath at 37 °C and 50 mL of citrate buffer was added to the flask. The flask was swirled until the lipid membranes dissolved in the buffer solution. A white emulsion formed indicating the solubilization of the membranes into the buffer solution. Dynamic Light Scattering (DLS) showed membranes vesicles with a diameter of roughly 5 microns formed when buffer pH 4 or 7 was used.

3.7 Membrane interaction experiment

First 2 mL of membrane solution at pH 7 were added to 4 viles (3 samples and 1 blank). Then 200 µL of polymer stock solution was added to all 3 viles containing buffer and membranes. These solutions were titrated to pH 8 and 11 with 0.7 M KOH and to pH 3 with 1 M HCl. A polymer stock solution was made by dissolving 1.42 mg PAHA-20-E in 4 mL of buffer pH 6.2. A 2mm thick glass capillary was filled with sample and sealed on both sides with clay. The capillaries were analysed using a Nikon TiE microscope in brightfield- and fluorescent mode to see where the polymer moved at different pH values.

4 Results and discussion

The experimental results were obtained by following the methods described in chapter 3. Some experiments deviated slightly from the protocol and this will be indicated.

4.1 pH calibration

The experiments performed in this research depended highly on an accurate measurement of the pH. So, when making the buffers a complication occurred. At first the buffers were made using citric acid, trisodium citrate, sodium hydroxide and sodium chloride. After titrating the buffers to the desired pH, sodium chloride was added to account for the difference in ionic strength of the buffers. Upon adding the NaCl the pH of the solution went down. The effect was also present at high ionic strength where it seemed that the pH became lower and that the change in pH became even larger. This was unusual since the activity coefficient does not change a lot at high ionic strength [29]. An explanation was found when looking into the alkali error. The alkali error occurs at high sodium concentration and low proton concentration. It is hypothesized that sodium ions can interact with the glass membrane of the pH meter, creating a larger potential measured by the meter and this results in a lower measured pH. The effect is mostly present at high pH when the concentration of H^+ is very low [37]. The experiments in this research showed however that also at low pH values of 4-7 at high ionic strength, a shift in pH to lower values was observed when adding salt. This made it hard to tell whether the pH shift came from the change in activity coefficient or from the alkali error. For the 2-phase oil/water experiment it would not be a problem if the pH shift came from a change in activity coefficient since this is in essence also the driving force for the polymer to change phase. An alkali error could be a problem since it would make the determination of the final pH of the solutions harder because it is unknown how the alkali error scales with respect to the sodium concentration.

To test the origin of the pH-shift a titration series was performed. The alkali error could be reduced if potassium salts were used instead of sodium. A possible explanation for this could be that due to the smaller ionic radius of potassium it interacts less with the glass membrane of the electrode. A diluted pH 2.5 HCl solution was made with a 700 mM KCl concentration. This solution was titrated with 700 mM KOH solution. By keeping the potassium concentration constant, the alkali error should stay constant and it was possible to make a pH calibration curve (figure 10).

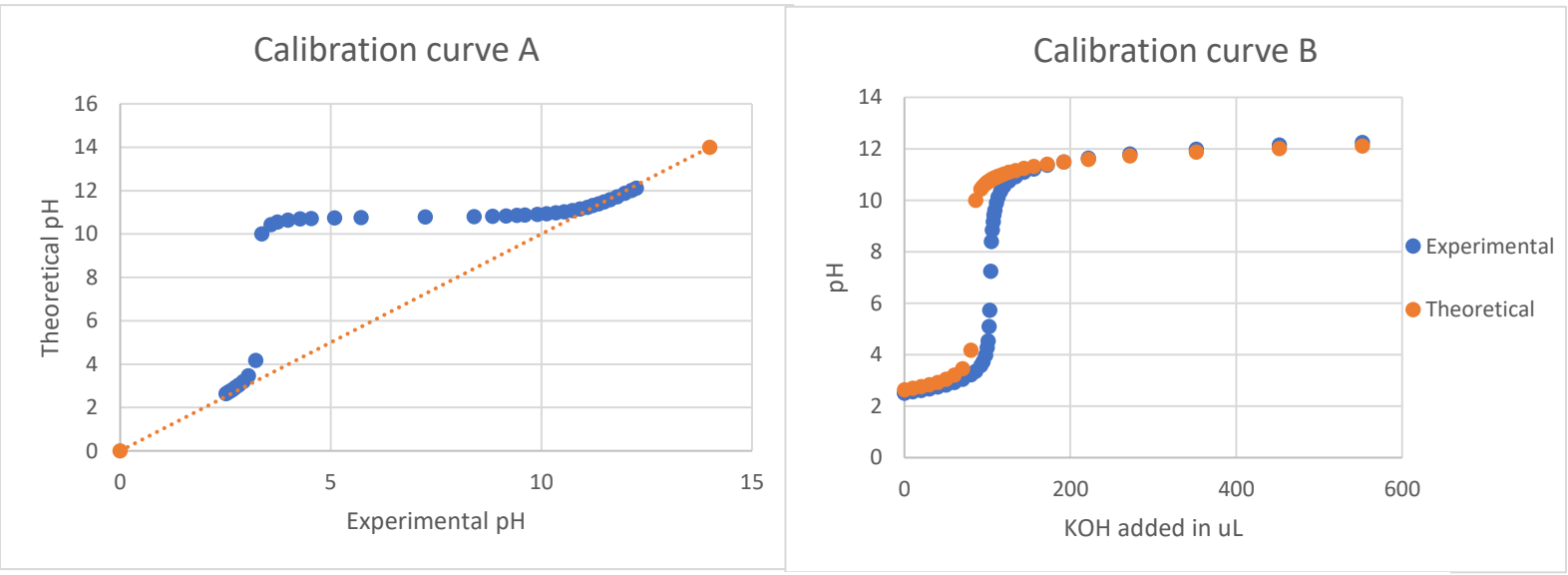

Figure 10: Right: experimental vs theoretical pH of the calibration experiment. The sharp deviation from the theoretical pH is due to titration inaccuracies. Left) Display of how the experimental and theoretical amount of KOH added is influenced by a constant offset.

Figure 10a illustrates the difficulties when accurately measuring the pH using titration. The method is very prone to titration errors and it is very easy to over- or underestimate the amount of base that is

added. The KOH was added by a small plastic tube that was inside the solution using a syringe pump. Inaccuracies in the amount of KOH added could occur due to syringe pump inaccuracies or via diffusion of KOH from the tube into the solution.

Figure 10a does show that experimental and theoretical match with the theoretical values for pH 2-3.5 and 10-12. This is because the H+ or OH- concentration is higher here. The figure also shows that the experimental pH is lower than the theoretical pH. This is expected at high pH where the alkali error is biggest but the experiment shows that it also occurs at low pH. Figure 10b shows that the theoretical and experimental titration curve have a similar shape but with a small offset. This seems to indicate that the alkali error stays mostly constant during the measurement since the potassium concentration also stays constant. This was a good result since for the 2-phase system we are mostly interested in the pH range in which the transition occurs (sharpness of transition). A constant pH offset will not influence this because it is, in theory, equal for all different buffer solution so the sharpness would not be influenced. The potassium error could be a problem when looking at the pH at which the polymer interacts with membranes since calibration will be necessary in order to calculate an accurate absolute value for the pH. The focus of this research was mostly on the 2-phase experiment so due to some time constraints it was chosen to not further investigate the alkali error. The decision was made to use potassium over sodium when making the buffers and also to measure at high potassium concentration since this seemed to minimize pH shifts between individual buffers. Measuring at high ionic strength is also advantageous because it minimizes Columbic interactions which can influence the sharpness of the transition.

4.2 Determination of the length of the polymers

One of the main goals of this research was to determine the influence of the length of the polymers on the sharpness of the transition. In order to properly investigate this, three polymers were synthesized from monomer 2, with targeted chain lengths of 20, 40 and 80 monomer units. The first method that was tried to measure length of the polymers was SEC-HPLC. This method could give an indication of the polydispersity of the polymer samples and give a rough estimate of the length of the polymers. This could be done by comparing the retention times to the poly (ethylene glycol) (PEG) standard red, yellow and green (appendix B6-B8). The SEC-HPLC measurements did not give good results probably due to the fact that the concentration of polymer in the samples was too low. This resulted in a very small change in refractive index in the DMF solvent when the polymer passed by the detector. Due to time constraints it was not possible to redo the measurement. Another method that was considered to perform was matrix assisted laser desorption ionisation (MALDI) but again due to time constraints it was not possible to perform this method.

A new method needed to be found to calculate the chain length of the polymers. The thiocarbonylthio-group on the CTA showed a distinctive absorption peak at 308 nm. Since each ''living'' chain would have a thiocarbonylthio-group at the end of its chain, it was possible to calculate the chain length by directly measuring the absorbance of the CTA. Using Beer Lambert's law, it is possible to calculate the absorbance of a single CTA molecule. This can be used to calculate the amount of chains and together with the mass of the polymer it was possible to calculate the average chain length. The absorbance from the peaks at 308 nm (Appendix C1) were taken and presented in table 4.

Polymer	Absorbance at 308 nm (blank corrected)	Concentration CTA (mg/mg pentanol)	Mole CTA in each sample	Moles of monomer	Estimate chain length
CTA	2.402138	6.03366E-05	7.60456E-07	X	X
PAHA-20-1	2.284496	5.73817E-05	3.49923E-07	9.22226E-06	26.3551
PAHA-40	0.715515	1.79722E-05	1.11497E-07	5.45847E-06	48.95602
PAHA-80	0.611687	1.53643E-05	9.49739E-08	8.73548E-06	91.97774
PAHA-20-E	2.751014	6.90996E-05	4.29032E-07	7.70008E-06	17.94756
CTA (on plate reader)	1.904	6.03366E-05	7.60456E-07	X	X

PAHA-20-2 (on plate reader)	1.4905	4.7233E-05	2.89786E-07	5.91981E-06	20.42819

The concentration of CTA in each vile was calculated by taking the fraction of the absorbance at 308 nm and multiplying this by the concentration of CTA in the reference vile. The amount of moles CTA could now be calculated by multiplying the concentration by the volume of the viles and dividing this by the molecular weight of CTA. The livingness of the polymer was estimated to be 83%, so this meant that only 83% of the polymers would have CTA on it. By dividing moles CTA by 0.83, the number of chains could be calculated. It was now possible to calculated the number of moles of monomer present in the sample by taking the weight of polymer, subtracting the weight of CTA and dividing this by the molecular weight of the monomer. By dividing the moles of monomer by the moles of CTA an estimate chain length could be calculated.

The chain lengths are close to the target lengths of 20, 40 and 80. The most important thing is that the ratio is roughly 1:2:4 which was the goal in order to investigate the effect of chain length on the sharpness of the transition. This method however is very limited because if unreacted CTA is present in the polymer sample this would influence the estimated chain length by making it appear shorter than it is. This method gives no information about the PDI of the polymer but simply gives an average chain length. The argument could be made that by taking the livingness of the polymer it could account for the chains which are terminated early but there is still a very high change that there are chains present the are shorter or longer. This is unfortunately the only way for now to estimate the average chain length for the polymers. In the future it would be highly beneficial to perform new SEC-HPLC measurement in THF and with higher concentrations of polymer. New insights into the length of the polymer could also be gained by performing MALDI mass spectrometry.

4.3 Effects of polymer length on the sharpness of the transition

The sharpness of the transition of the pH dependent partitioning in a pentanol-water system was examined. This was done by dissolving polymer in pentanol and adding this to different buffer solutions.

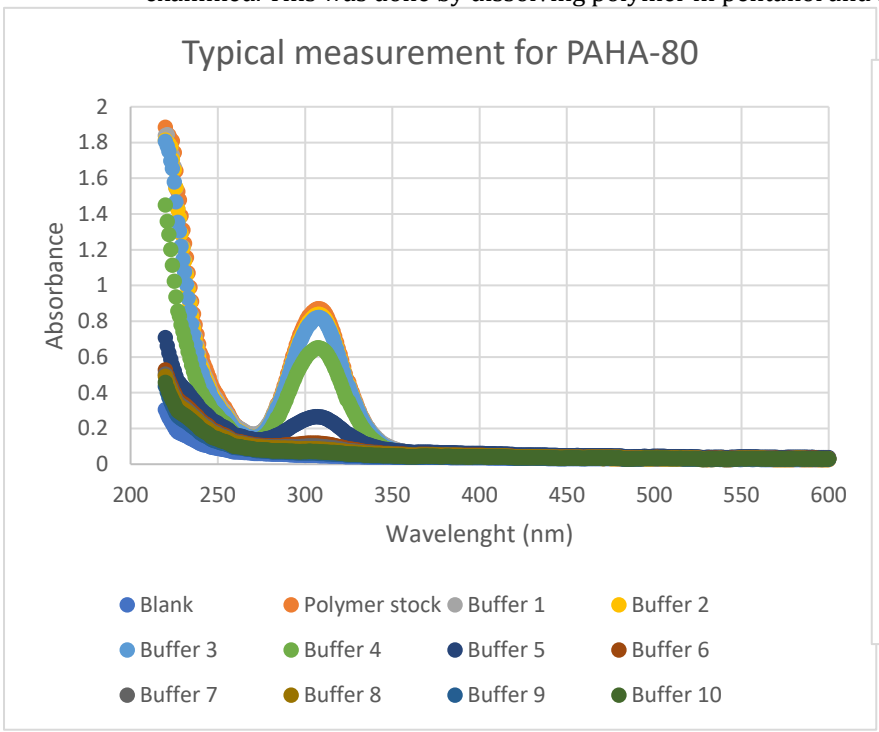

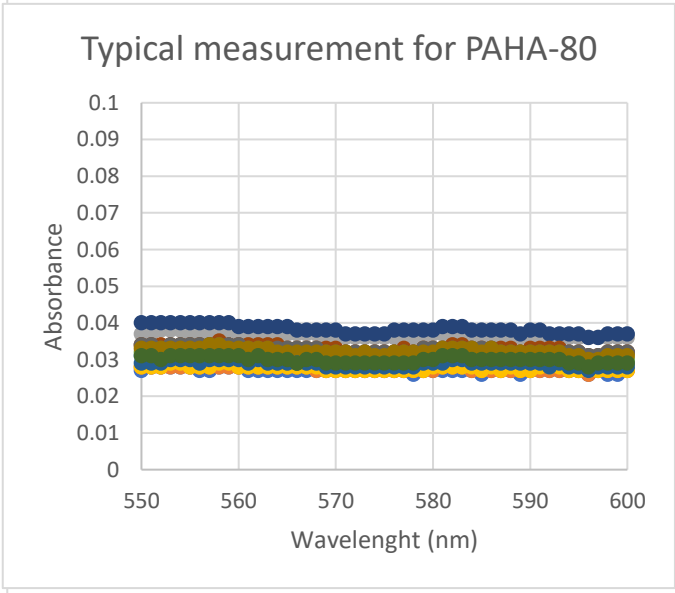

Figure 11: typical UV-VIS measurement. Note that the peak at 308 nm is distinctive for the thiocarbonylthio-group at the end of the chain.

The UV-VIS spectrum was measured with a BMG labtech Clario Star plus microplate reader and a typical measurement is figure 11.

The right graph shows that the baselines of all the measurement series are slightly elevated above 0. The peak at 308 nm is distinctive for the polymer so in order to accurately measure the fraction of polymer a baseline correction is performed. The average value for the baseline between 550-600 nm is subtracted from all values for every single measurement. The peak at 215 nm is contributed to the UV- cut off of the 1-pentanol solvent (Appendix E7).

It was now possible to measure the fraction of polymer by dividing the absorbance at 308 of the sample by the absorbance of the stock. These datapoints were the fitted using Eq. 36 in order to calculate the values for M and g_H. This was plotted against the pH of the buffer measured at the end of the experiment. After a pH measurement, the standard buffer solutions were remeasured in order to see if the pH had drifted during the pH measurement. To account for this, calibration curves were made by taking the pH values of standard buffers at the end of the measurement and plotting them against the actual pH values (Appendix E2-E6). The effect of applying the pH correction is depicted below in figure 12.

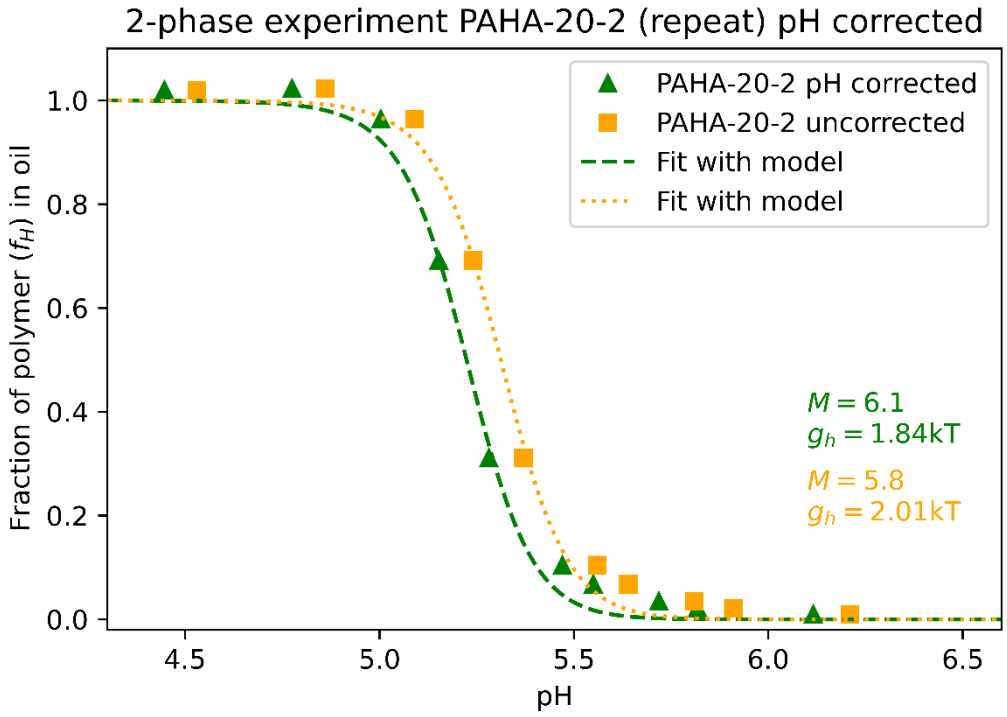

Figure 12: 2-phase experiment of PAHA-20-2 (repeat) where only one series of pH points is corrected.

The pH correction mostly influence the value for g_H. This is because a very simple, linear correction curve is used which mostly lowers the values for the pH. By doing this the pH can me more accurately and evenly measured and this will correct for pH drifts during the different measurements.

After applying a blank, baseline and pH correction, the results for the 2-phase experiments are depicted in figure 13.

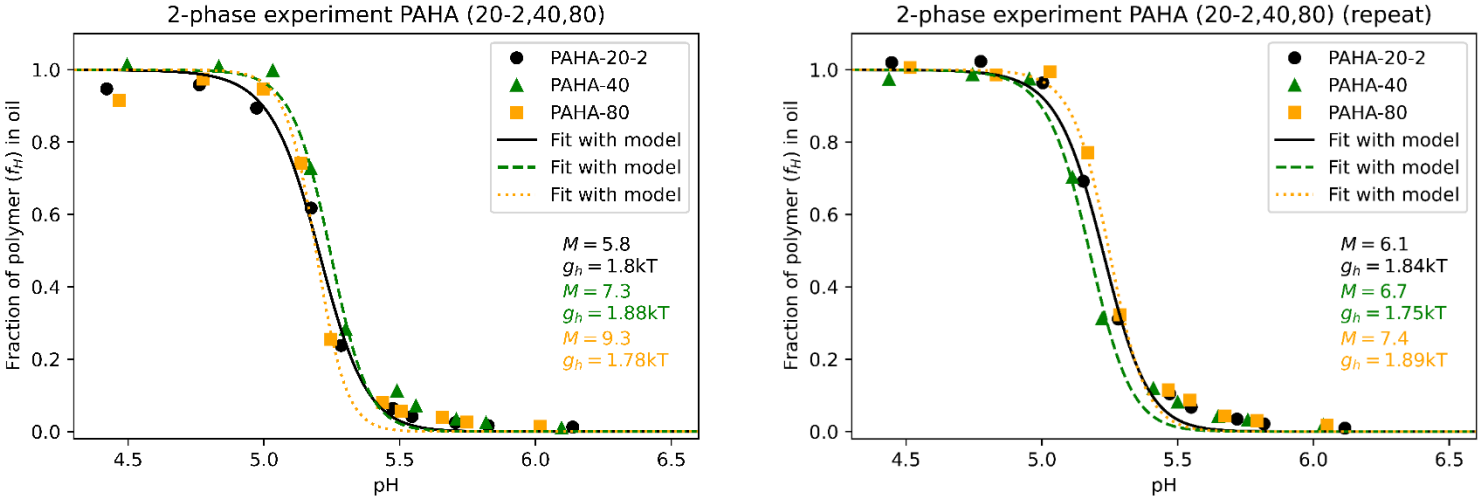

Figure 13: Results of the 2-phase experiments for PAHA 20-2, 40 and 80.

Figure 13 shows that the polymers all display cooperative behaviour and the transitions are quite sharp. The first and the repeat measurement show a clear trend in that the value of M increases with increasing polymer length. This follows the theoretical model because a longer polymer will have a more ionizable sites and will display more cooperative behaviour. The value of the experimental M increases with respect to the length of the polymer in both experiments (figure 14). The correlation coefficients for both measurements are both close to 1 which seems to indicate that there is a linear relationship.

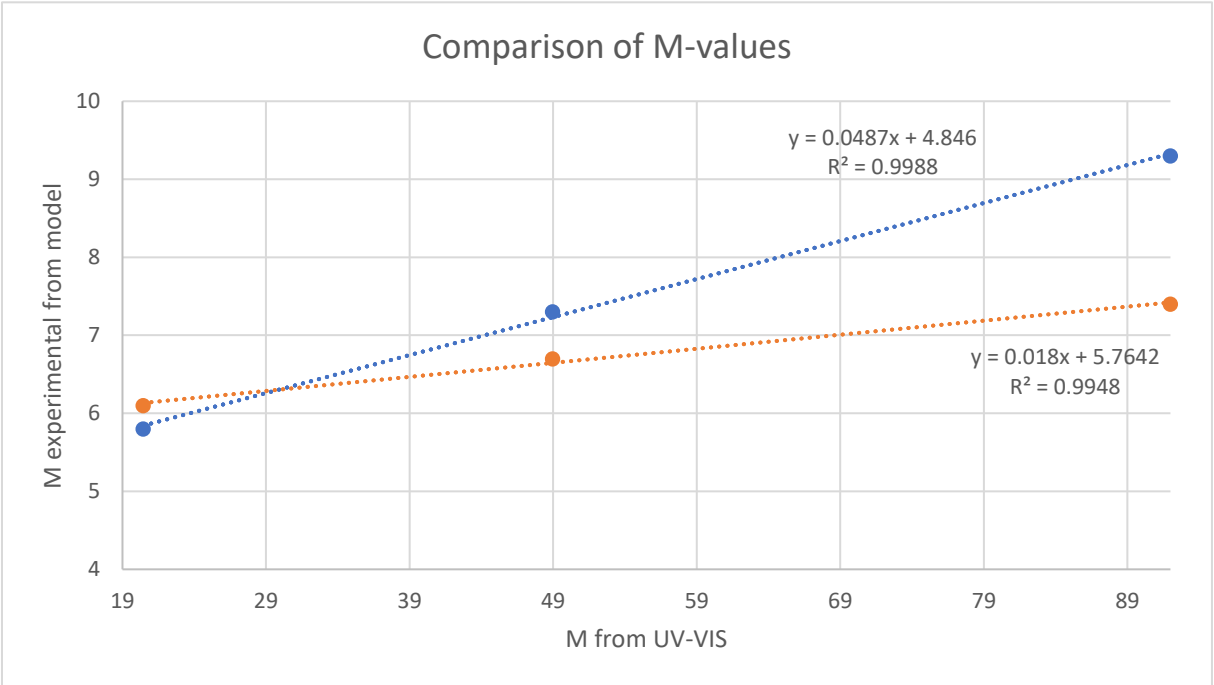

Figure 14: Comparison of the M value calculated by UV-VIS with the experimental M-value. Note that the blue line corresponds with the first measurement and the orange line with the repeat measurement.

The results of the 2-phase experiments show that even short polymers (PAHA-20) can display cooperative behaviour with sharp transitions. The increase in sharpness with increasing polymer length was accurately predicted by the theoretical model and figure 14 shows that the relationship between the two seems to be linear.

There is a difference in the sharpness of transition between the two measurements. This is due to inaccuracies in the pH meter. The pH meter has an error of roughly 0.1 pH unit which can make an accurate determination of the pH very hard. This has consequences for the determination of M, since a difference between M=6 and M=9 falls in the window of error and this explains the mismatch in M values between the measurements. Insights could be gained by synthesizing polymers with 5 or 10 monomer units to see if the linear relationship is still present. Shorter polymers will have a broader transition and this would make it easier to measure them and show the trend in increasing M value with increasing polymer length. It will also help to confirm or deny the linear increase in experimental M that is observed in figure 14. More datapoints will help to see if this linearity still holds.

4.4 Effects on the transition pH

The model predicts that the transition pH is dependent on the ratio between hydrophobic and hydrophilic monomer units (Eq. 38). For PAHA the hydrophobic and hydrophilic parts of the monomer are on the same unit so the $\frac{M_H}{M}$ – ratio is 1. This changes Eq. 38 into:

$$pH_{trans} = pK_a + 0.4343\,\frac{g_H}{kT} \qquad (44)$$

Eq. 44 shows that the transition point is only dependent on the hydrophobic penalty of each individual monomer unit. This is the same for PAHA 20-2, 40 and 80 so the model predicts that these three polymers would have the same transition pH. The transition pH values for the polymers are calculated from figure 13 by taking the values for M and g_H and solving Eq. 36 when it is 0.5.

Polymer	pH_{trans} first measurement	pH_{trans} repeat measurement
PAHA-20-2	5.203	5.224
PAHA-40	5.245	5.177
PAHA-80	5.193	5.250

The table above shows that the transition pH is very similar for each polymer and it is roughly 5.2. The value for g_H is scaled for each polymer by dividing the total conformational energy penalty (G_H) by the experimental value for M. By doing this it is possible to compare the different conformational energy penalties of the individual monomer units between the three polymers. Figure 13 shows that the value for g_H is also very similar for all 6 measurements. This supports the theory of the model that the transition pH of the three PAHA polymers should be the same, since the $\frac{M_H}{M}$ – ratio is 1. The differences in transition pH lay well within the margin of error so this seems to confirm the model. The limitations of the pH accuracy between runs can explain the small differences in transition pH between runs and between the different polymers.

The calculated values for g_H in figure 13 can also be used to calculate the transition pH for all three polymers by using Eq. 44.

Polymer	pH_{trans} first measurement	pH_{trans} repeat measurement
PAHA-20-2	5.282	5.300
PAHA-40	5.316	5.260
PAHA-80	5.273	5.320

The values for the transition pH calculated by Eq. 44 deviate slightly from the actual values obtained from figure 13. This is due to the fact that the assumption is made in Eq .38 that $(1 + 10^x) \approx 10^x$, which is only valid for when the pH_{trans}-pKa > 1. The pKa for the acid groups is estimated to be 4.5 [38] and this is not far below the value of the transition pH. The values calculated by Eq. 44 are still close to the values taken from figure 13 so this again supports the theory that the transition pH is dependent on the hydrophobic energy penalty of the individual monomer units and not of the entire polymer.

4.5 Effects of ionic strength

As mentioned in chapter 2.4, it is expected that the ionic strength can have an influence on the sharpness of the transition. The model predicted that intermediate states can cause transition broadening since the intermediate states will have different conformational energy penalties. The statistical weight of the intermediate states has to be added to the GPF. The experimentally observed hydrophobic fraction of polymer can now also contain a fraction of the intermediate states because they move to the aqueous phase at slightly different pH. This gives rise to transition broadening because it now appears that the polymer moves to the aqueous phase over a wider pH range.

The transition in a 2-phase pentanol/water system was examined at 70 mM, 270 mM and 700 mM ionic strength (figure 15).

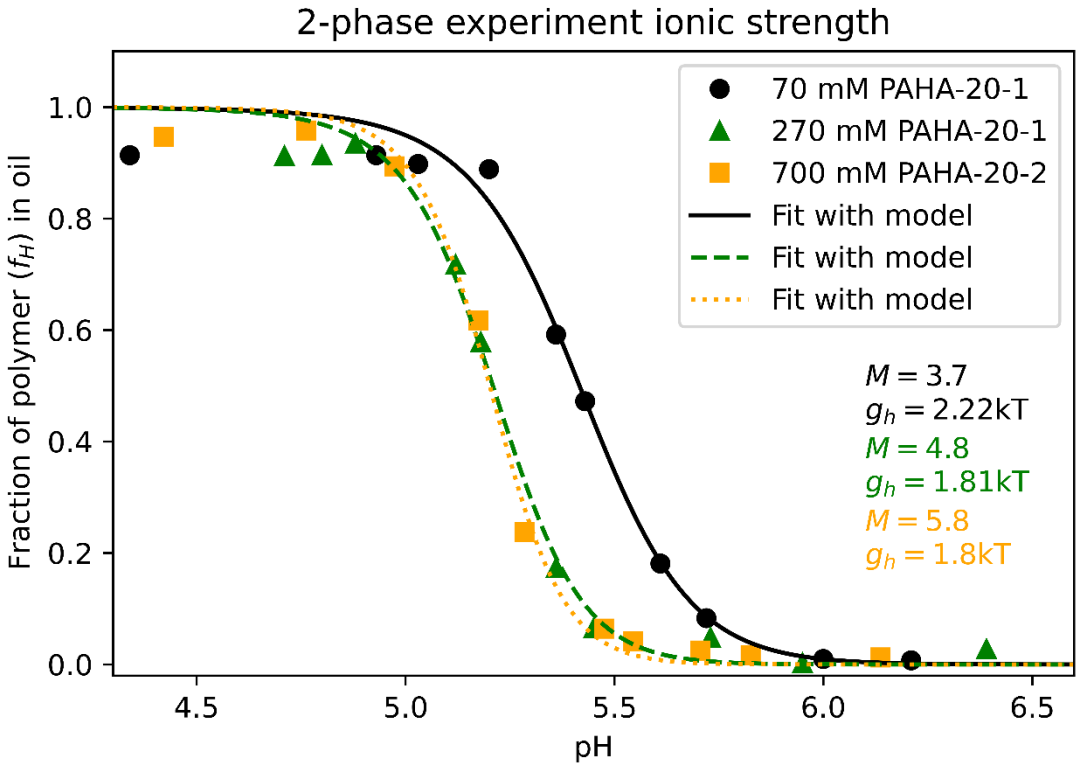

Figure 15: 2-Phase experiment for PAHA-20-1 at 70 mM, 270 mM and 700 mM ionic strength. Note that the 700 mM data was taken from the first 2-phase experiment in figure 13.

It is good to point out that the measurements at 70- and 270 mM ionic strength, were performed before the sodium complications were discovered so the buffers were still made with sodium. These experiments were measured with the UV-VIS machine and not the plate reader. Also, the initial pH of the buffer solutions is plotted and not the pH after the experiment. The results of the experiment are nonetheless still very interesting. The graph shows that the transition gets broader when the ionic strength decreases. This is due to the fact that at low ionic strength, the Debye screening length increases. The result of this is that the charged acid groups will experience more Coulombic repulsion between neighbouring groups. This can lead to a split in the pKa values of different acid groups on the polymer. A split in pKa values also creates a split in conformational energy penalty of the polymer and this results in more intermediate state and transition broadening. The PAHA-20-2 polymer in figure 15 was measured at 700 mM ionic strength (potassium buffer) and it seems to follow the trend that the transition gets sharper with increasing ionic strength. It is however, hard to compare the two experiments with each other since different buffers (sodium vs potassium) and polymers were used which could all influence the transition.

Another interesting observation is that the transition pH becomes lower when the ionic strength increases. At 70 mM ionic strength the transition pH is 5.414 and at 270 mM it is 5.208. This probably because at higher ionic strength it becomes less unfavourable to move to the aqueous phase since the

charges are more screened. This lowers the hydrophobic conformational energy penalty (g_H) and this results in a lower transition pH at high ionic strength. The transition point at 270 mM is very similar to the ones at 700 mM for PAHA-20-2. The Debye length decreases with the square root of the ionic strength so it could be the case that at a certain ionic strength the Debye length becomes so small that it does not influences the transition pH anymore. Repeat experiments need to be performed in order to accurately measure this.

The data points in figure 15 show that the highest fraction of PAHA-20-1 is only about 0.9. This is because in these experiments no water saturated pentanol and pentanol saturated buffer were used. The importance of the equal volumes became known later and that is why the highest fractions in figure 13 are 1. It also has to do with the fact that the absorbance of the polymer changes slightly when it is in water saturated pentanol. This influences the value of f_H because for the PAHA-20-1 experiments the polymer stock was not saturated with water.

4.6 Membrane interaction experiments

The membrane interaction experiments were inspired by research performed by Brodszkij et al. where 6-hydroxy hexanoic acid acrylate polymers interacted with giant unilamellar vesicles (GUV). The GUVs were made from 1,2-dioleoyl-sn-glycero-3-phosphocholine (DOPC) and 1,2-dimyristoyl-sn-glycero-3-phosphoethanolamine-N-(lissamine rhodamine B sulfonyl) lipids (PE-Rh). The study showed that the polymers were able to move into the membrane when the pH was below the transition point (pH 5). When the pH was then increased it was even possible for the polymers to permeate the membranes and move into the GUV. The data was analysed by taking confocal laser scanning microscopy (CLSM) images and performing a line scan to highlight the difference in contrast between the membranes and background [39]. The model predicts that at low pH, the polymer would move from the aqueous phase to the hydrophobic phase in and around the membranes. This is because at low pH there is too little favourable adsorption energy from the solution available to overcome the hydrophobic energy penalty of the polymer. The result of this is that the polymer tries to find other ways to minimize the hydrophobic energy penalty and does this by migrating into the hydrophobic reservoirs in and around the membranes. At high pH there is more favourable adsorption energy available (more OH^-) so the polymer will stay more in the aqueous phase.

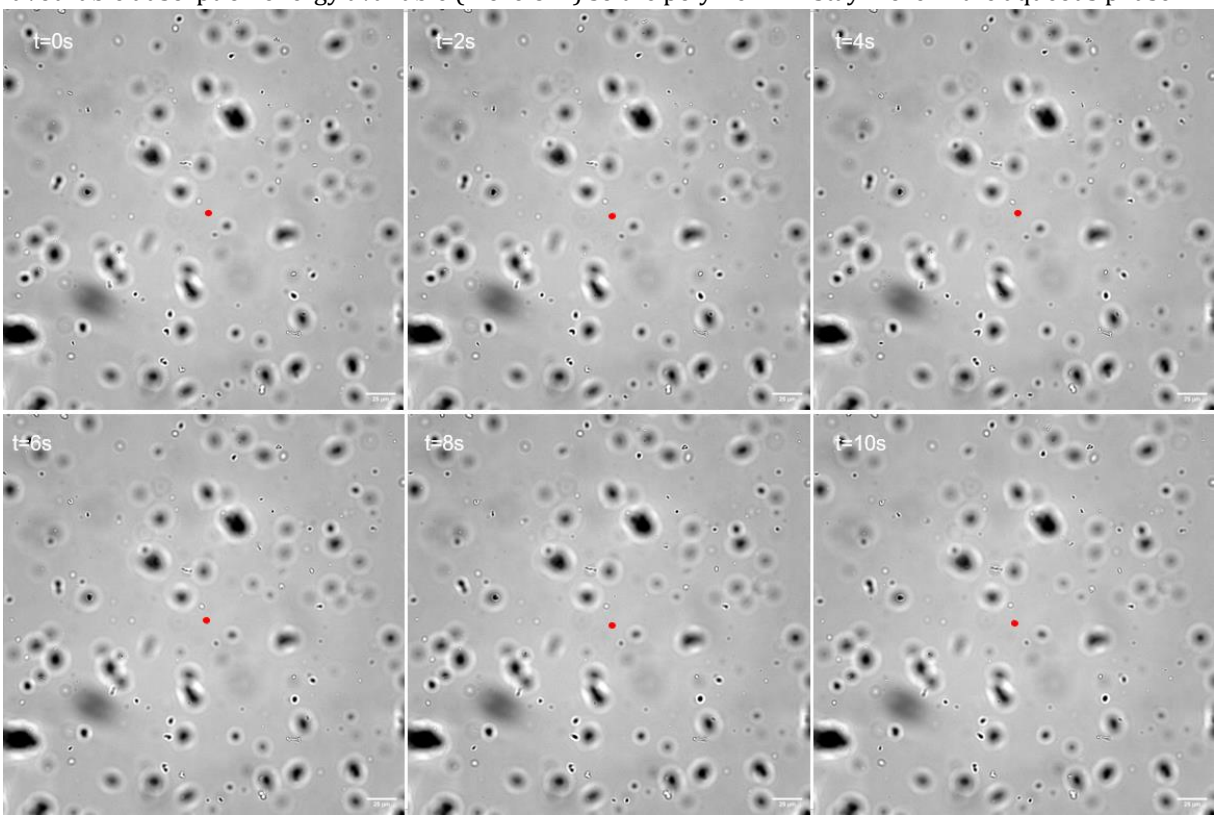

Figure 16: Bright field image of the membranes at pH 11. 10 second overview to illustrate how the membranes move through the solution.

The difference between the membrane interaction experiments in this research and the Brodszkij research is that in this research membrane vesicles with a size of roughly 5 microns were used and in the Brodszkij research they were around 50 microns. In this research the membranes were also not fluorescently labelled so it was not possible to fluorescently image the membranes by themselves. A Nikon TiE microscope with a 40x objective was used to take brightfield and fluorescent images. Figure 16 shows that when imaging the middle of the capillary, the membrane vesicles diffuse freely in solution. This was a clear indication that the membranes were actually formed (figure 16).

PAHA-20-E was added to membranes at pH 3, 8 and 11 and fluorescent images were taken. This was possible due to the fact that Eosin Y shows a distinctive emission peak at 540 nm. The goal of this experiment was to see how the polymers would interact with membranes and if a change in pH would result in a migration of the polymer from the aqueous solution into the membranes. It was expected that at low pH the polymer would move in and around the membranes because it would want to minimize its hydrophobic interaction with the solvent. This would result in a higher contrast between the membrane and the background. At high pH values the polymer would likely be more present in the solvent because the charges would prevent the polymer from moving into the membrane and this would result in a smaller contrast between the membrane and the background. Appendix D4 shows that the membranes without polymer do not show any fluorescent signal so the signal only comes from localized polymer.

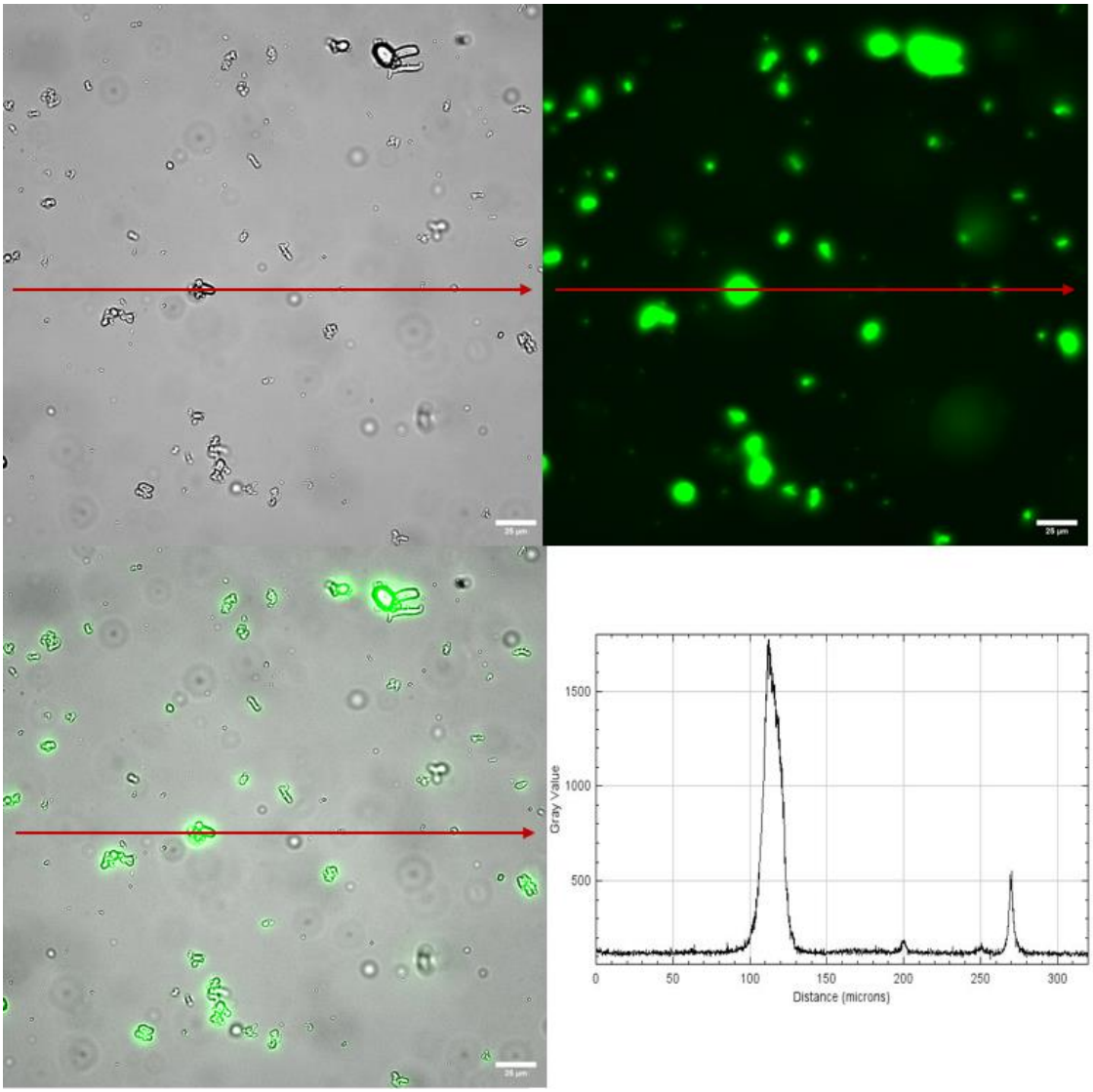

Figure 17: Membranes + PAHA-20-E at pH 3. Top left) Brightfield image. Top right) Fluorescent image. Bottom left) Overlap of BF and fluorescent image. Bottom right) Line scant taken from the fluorescent image on the red arrow . Scalebar 25 microns.

A complication occurred when fluorescently imaging the free membranes in the middle of the solution. Because of the movement of the membranes they seemed to move in and out of focus which resulted in a very weak fluorescent signal. The background was often also dominated by signal coming from larger clumps of membranes which were stuck to the glass. This is depicted appendix D1-D3, where the line scan shows that the contrast between background and moving membrane is very low. Because of this it was chosen to image the membranes which were stuck to the inside of the glass. These membranes did not move anymore and this resulted in far more clear images. The images of the three different pH solutions are depicted in figure 17, 18 and 19.

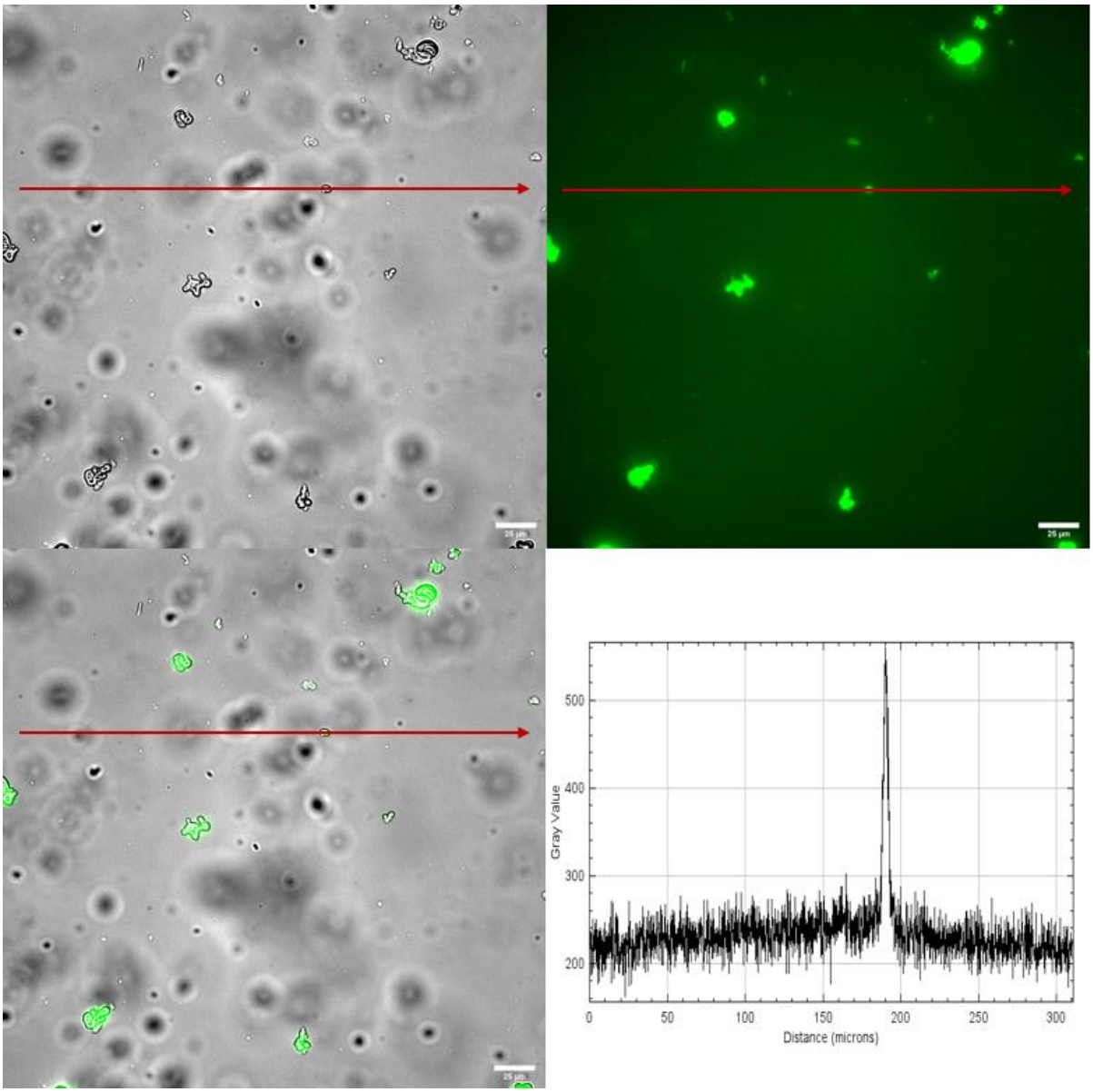

Figure 18: Membranes + PAHA-20-E at pH 8. Top left) Brightfield image. Top right) Fluorescent image. Bottom left) Overlap of BF and fluorescent image. Bottom right) Line scant taken from the fluorescent image on the red arrow . Scalebar 25 microns.

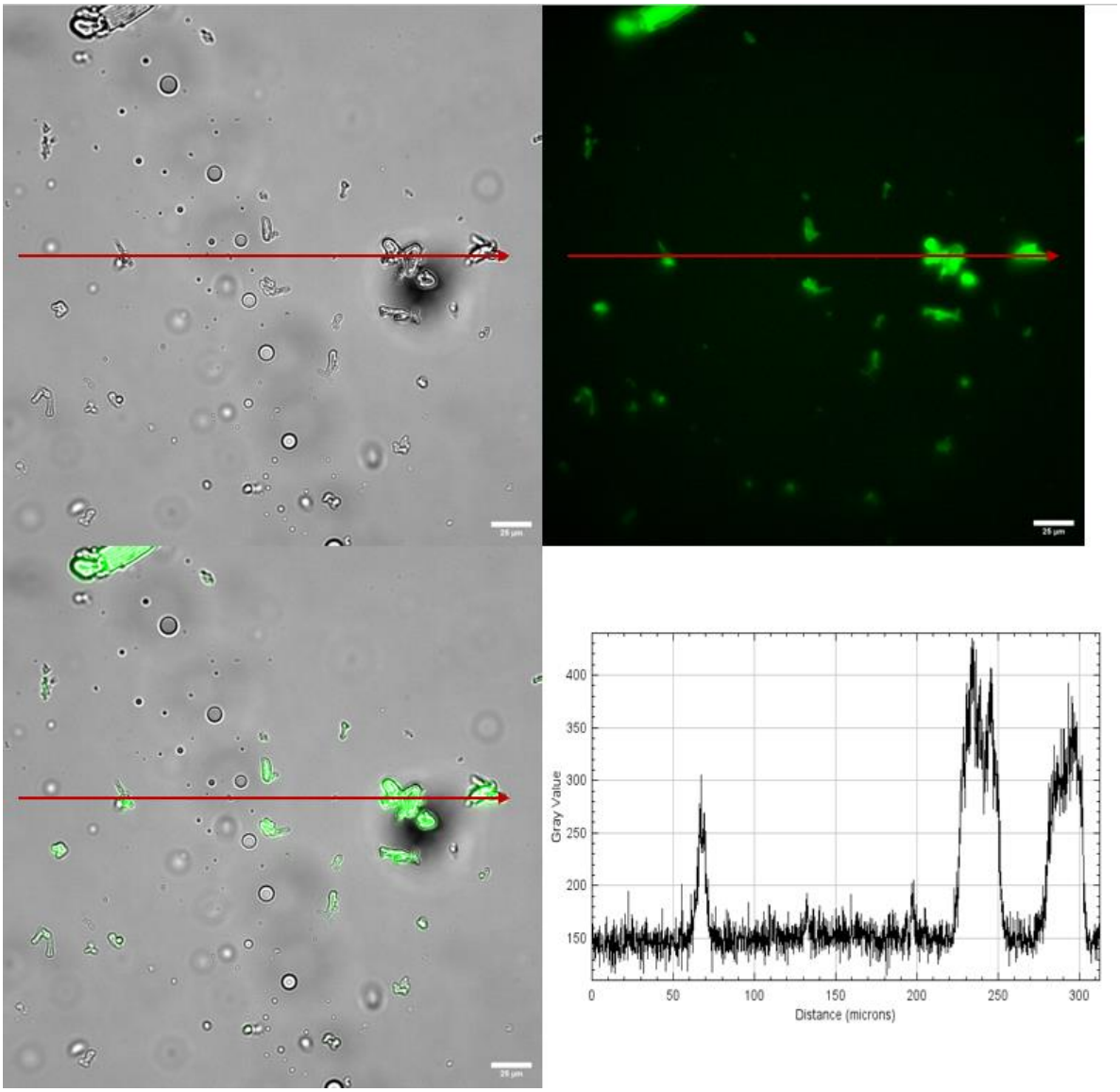

Figure 19: Membranes + PAHA-20-E at pH 11. Top left) Brightfield image. Top right) Fluorescent image. Bottom left) Overlap of BF and fluorescent image. Bottom right) Line scant taken from the fluorescent image on the red arrow . Scalebar 25 microns. Note that the round bright spots in the middle of the image are contamination on the glass since they appear in a line and do not show any fluorescent signal.

The first important observation is the fact that the polymer did not solubilize the membranes. This was also confirmed when looking at the membrane solution by eye (appendix E1). For Poly 6-aminohexanoinc acid (PAHA), the hydrophobic and hydrophilic group are on the same monomer unit. A polymer like SMA has the hydrophobic and hydrophilic group on different monomer units and due to the flexible backbone of the polymer it can twist the groups depending on which orientation is most favourable. This makes SMA more surface active then PAHA and this could explain why SMA can solubilize membranes and PAHA cannot.

The overlap images of figure 17, 18 and 19 all seem to indicate that the polymer migrates in and around the membranes at a pH range between 3-11. This was expected at low pH but was a bit surprising at high pH since the acid groups will be charged at pH 7 and 11 and interaction with the membrane is unfavourable then. The acid group is connected to the backbone by 6 carbon atoms. This can be a possible explanation as to why even at high pH the polymer is still localized mostly in and around the membranes. It is possible that at high pH, due to the large sidechain length, the polymer can partly insert into the membrane bilayer and stick its acid groups outside into the solution. The large side chain could help keep the charges apart for each other and this would minimize unfavourable Coulombic repulsion.

The line scan graphs show that the biggest contrast between membrane and solution is present at pH 3. It is hard to pinpoint exactly how much brighter the membranes appear in comparison to the background. In each image one of the brightest membrane spots was taken and the difference in grey values between the background and the membranes is clearly the highest at pH 3. At pH 3 the acid groups will be protonated so it will be highly unfavourable for the polymer to stay in solution so it will move in and around the membranes to minimize the hydrophobic interaction with the solvent. At pH 7 and 11 the acid groups are deprotonated so the polymer will likely be more localized in the solution. To test this further, it was decided to measure the fluorescence of the solution using fluorescent spectroscopy. The membranes were centrifuged at 2616 g for 10 minutes and the fluorescence of the supernatant was measured (figure 20).

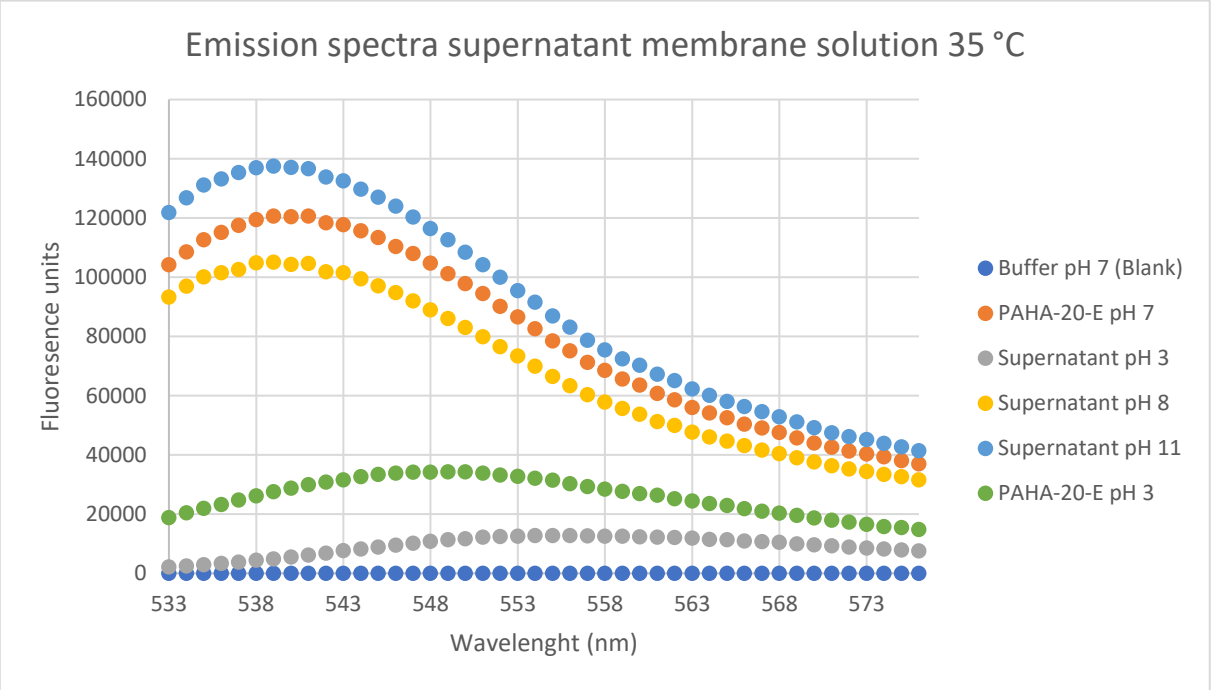

Figure 20: Emission spectra of the supernatant taken after centrifuging the membrane solutions. The spectra show that the fluorescence intensity of Eosin Y greatly diminishes at pH 3. Excitation wavelength was 508 nm ±5nm.

At first glance it seemed that the fluorescence of the supernatant decreased from pH 11 to pH 3 and this corresponded with the line scans, which showed that the contrast between membranes and solution was highest at pH 3. The spectrum shows that the fluorescence intensity of PAHA-20-E greatly diminishes at pH 3. This was an indication that the decrease in fluorescent intensity at pH 3 also occurs when no membranes are present in the sample and this is explained by figure 21.

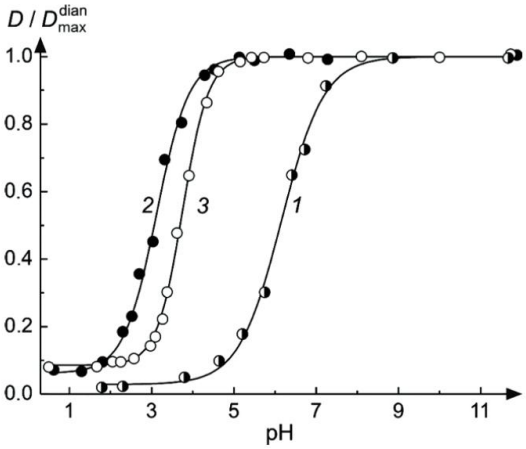

Figure 21: Fluorescence yield of fluorescein (1), Eosin Y (2) and erythrosin B (3). Normalized by the maximum of the absorbance spectrum. Figure taken from [32].

Figure 21 shows that the fluorescence yield of Eosin Y starts to decrease around pH 4. This explains why the fluorescence intensity of the PAHA-20-E solution decreases a lot at pH 3. This makes it harder to compare the line scans in figure 17, 18 and 19. Because the fluorescence intensity decreases at pH 3, it is now hard to tell whether the decrease in fluorescent signal in the solution in figure 17 is due to the fact that polymer concentration is actually lower there or that it is simply due to the fact that the intensity decreases due to the low pH. The argument can be made that the fluorescent signal at pH 3 equally decreases for the polymer free in solution as for the polymer inside the membranes and that the ratio between the two peaks in the line scan is still a valid method to determine this. It is unlikely that this is the case since the hydrophobic environment inside the membrane will likely influence the polarity and charge of the Eosin Y and it is not known where the polymer exactly is.

As of now it is not possible to say for certain that PAHA-20-E polymer localizes more inside the membranes at low pH due to the fact that fluorescence intensity decreases at pH values below 4. Using a lower polymer concentration and measuring above pH 4 could help increase the contrast between membrane and background. Confocal microscopy would be a more suitable way of analysing the results since this could be used to take images of slices in the z-space of the sample. This could help image the inside of the membranes that are stuck on the glass and this can give insights into where the polymer is in and around the membranes.

The experiments did show that PAHA-20-E polymer is able to move in and around the membranes and that this happens over a pH range of 3 to 11. The experiments also showed that PAHA-20-E was not able to solubilize membranes.

5 Conclusions and outlook

The goal of this research is to investigate the pH induced cooperative conformational changes displayed by HPEs while transitioning between a hydrophobic- and a hydrophilic state via a statistical mechanical model developed by *Martin Robinson et al.* [1] and secondly, investigate the interaction of the HPEs at different pH with respect to lipid bilayer membranes.

The experimental results show that poly (amino hexanoic acid) (PAHA) displays cooperative behaviour when transitioning in a 2-phase pentanol and water system. It shows that even very short polymers (PAHA-20) can display cooperative behaviour. The value of M, which is an indication for the cooperativity of the transition, increases with increasing polymer length and the transition becomes sharper. This is in compliance with the model since it predicts that the transition becomes sharper with increasing M value. The results also show that the transition pH stays roughly the same for all three different lengths of PAHA polymer. This is again confirmation of the model since the transition pH is dictated by the $\frac{M_H}{M}$ – ratio and the hydrophobic energy penalty of each individual monomer unit and this is the same for all three different polymers.

The differences between first- and the repeat measurements are explained by the sensitivity of the pH meter that is used. This highlights the sensitivity of the system because it is highly dependent on an accurate measurement for the pH. The differences in sharpness and the resulting M values are very small and a small deviation between runs can influence this. An attempt is made to avoid this problem by using high ionic strength potassium buffers and performing pH corrections after each measurement.

The results of the ionic strength experiment show that the transition becomes shaper with increasing ionic strength. This is because low ionic strength can lead to a split in pKa values between individual acid groups which results in more intermediate states and this causes transition broadening. The results also show that the transition pH shifts to higher values with decreasing ionic strength. This is due to a decrease in hydrophobic conformational energy penalty since less charge screening occurs at low ionic strength. The shift in transition pH does seem to become smaller with increasing ionic strength which is due to the fast decay of the Debye length. The effect that the ionic strength has on different parameters in the model and the resulting effect of this on the sharpness of transition and transition pH both complies with the model.

The interaction of PAHA with lipid membranes is examined by fluorescently labelling PAHA with Eosin Y (PAHA-20-E). The fluorescent and bight field images show that the polymer is able to move in and around the membranes at pH 3, 8 and 11. The line scans seem to show that the contrast between polymer inside the membranes and free in solution is the biggest at pH 3. This is expected since at pH 3 the acid groups are hydrophobic (protonated) and want to minimize hydrophobic area in contact with solution and move into the membranes. Emission spectra shows that the PAHA-20-E greatly decreases in emission intensity at pH 3. This makes the line scans more unreliable since the diminished background can also be caused by the decreased pH. Because of this, the only conclusion that can be made by this experiment is that the polymers move in and around the membranes at all three pH and that they do not solubilize membranes.

In the future it would be good to conduct new SEC-HPLC and MALDI experiments to get an accurate measurement of the length of the polymers. It would also be good to repeat the 2-phase experiments one more time to get more data on the values of M to see if the trend of increasing sharpness still occurs. Research that would be interesting to conduct is varying the side chain length on the polymers. The model predicts that this would only change the transition pH but not the sharpness of the transition. By making polymers with the same length but with different sidechain length this could be investigated. It would also be very interesting to synthesize polymers smaller in size (5-10 monomer units). This could give more insights in whether the transition really gets sharper with increasing polymer size. It could also help to confirm or refute the claim that the experimental value of M linearly depends on the polymer length.

It would be good to repeat the membrane interaction experiments but at a pH of 4 instead of 3. This would not diminish the fluorescence intensity of the Eosin Y as much and this could lead to more insights being gained from the line scans. It would also be good to image the membranes with a confocal microscope

instead of a widefield fluorescent microscope. A confocal microscope should be used to make images in the z-space of the sample and this can make it easier to image the inside of the membranes stuck to the glass of the capillary and it would also remove out of focus light. Using a lower polymer concentration could help increase the contrast between the membranes and the solution. It would be good to synthesize larger membranes because this can make it easier to see if the polymer is actually able to permeate the membranes or only stays in and around the lipid bilayer.

This research shows that accurately determining the transition pH can be challenging and that the absolute value depends on the type of transition and system. Gaining a better control and understanding of the transition pH in membrane interaction experiments will be necessary in order to use HPEs for selective tumour treatment. The sharpness of the transition can be quite sharp, even for smaller HPEs. This can be helpful when designing HPEs for tumour treatment because it indicates that the HPEs do not necessarily need to be very long in order to display cooperative behaviour. This could help with making a more sustainable and effective HPE medicine, because more smaller polymers could be synthesized from the same amount of monomers. The research shows that the statistical mechanical model can be used to make predictions about the sharpness of the transition and the transition pH of the HPEs and this can definitely be useful when designing HPEs for selective tumour treatment.

6 Acknowledgements

I would like to start with thanking Prof. Dr. Willem Kegel, who was my supervisor for this research project. Willem, thanks for all the help and useful discussions about HPEs and statistical mechanics. You were always very kind and helpful when I came walking into your office with questions, I learned so much from you during this project and I am very thankful for that!

I want to thank James Martin Robinson, who was my daily supervisor for this research project. James, you helped me daily with all my struggles when performing this research. You helped me in- and outside the lab and your nice and calm approach made me feel very comfortable. You showed me the ins and outs of polymer synthesis and the model from which I gained so much knowledge. During our discussions you treated me like an equal which motivated me to look at the subject with different views. Thanks for all the help James, it was a great pleasure to work with you!

I want to thank Alex van Silfhout, who was also my daily supervisor for this research project. Alex, our discussions were always very fruitful and your knowledge about the lab was amazing. You came with a lot of good suggestions on how to synthesise and analyse the polymers in the best way. Your funny and relaxed attitude made it very nice to work with you. Thanks for all the help and smiles!

I would like to thank everyone in the Kegel group for our interesting and useful discussions. I would like to thank Bas van Ravenstein for helping us with the organic synthesis of the polymers and I want to thank Mies van Steenbergen for helping us with the SEC-HPLC measurements.

I would like to thank everyone at FCC for being kind, helpful and creating a very nice work environment to conduct research in. I want to thank my office mates Tessa, Bo, Steffen, Kevin, Ariane and Simon for being so kind, funny, helpful and patient while listen to my rambles about ionic strength and buffers.

At last I want to say something about my two grandfathers who unfortunately passed away while I was conducting this research. I find it hard to describe with words how big of an impact you both had on me as a person and on my life. People say wisdom comes with age and that was certainly true for both of you. Opa Dirk, I remember our cycles trough the countryside and you explaining the different plants and animals that inhabited the area. This is where my interest in nature and science began and I am very grateful for these memories. Opa Niek, you let me ''work'' in your lab when I was little, where I pretended to make fake teeth just like you did. I think this is where my interest in chemistry must have started and these memories of you are so precious to me. You were both role models to me and you shaped me into the person I am today and I am proud to be your grandson.

7 References

1. Martin Robinson, J. L. & Kegel, W. K. Cooperative transitions involving hydrophobic polyelectrolytes. *PNAS* **120**, (2023).
2. Aguilar, M. R. & San Román, J. *Advances in shape memory polymers*. (Woodhead Publishing, 2014).
3. Kegel, W. K. *Toy Models in physical chemistry and molecular biology*. (2019).
4. Monod, J., Wyman, J. & Changeux, J. P. On the nature of allosteric transitions: A plausible model. *J Mol Biol* **12**, 88–118 (1965).
5. Di Mauro, G. M., La Rosa, C., Condorelli, M. & Ramamoorthy, A. Benchmarks of SMA-Copolymer Derivatives and Nanodisc Integrity. *Langmuir* **37**, 3113–3121 (2021).
6. Scheidelaar, S. *et al.* Molecular Model for the solubilization of membranes into nanodisks by styrene maleic acid copolymers. *Biophys J* **108**, 279–290 (2015).
7. Dörr, J. M. *et al.* The styrene–maleic acid copolymer: a versatile tool in membrane research. *European Biophysics Journal* vol. 45 3–21 (2016).
8. Scheidelaar, S. *et al.* Effect of Polymer Composition and pH on Membrane Solubilization by Styrene-Maleic Acid Copolymers. *Biophys J* **111**, 1974–1986 (2016).
9. Hao, G., Xu, Z. P. & Li, L. Manipulating extracellular tumour pH: An effective target for cancer therapy. *RSC Advances* vol. 8 22182–22192 (2018).
10. Kuriyan, J., Konforti, B. & Wemmer, D. *The molecules of life, Pysical and chemical principles*. (Garland science, 2013).
11. Swenson, H. & Stadie, N. P. Langmuir's Theory of Adsorption: A Centennial Review. *Langmuir* **35**, 5409–5426 (2019).
12. Wodak, S. J. *et al.* Allostery in Its Many Disguises: From Theory to Applications. *Structure* vol. 27 566–578 (2019).
13. Hilser, V. J., Wrabl, J. O. & Motlagh, H. N. Structural and energetic basis of allostery. *Annual Review of Biophysics* vol. 41 585–609 (2012).
14. Ma, X. *et al.* Ultra-pH-sensitive nanoprobe library with broad pH tunability and fluorescence emissions. *J Am Chem Soc* **136**, 11085–11092 (2014).
15. Kegel, W. K. *Physical Chemistry 2: Classical Thermodynamics and introduction to Statistical Thermodynamics*. (2021).
16. Schrödinger, E. Statistical Thermodynamics. 1–14 (1948).
17. Hill, T. L. *An introduction to statistical thermodynamics*. (Dover Publications, 1986).
18. De Oliveira, C. R. & Werlang, T. Ergodic hypothesis in classical statistical mechanics. *Revista Brasileira de Ensino de Física* **29**, 189–201 (2007).
19. Atkins, P. & de Paula, J. *ATKINS' PHYSICAL CHEMISTRY*. vol. 8 (W. H. Freeman and Company, 2006).
20. Steiner, E. *The Chemistry Maths Book*. vol. 8 (Oxford University press, 2008).
21. Martin Robinson, J. L. & Kegel, W. K. Supplementary Information for Cooperative transitions involving hydrophobic polyelectrolytes. *PNAS* **120**, (2023).
22. Chiefari, J. *et al.* Living Free-Radical Polymerization by Reversible Addition-Fragmentation Chain Transfer: The RAFT Process. *Macromolecules* **31**, 5559–5562 (1998).

23. Lovell, P. A. & Young, R. J. *Introduction to Polymers*. (Chapman & Hall, 1991).

24. Brodszkij, E. *et al.* SUPPORTING INFORMATION Interaction of pH-Responsive Polyanions with Phospholipid Membranes. *Polym Chem* **10**, 5992–5997 (2019).

25. Perrier, S. 50th Anniversary Perspective: RAFT Polymerization - A User Guide. *Macromolecules* vol. 50 7433–7447 (2017).

26. Matyjaszewski, K. Atom Transfer Radical Polymerization (ATRP): Current status and future perspectives. *Macromolecules* **45**, 4015–4039 (2012).

27. Lorandi, F. *et al.* Atom Transfer Radical Polymerization of Acrylic and Methacrylic Acids: Preparation of Acidic Polymers with Various Architectures. *ACS Macro Lett* **9**, 693–699 (2020).

28. Weller, M., Overton, T., Rourke, J. & Armstrong, F. *Inorganic chemistry*. vol. 7 (Oxford University Press, 2018).

29. Harris, D. C. & Lucy, C. A. *Quantitative chemical analysis*. vol. 9 (2017).

30. Erné, B. *Colloid Science: Colloidal Analysis Techniques*. (2022).

31. Antonini, A., Butturi, M. A., Zurru, P., Norton, M. & Parretta, A. Development of a high/low concentration photovoltaic module with dichroic spectrum splitting. *Progress in Photovoltaics: Research and Applications* **23**, 1190–1201 (2015).

32. Slyusareva, E. A. & Gerasimova, M. A. *pH-DEPENDENCE OF THE ABSORPTION AND FLUORESCENT PROPERTIES OF FLUORONE DYES IN AQUEOUS SOLUTIONS*. *Russian Physics Journal* vol. 56 (2014).

33. Hetzer, M., Schmidt, B. V. K. J., Barner-Kowollik, C. & Ritter, H. Limitations of cyclodextrin-mediated RAFT homopolymerization and block copolymer formation. *J Polym Sci A Polym Chem* **51**, 2504–2517 (2013).

34. Esquivel-Guzmán, J. A., Zaragoza-Galán, G., Ortíz-Palacios, J. & Rivera, E. Synthesis and characterization of novel polymers bearing fluorescein units: Thermal and optical properties. *Des Monomers Polym* **15**, 561–574 (2012).

35. Skrabania, K., Miasnikova, A., Bivigou-Koumba, A. M., Zehm, D. & Laschewsky, A. Examining the UV-vis absorption of RAFT chain transfer agents and their use for polymer analysis. *Polym Chem* **2**, 2074–2083 (2011).

36. Kopf, A. H. Membrane Solubilization by Amphipathic Copolymers. (Utrecht University, 2022). doi:10.33540/1181.

37. Boisen, O., Corral, A., Pope, E. & Goeltz, J. C. Quantifying the Cross-Sensitivity of Glass pH Electrodes in Alkaline Solutions. *J Chem Educ* **96**, 1418–1423 (2019).

38. Haslak, Z. P., Zareb, S., Dogan, I., Aviyente, V. & Monard, G. Using Atomic Charges to Describe the pKa of Carboxylic Acids. *J Chem Inf Model* **61**, 2733–2743 (2021).

39. Brodszkij, E. *et al.* Interaction of pH-responsive polyanions with phospholipid membranes. *Polym Chem* **10**, 5992–5997 (2019).

40. Ball, D. W. & Baer, T. *Physical Chemistry*. vol. 2 (2011).

41. Veloz Martínez, I., Ek, J. I., Ahn, E. C. & Sustaita, A. O. Molecularly imprinted polymers via reversible addition-fragmentation chain-transfer synthesis in sensing and environmental applications. *RSC Advances* vol. 12 9186–9201 (2022).

8 Appendix

Appendix A ^{1}HNMR-spectra

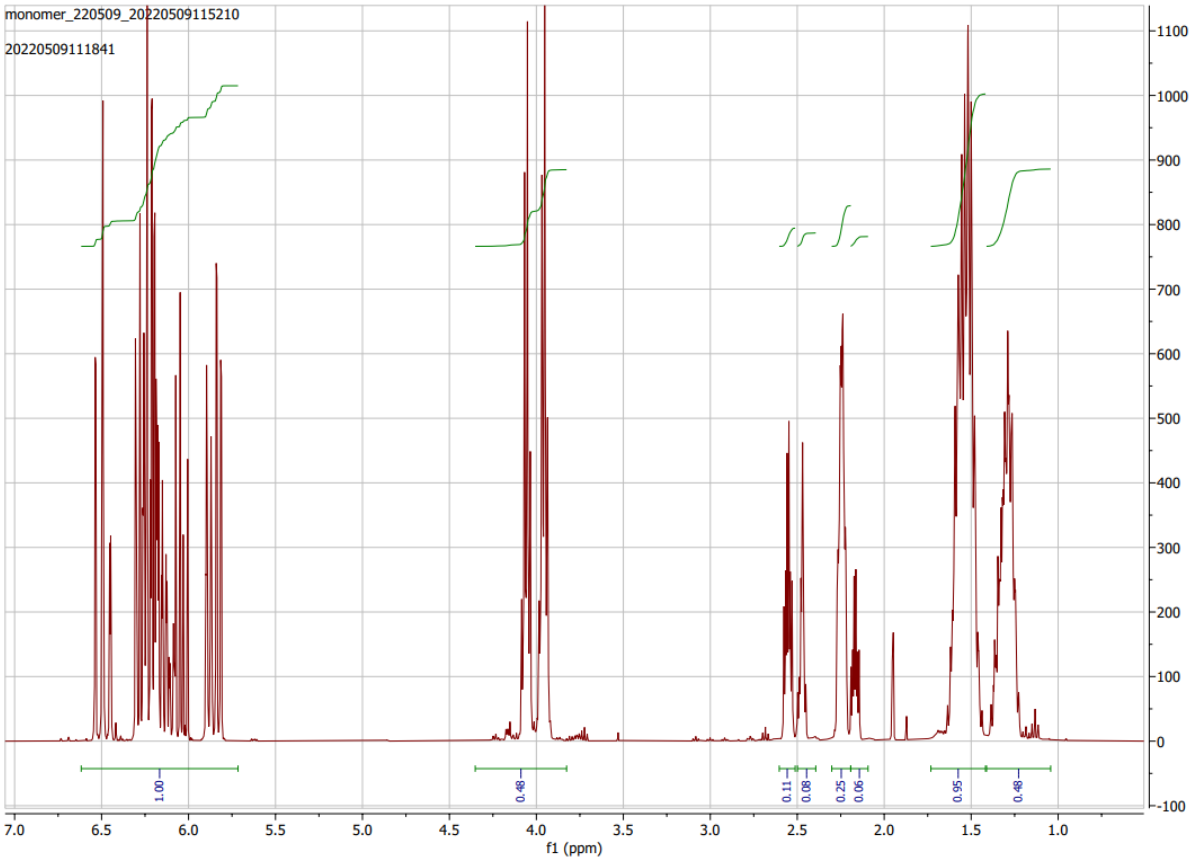

A1: 6-hydroxyhexanoic acid acrylate spectrum (DMSO)

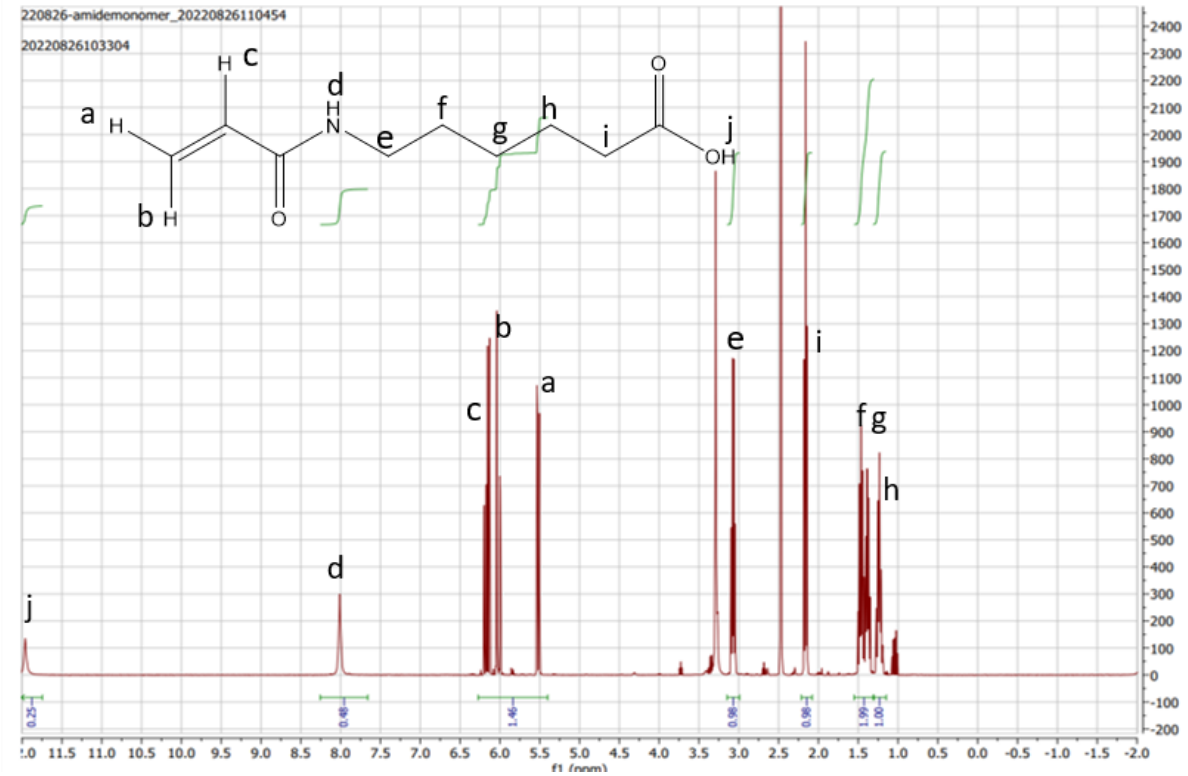

A2: 6-aminohexanoic acid acrylate (DMSO)

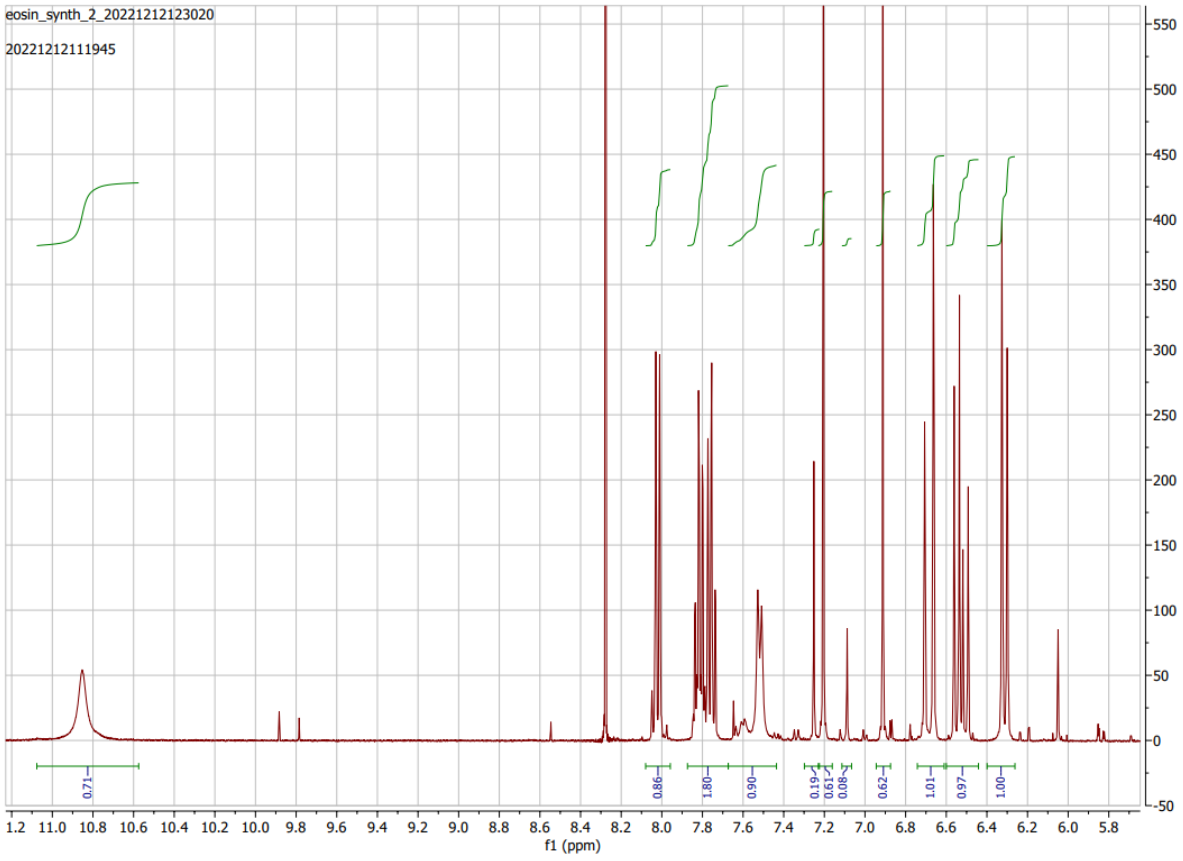

A3: Eosin Y acrylate (DMSO)

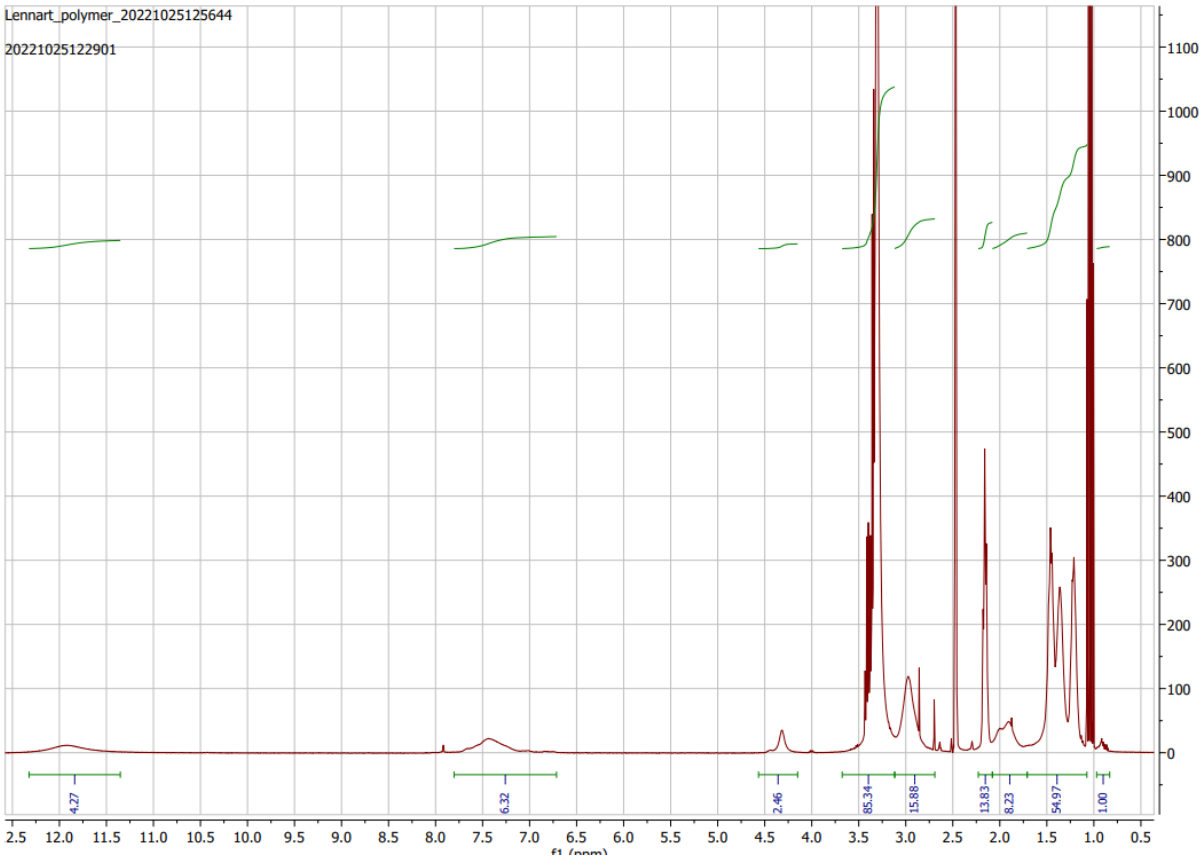

A4: PAHA-20-1 (20 length) (DMSO)

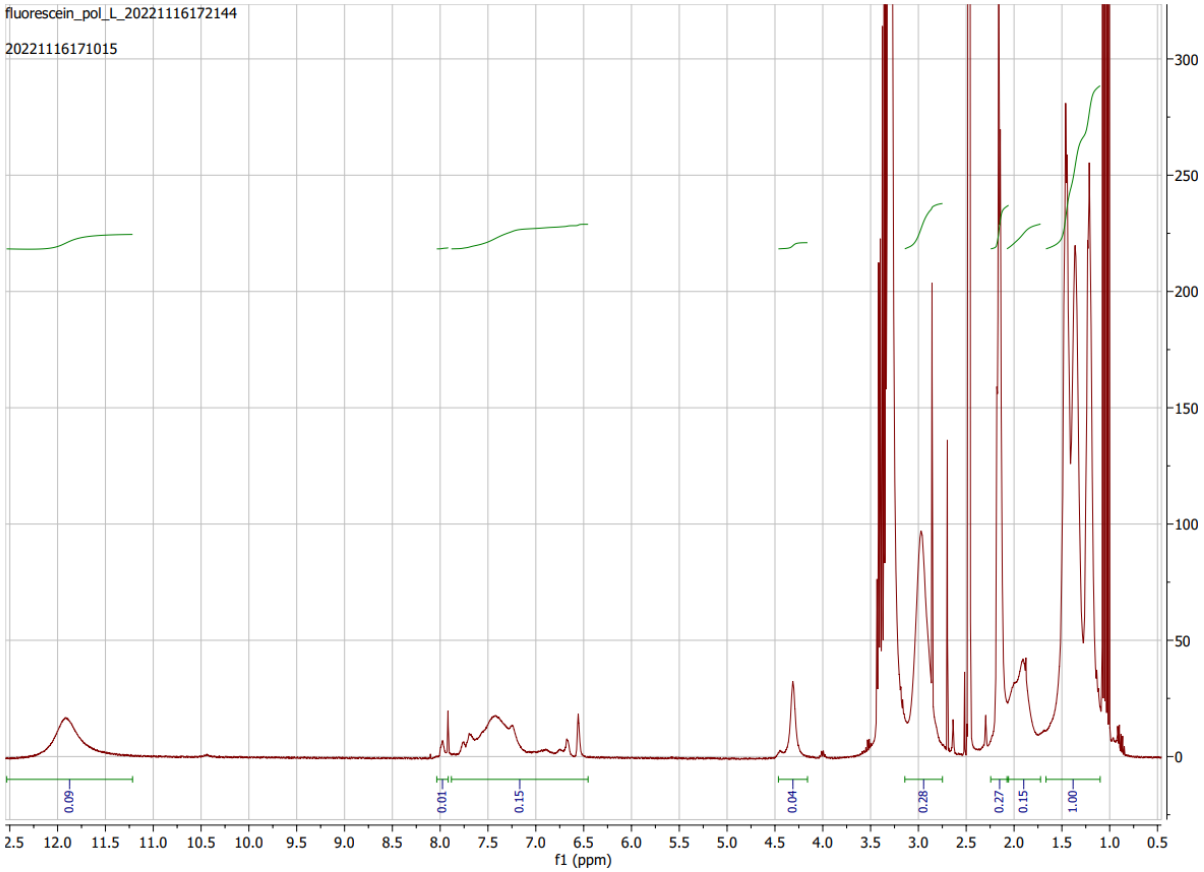

A5: PAHA-20-F (DMSO)

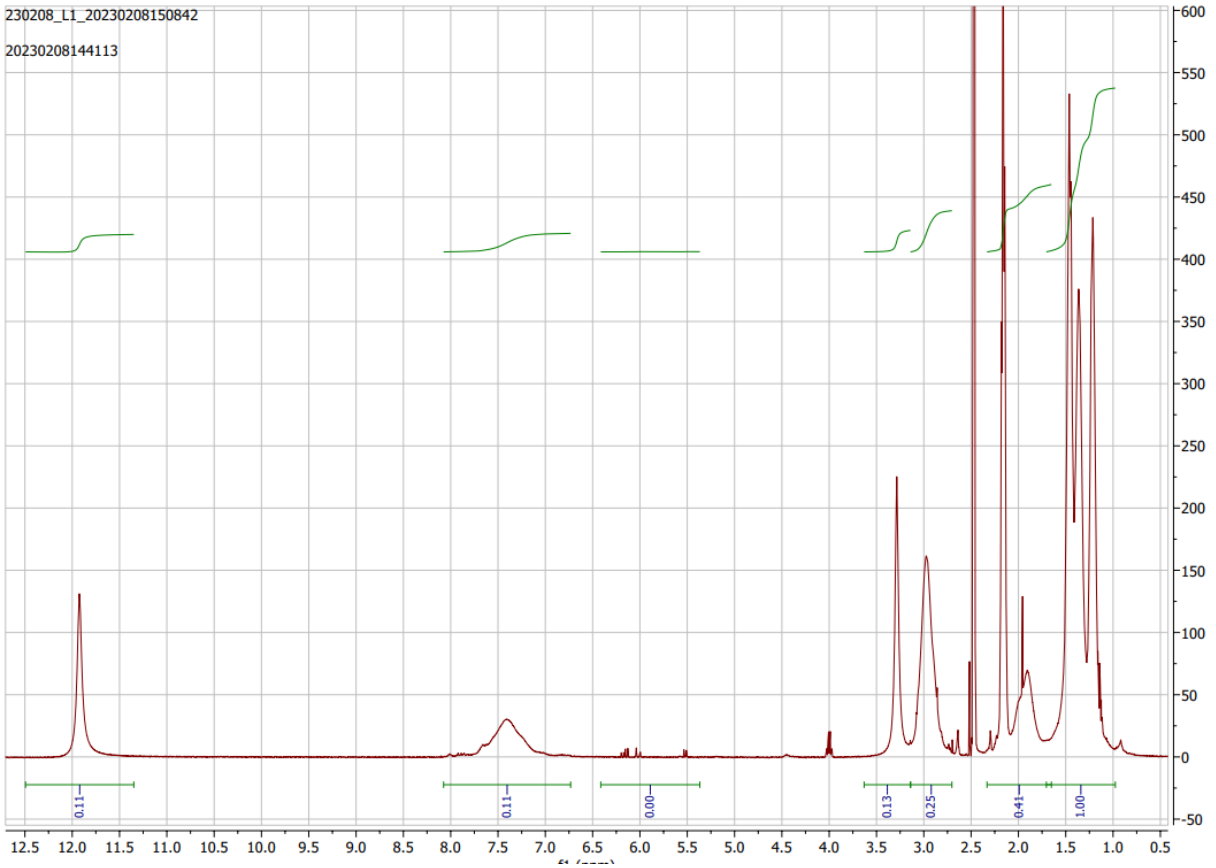

A6: PAHA-40 (40 length) (DMSO)

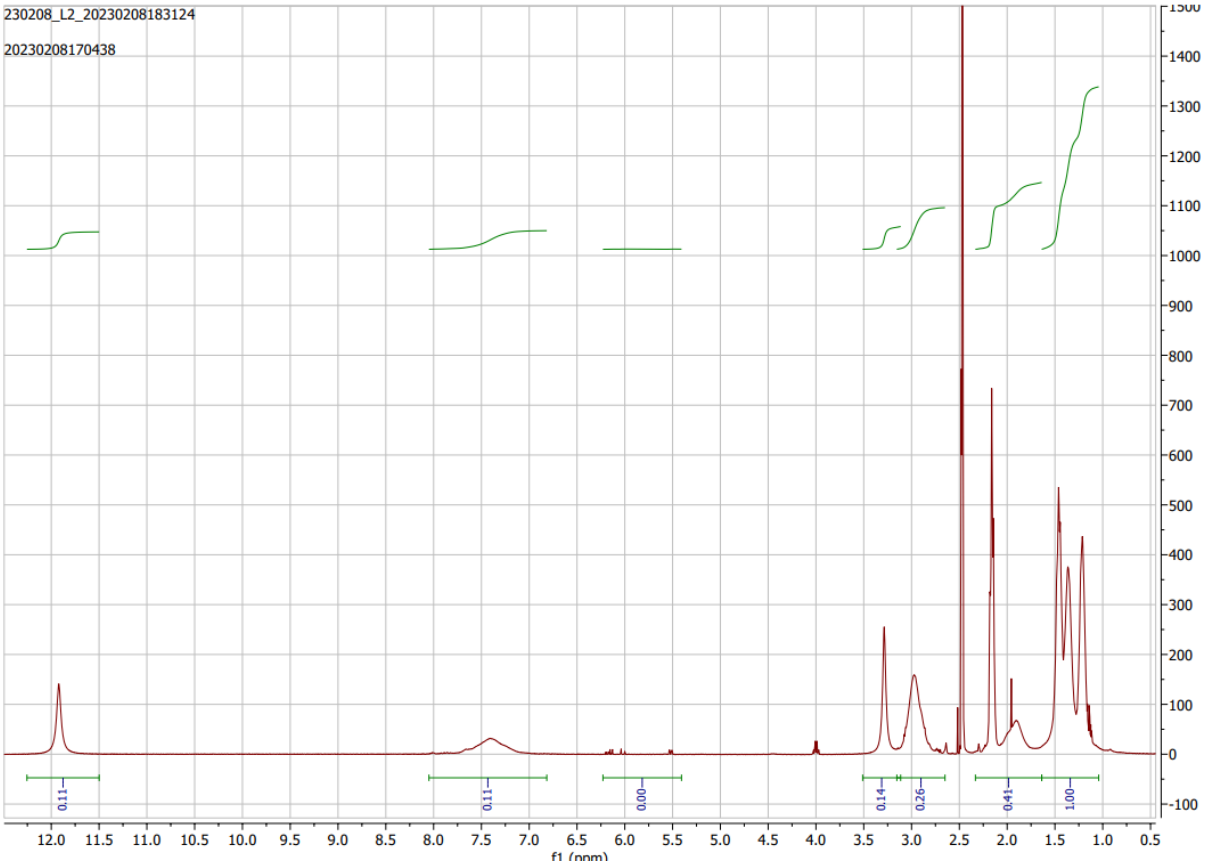

A7: PAHA-80 (80 Length) (DMSO)

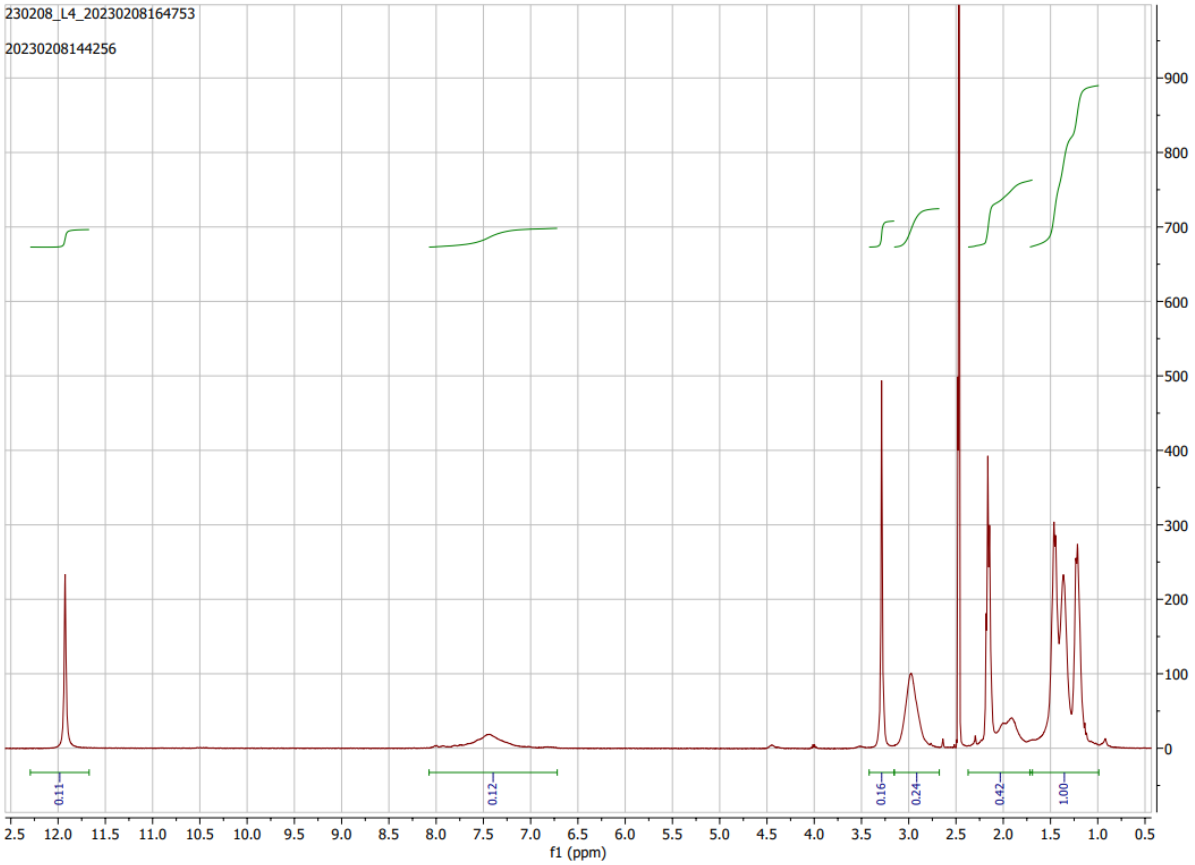

A8: PAHA-20-E (DMSO)

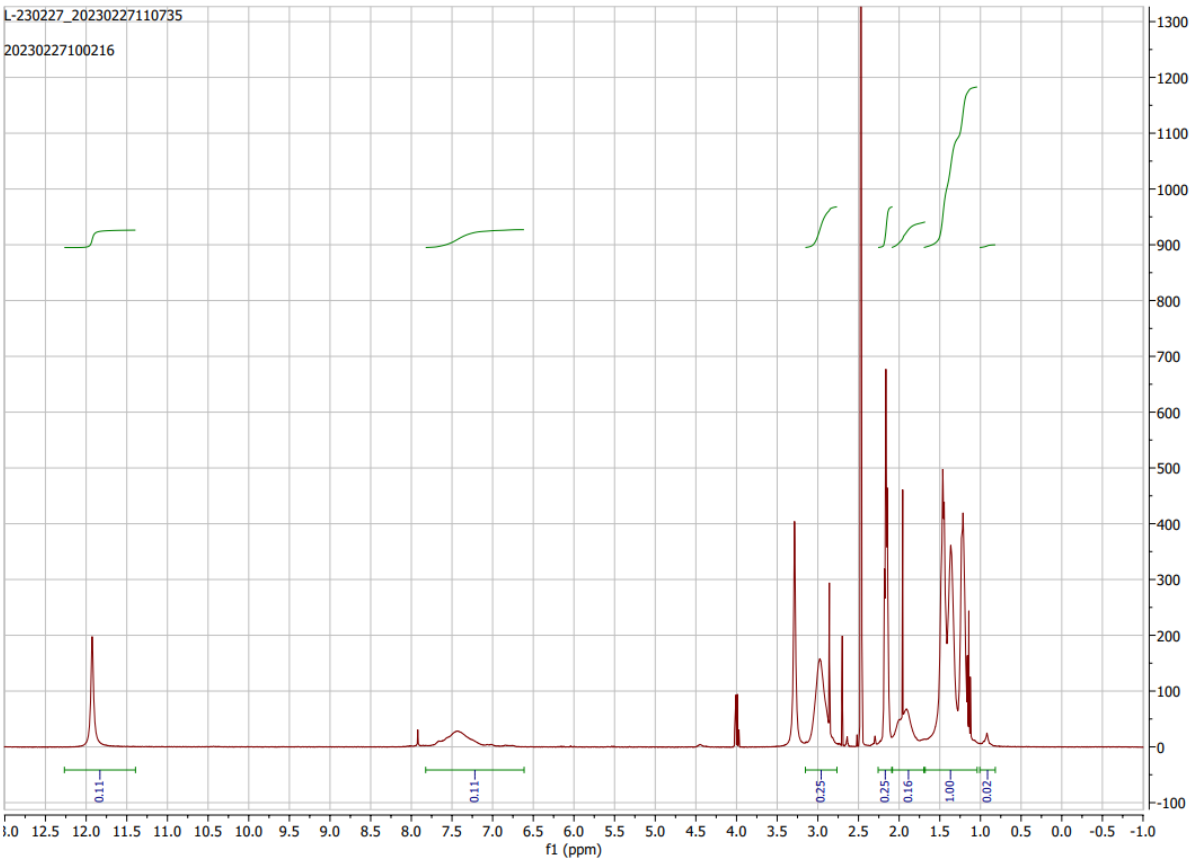

A9: PAHA-20-2 (20 length) (DMSO)

Appendix B HPLC

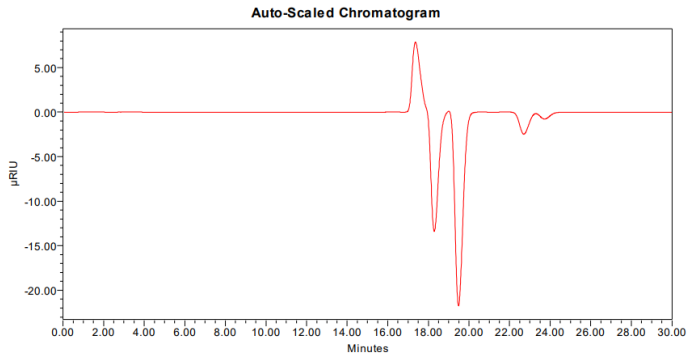

GPC Results

	Dist Name	Mn	Mw	MP	Mz	Mz+1	Mv	Polydispersity	MW Marker 1	MW Marker 2
1										

B1: PAHA-20-1

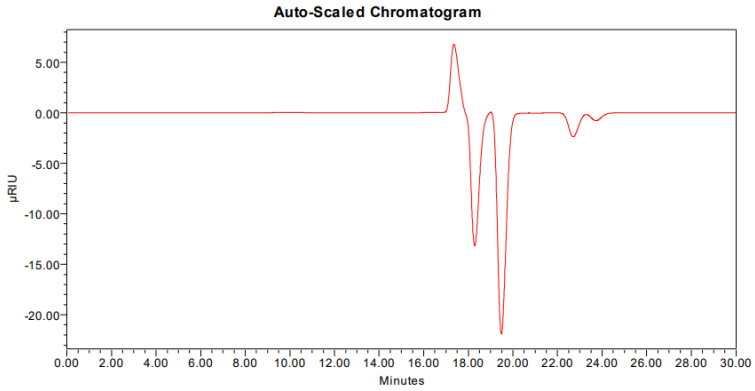

GPC Results

	Dist Name	Mn	Mw	MP	Mz	Mz+1	Mv	Polydispersity	MW Marker 1	MW Marker 2
1										

B2: PAHA-20-F

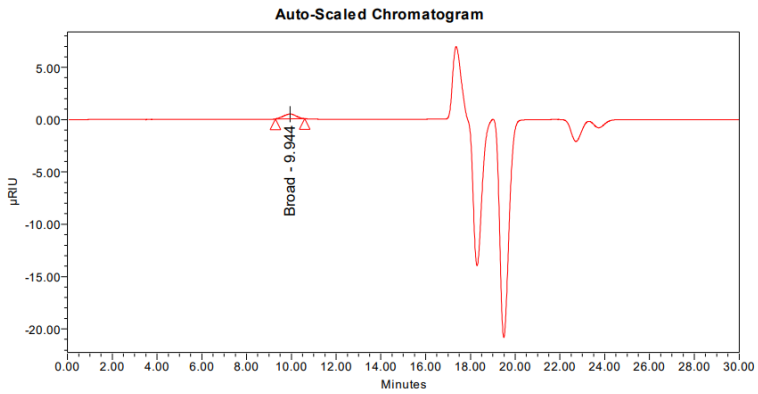

GPC Results

	Dist Name	Mn	Mw	MP	Mz	Mz+1	Mv	Polydispersity	MW Marker 1	MW Marker 2
1										

B3: PAHA-40

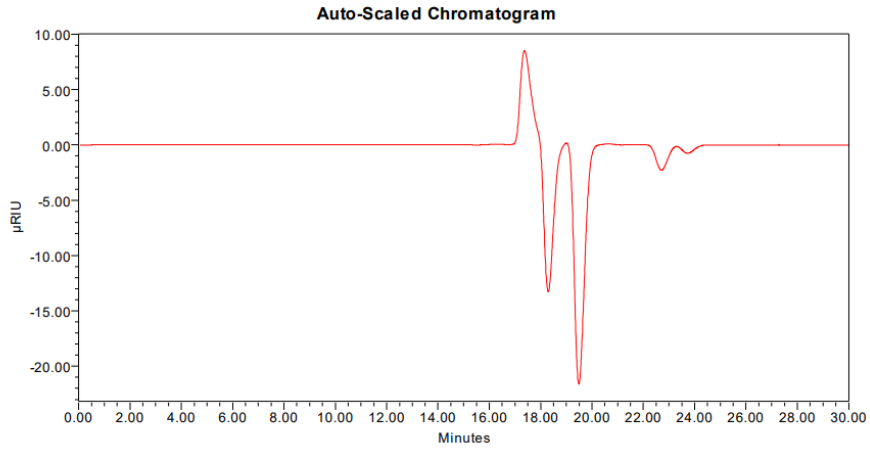

GPC Results

	Dist Name	Mn	Mw	MP	Mz	Mz+1	Mv	Polydispersity	MW Marker 1	MW Marker 2
1										

B4: PAHA-80

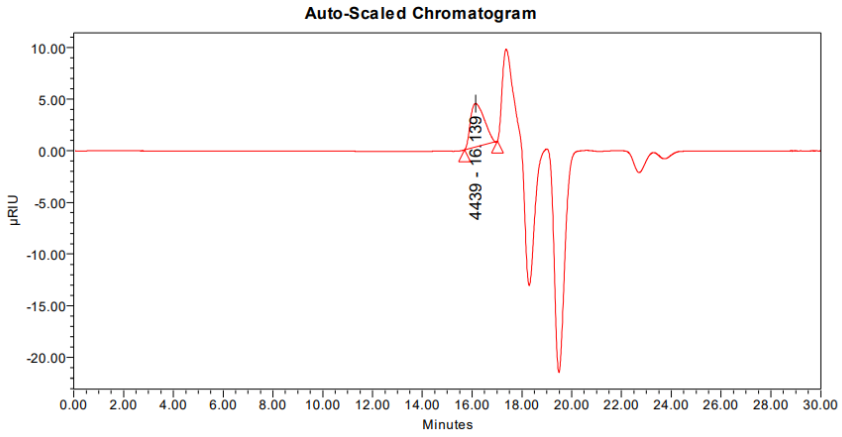

GPC Results

	Dist Name	Mn	Mw	MP	Mz	Mz+1	Mv	Polydispersity	MW Marker 1	MW Marker 2
1		4220	4264	4439	4308	4349		1.010493		

B5: PAHA-20-E

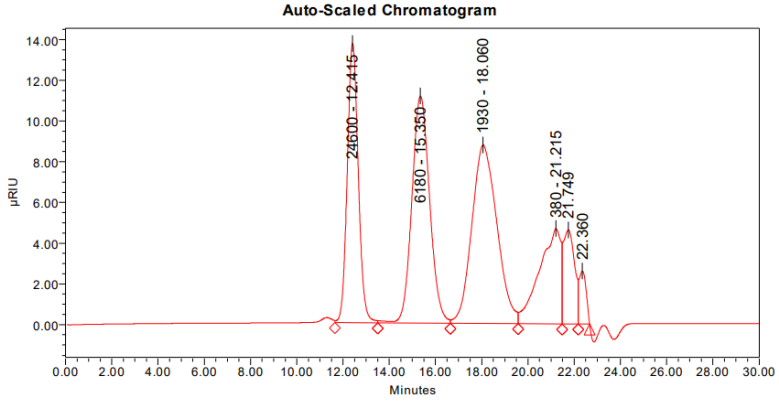

GPC Results

	Dist Name	Mn	Mw	MP	Mz	Mz+1	Mv	Polydispersity	MW Marker 1	MW Marker 2
1				24600						
2				6180						
3				1930						
4				380						

B6: Standard Yellow (PEG)

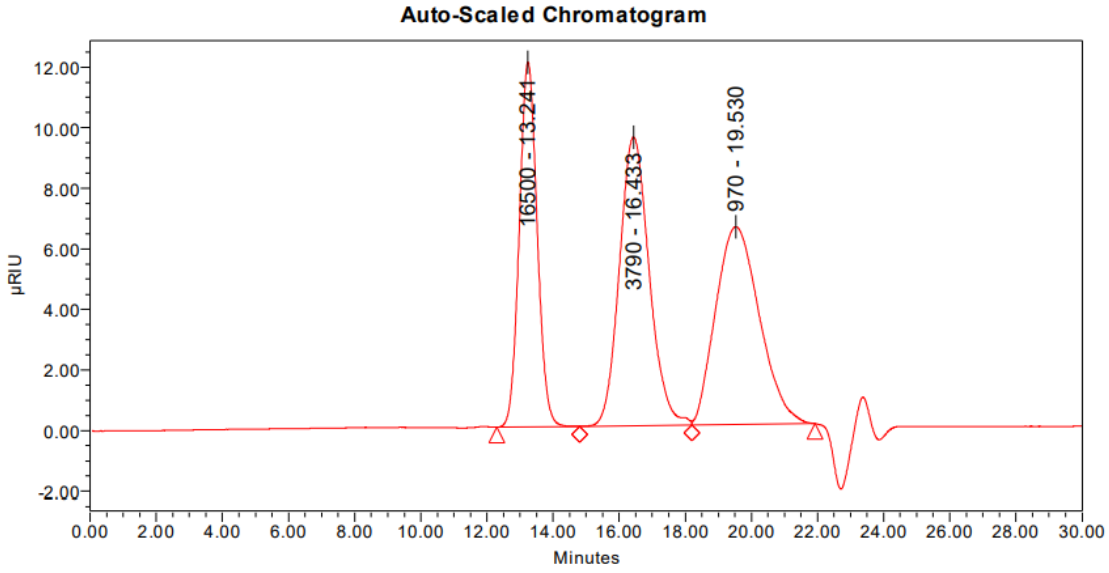

GPC Results

	Dist Name	Mn	Mw	MP	Mz	Mz+1	Mv	Polydispersity	MW Marker 1	MW Marker 2
1				16500						
2				3790						
3				970						

B7: Standard Green (PEG)

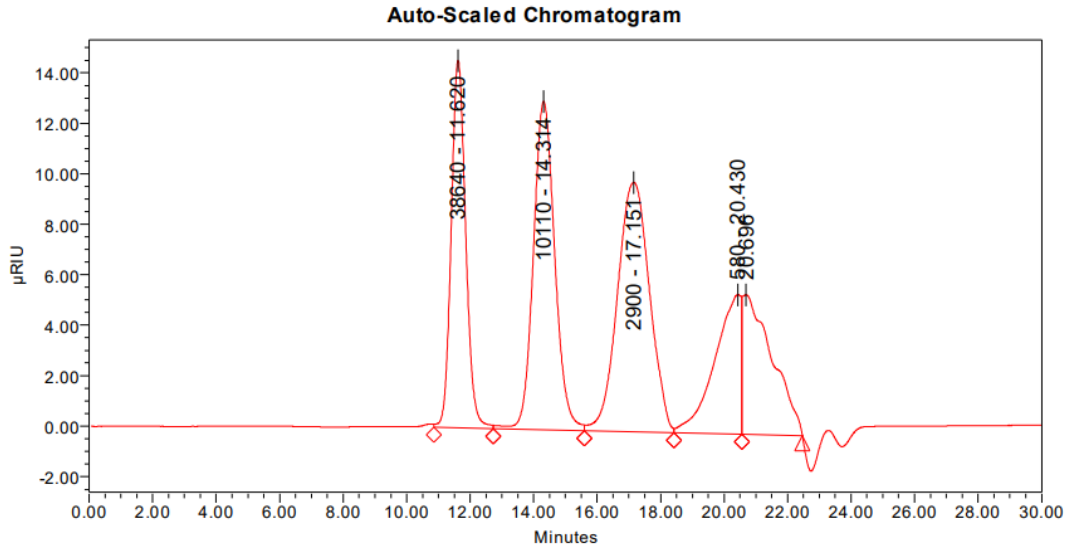

GPC Results

	Dist Name	Mn	Mw	MP	Mz	Mz+1	Mv	Polydispersity	MW Marker 1	MW Marker 2
1				38640						
2				10110						
3				2900						
4				580						

B8: Standard Red (PEG)

Appendix C UV-VIS measurements

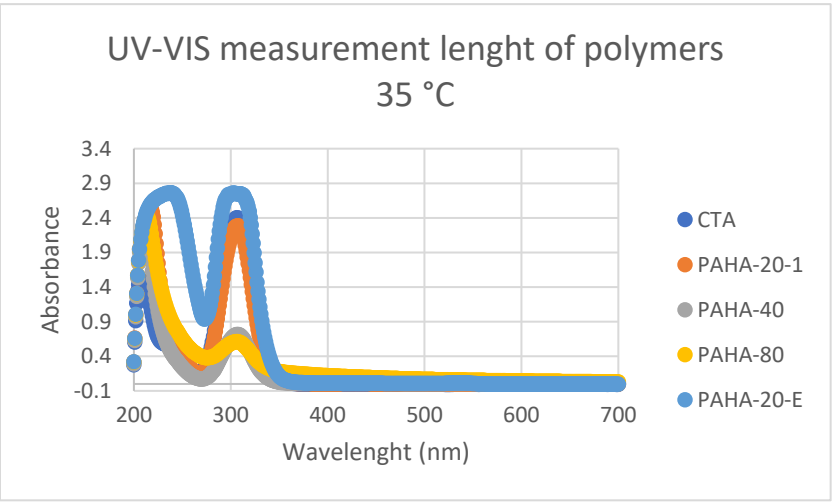

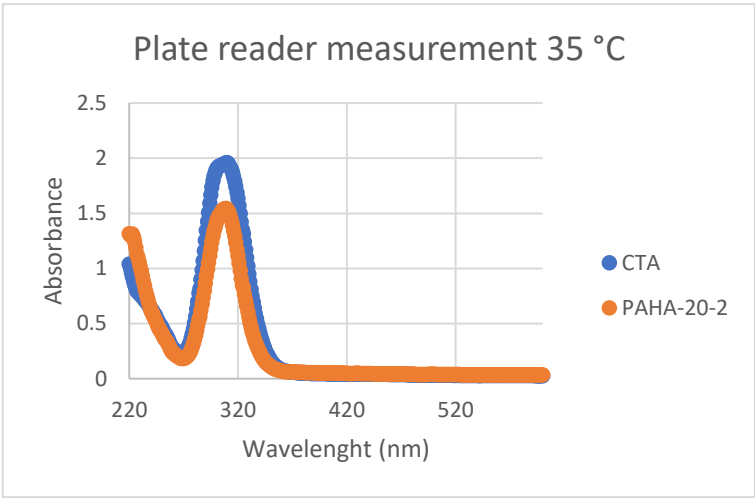

C1: UV-VIS measurement for determination of length of polymers. Left data from UV-VIS machine and on the right data from the plate reader.

Appendix D Microscopy images

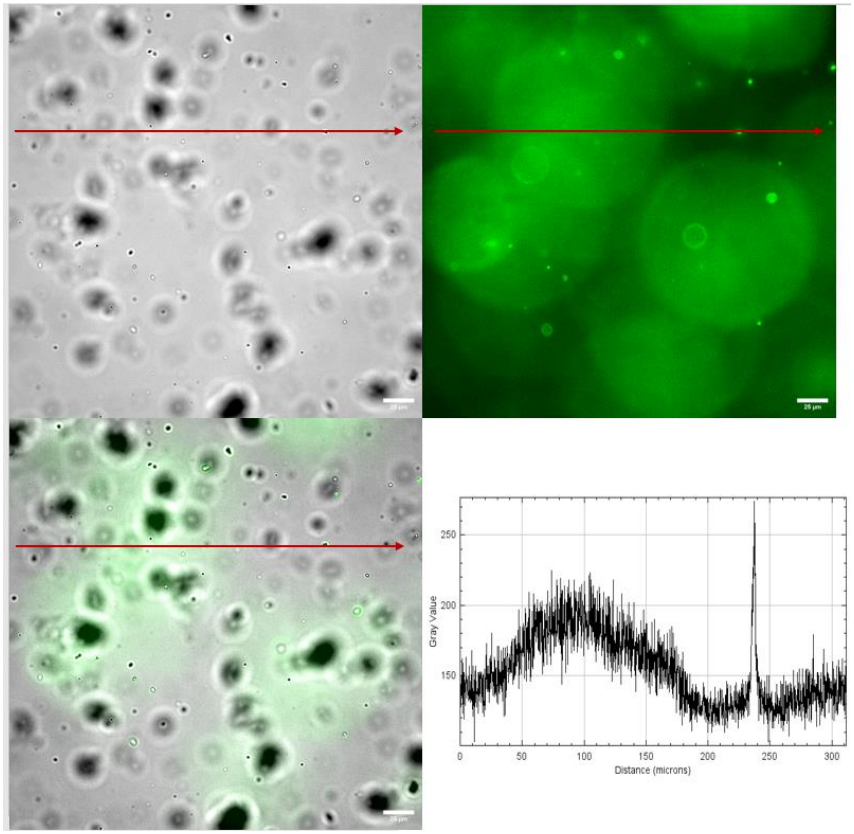

D1: Membranes and PAHA-E-6 at pH 3 in the middle of the capillary. Scalebar 25 microns.

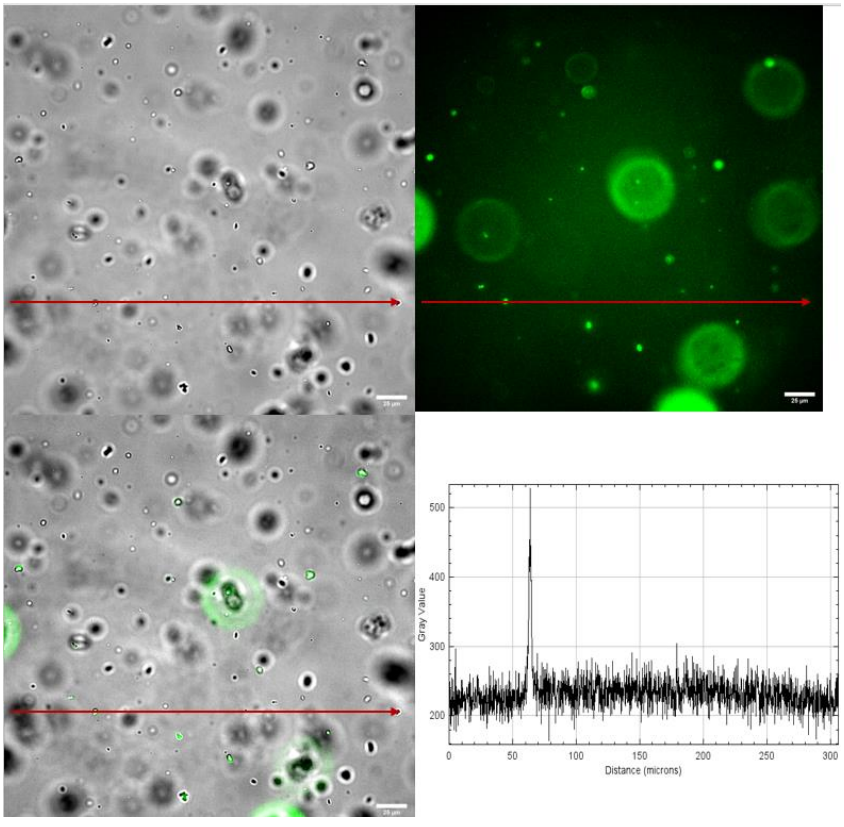

D2: Membranes and PAHA-E-6 at pH 3 in the middle of the capillary. Scalebar 25 microns.

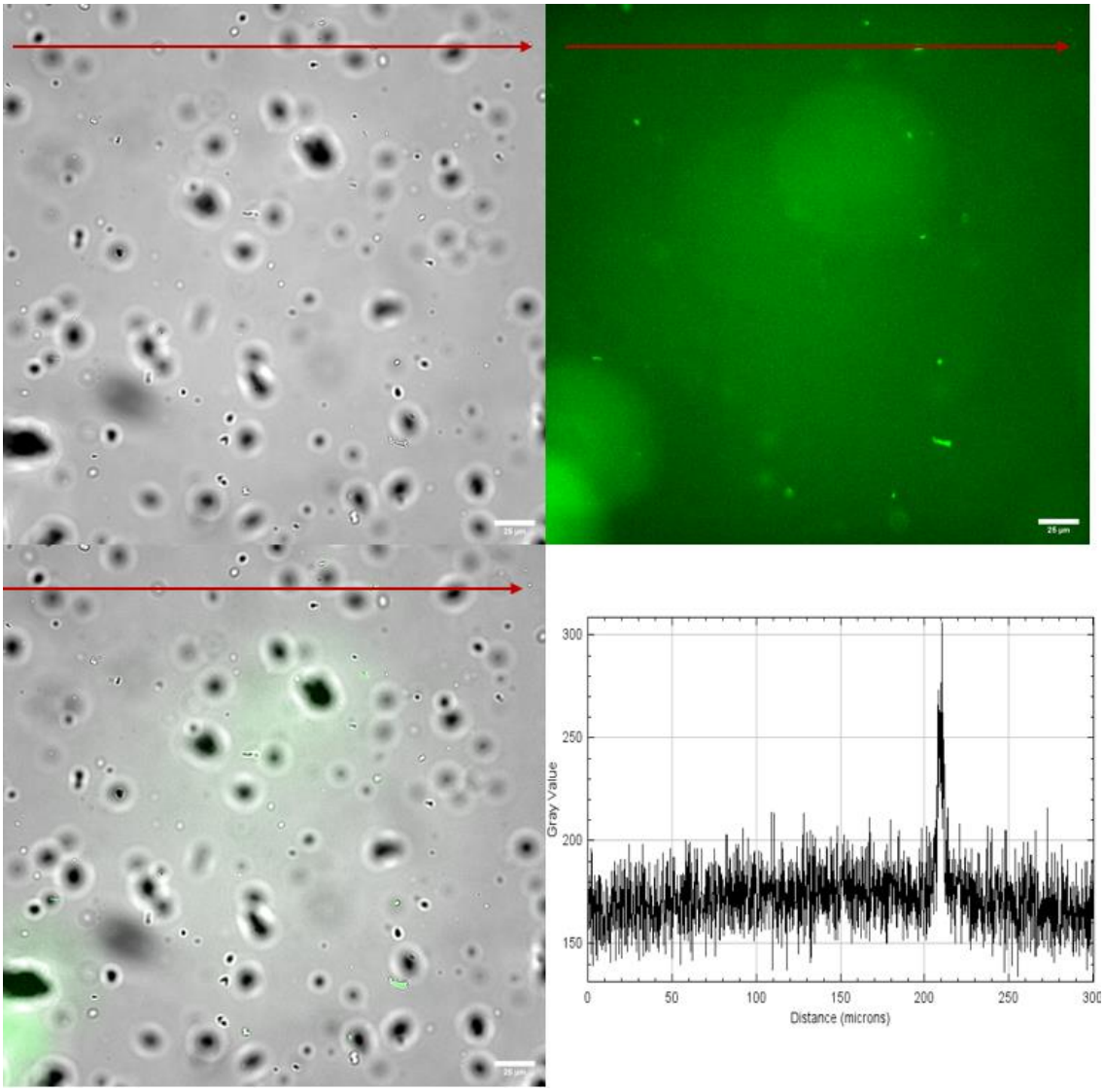

D3: Membranes and PAHA-E-6 at pH 3 in the middle of the capillary. Scalebar 25 microns.

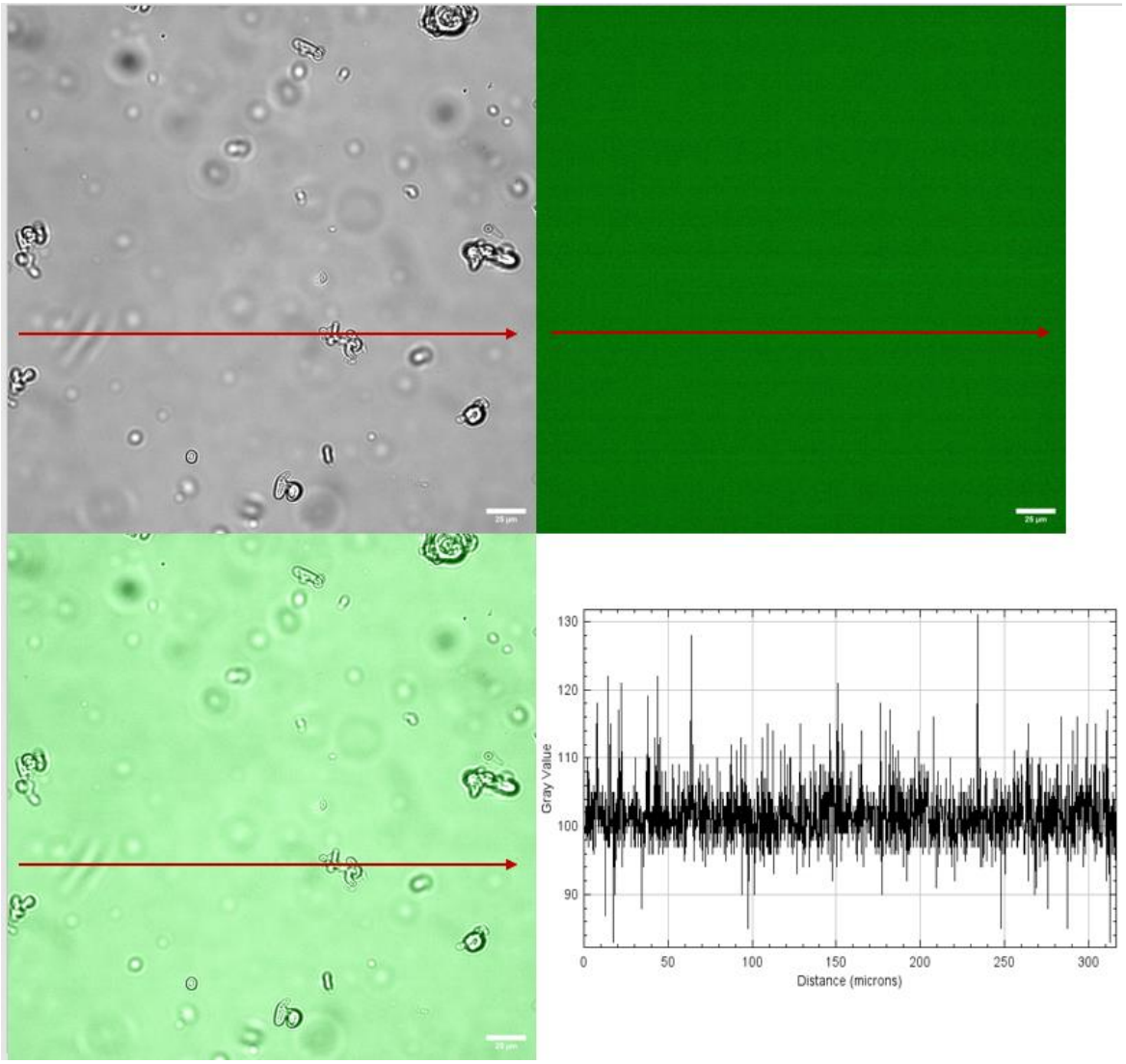

D4: Membranes at pH 7 in the middle of the capillary. Scalebar 25 microns.

Appendix E additional figures

E1: PAHA (left), No polymer (middle), SMA (right) with lipid membranes

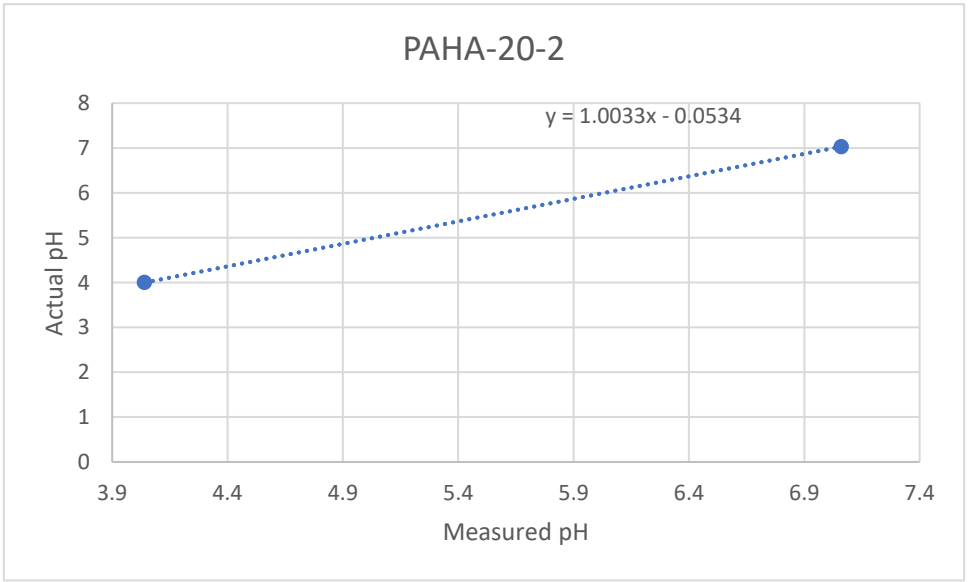

E2: pH correction graph PAHA-20-2

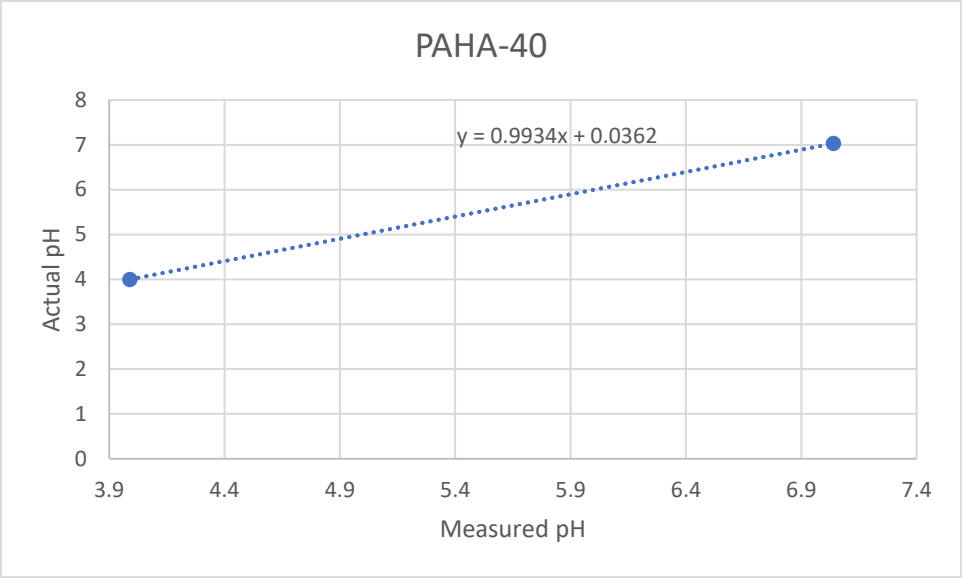

E3: pH correction graph PAHA-40

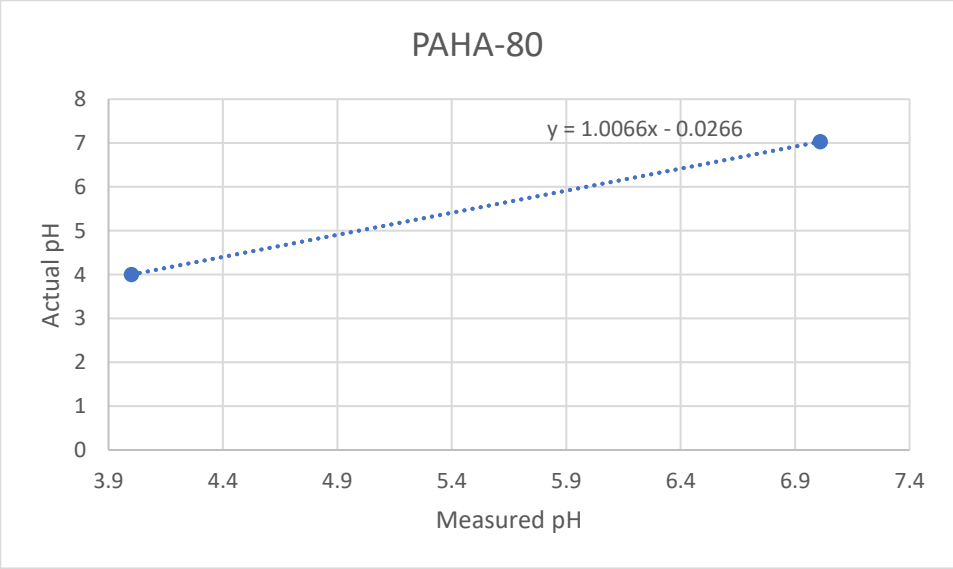

E4: pH correction graph PAHA-80

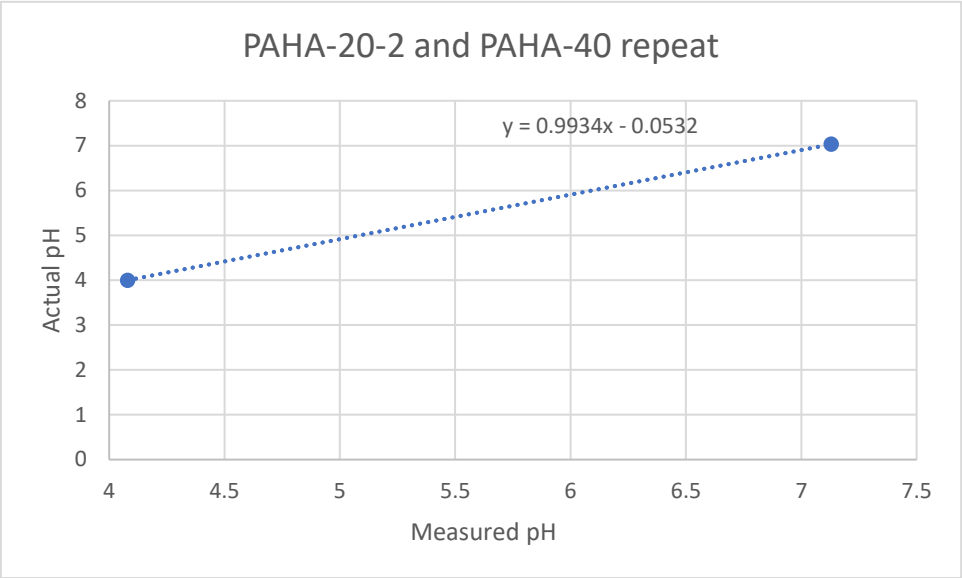

E5: pH correction graph PAHA-20-2 and PAHA-40 (repeats) since these were both measured in one measurement

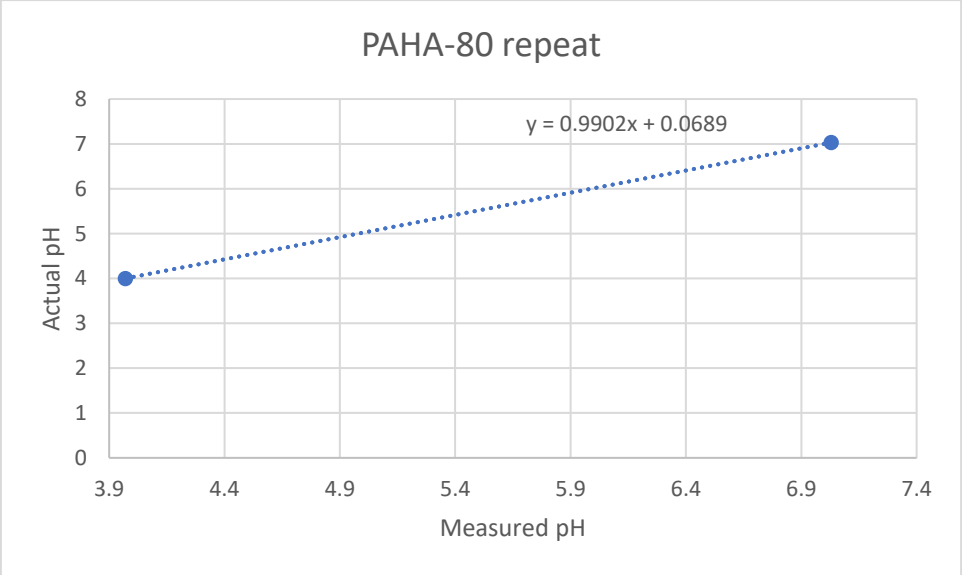

E6: pH correction graph PAHA-80 (repeats)

	UV Cutoff (nm)
Acetonitrile UV	190
Pentane	190
Water	190
Hexane UV	195
Cyclopentane	198
Cyclohexane	200
Heptane	200
Isopropyl Alcohol	205
Methanol	205
Ethyl Alcohol	210
2-Methoxyethanol	210
Methyl *t*-Butyl Ether	210
n-Propyl Alcohol	210
Trifluoroacetic Acid	210
Tetrahydrofuran UV	212
n-Butyl Alcohol	215
1,4-Dioxane	215
Ethyl Ether	215
Iso-Octane	215
n-Butyl Chloride	220
Glyme	220
Isobutyl Alcohol	220
Propylene Carbonate	220

E7: List with UV cut off values for different solvents. Note that there is no 1-pentanol but all alcohols display a cut off around 210 nm. From: https://macro.lsu.edu/HowTo/solvents/UV%20Cutoff.htm